



AMPEROMETRIC ENZYME-BASED DETECTION OF AGRICULTURAL PESTICIDES ON NOVEL CARBON NANO-ONION COMPOSITES

Vibol Sok

ADVERTIMENT. L'accés als continguts d'aquesta tesi doctoral i la seva utilització ha de respectar els drets de la persona autora. Pot ser utilitzada per a consulta o estudi personal, així com en activitats o materials d'investigació i docència en els termes establerts a l'art. 32 del Text Refós de la Llei de Propietat Intel·lectual (RDL 1/1996). Per altres utilitzacions es requereix l'autorització prèvia i expressa de la persona autora. En qualsevol cas, en la utilització dels seus continguts caldrà indicar de forma clara el nom i cognoms de la persona autora i el títol de la tesi doctoral. No s'autoritza la seva reproducció o altres formes d'explotació efectuades amb finalitats de lucre ni la seva comunicació pública des d'un lloc aliè al servei TDX. Tampoc s'autoritza la presentació del seu contingut en una finestra o marc aliè a TDX (framing). Aquesta reserva de drets afecta tant als continguts de la tesi com als seus resums i índexs.

ADVERTENCIA. El acceso a los contenidos de esta tesis doctoral y su utilización debe respetar los derechos de la persona autora. Puede ser utilizada para consulta o estudio personal, así como en actividades o materiales de investigación y docencia en los términos establecidos en el art. 32 del Texto Refundido de la Ley de Propiedad Intelectual (RDL 1/1996). Para otros usos se requiere la autorización previa y expresa de la persona autora. En cualquier caso, en la utilización de sus contenidos se deberá indicar de forma clara el nombre y apellidos de la persona autora y el título de la tesis doctoral. No se autoriza su reproducción u otras formas de explotación efectuadas con fines lucrativos ni su comunicación pública desde un sitio ajeno al servicio TDR. Tampoco se autoriza la presentación de su contenido en una ventana o marco ajeno a TDR (framing). Esta reserva de derechos afecta tanto al contenido de la tesis como a sus resúmenes e índices.

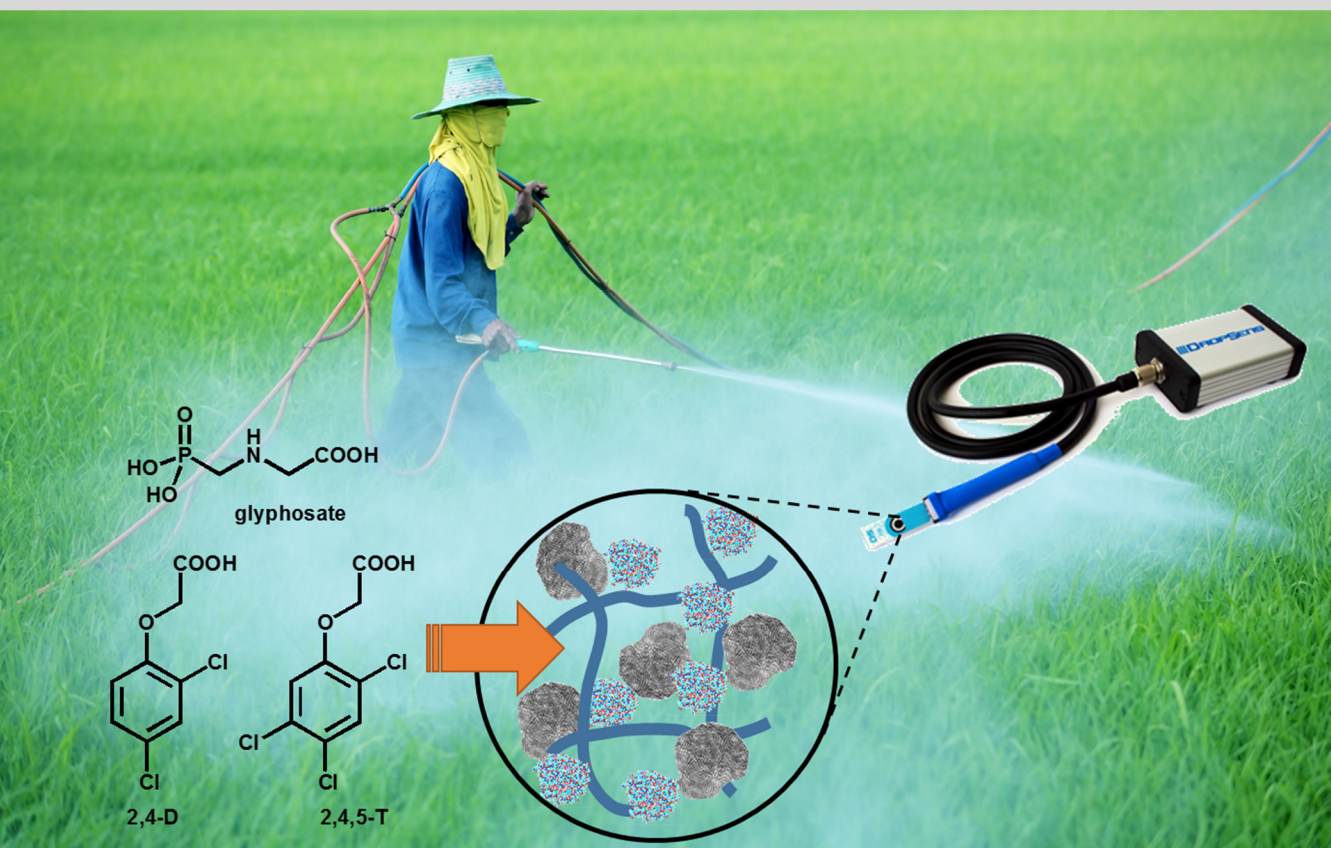
WARNING. Access to the contents of this doctoral thesis and its use must respect the rights of the author. It can be used for reference or private study, as well as research and learning activities or materials in the terms established by the 32nd article of the Spanish Consolidated Copyright Act (RDL 1/1996). Express and previous authorization of the author is required for any other uses. In any case, when using its content, full name of the author and title of the thesis must be clearly indicated. Reproduction or other forms of for profit use or public communication from outside TDX service is not allowed. Presentation of its content in a window or frame external to TDX (framing) is not authorized either. These rights affect both the content of the thesis and its abstracts and indexes.



UNIVERSITAT
ROVIRA I VIRGILI

Amperometric enzyme-based detection of agricultural pesticides on novel carbon nano-onion composites

VIBOL SOK



DOCTORAL THESIS
2018

Vibol Sok

**AMPEROMETRIC ENZYME-BASED DETECTION OF
AGRICULTURAL PESTICIDES ON NOVEL CARBON
NANO-ONION COMPOSITES**

DOCTORAL THESIS

Supervised by Dr. Alex Frago

Departament d'Enginyeria Química



UNIVERSITAT ROVIRA I VIRGILI

Tarragona

2018

UNIVERSITAT ROVIRA I VIRGILI

AMPEROMETRIC ENZYME-BASED DETECTION OF AGRICULTURAL PESTICIDES ON NOVEL CARBON NANO-ONION COMPOSITES

Víbor Sòk



Departament d'Enginyeria Química

Universitat Rovira i Virgili

Campus Sescelades,

Avda. Països Catalans, 26

43007 Tarragona

Tel: 977 55 85 79

Fax: 977 55 96 67

Dr. Alex Fragoso

CERTIFIES:

That the present study, entitled “Amperometric enzyme-based detection of agricultural pesticides on novel carbon nano-onion composites” presented by Vibol Sok for the award of the degree of Doctor, has been carried out under my supervision at the Department of Chemical Engineering of Universitat Rovira i Virgili,

Tarragona, September 4th 2018.



Dr. Alex Fragoso

ACKNOWLEDGEMENTS

First of all, I am thankful and indebted to Dr. Alex Fragoso, my supervisor, for sharing expertise, continuous advice, valuable guidance and encouragement extended to me during the entire studies beginning in the Master until the end of my Doctoral studies.

I am expressing my sincere gratitude to all Interfibio group members, especially to Dr. Mayreli Ortiz, Julio César Zuaznabar and Carmen Bermudo for sharing ideas and helping me with some experimental work.

I am also grateful to my professors in Cuba where I studied Agricultural Engineering and from whom I learned some of the basic knowledge I applied in this work. To my family for supporting and encouraging me to reach this graduation.

I also thank Generalitat de Catalunya for a pre-doctoral scholarship (FI) through AGAUR and Interfibio for the additional scholarship that allowed me to complete this thesis.

And above all, may you all get the power of nature for the gift of wisdom.

Vibol

ABBREVIATIONS

2,4-D: 2,4 dichlorophenoxyacetic acid

2,4,5-T: 2,4,5- trichlorophenoxyacetic acid

ABTS: 2,2'-Azino-bis(3-ethylbenzthiazoline-6-sulfonic acid)

ALP: alkaline phosphatase

Chi: chitosan

CNO: carbon nano-onion

CNO-ox: oxidized Carbon nano-onion

EDC: 1-ethyl-3-(3-dimethyl-aminopropyl) carbodiimide

HRP: horseradish peroxidase

HRTEM: high-resolution transmission microscopy

GOX: glucose oxidase

L-DOPA: L-3,4-dihydroxyphenylalanine

PBS: phosphate buffered saline

pNPP: p-nitrophenyl phosphate

SPE- screen printed electrode

TEM: transmission electron microscopy

TGA: thermogravimetric analysis

TMB: 3,3',5,5'-tetramethylbenzidine

TYR: tyrosinase

Table of contents

SUMMARY	1
CHAPTER 1. INTRODUCTION	3
CHAPTER 2. ENZYME KINETICS STUDY ON THE INHIBITION OF FREE AND IMMOBILIZED HORSERADISH PEROXIDASE BY 2,4,5-T, 2,4-D AND GLYPHOSATE	51
CHAPTER 3. KINETIC, SPECTROSCOPIC AND COMPUTATIONAL DOCKING STUDY OF THE INHIBITORY EFFECT OF THE PESTICIDES 2,4,5-T, 2,4-D AND GLYPHOSATE ON THE DIPHENOLASE ACTIVITY OF MUSHROOM TYROSINASE	68
CHAPTER 4. PREPARATION AND CHARACTERIZATION OF ALKALINE PHOSPHATASE, HORSERADISH PEROXIDASE AND GLUCOSE OXIDASE CONJUGATES WITH CARBOXYLATED CARBON NANO-ONIONS	88
CHAPTER 5. AMPEROMETRIC ENZYMATIC BIOSENSORS BASED ON CNO - MODIFIED SURFACES FOR PESTICIDE DETECTION	109
CONCLUSIONS AND FUTURE WORK	143

Summary

The overall objective of this thesis is to study the mechanism of interaction of different pesticides with peroxidase and tyrosinase enzymes, with the aim to develop biosensors for pesticide detection based on CNO-modified electrodes.

Chapter 1 is a general introduction and literature review, which covers the general information on global challenges associated to pesticide use, methods for pesticide detection, enzymatic biosensors for pesticide detection and CNO properties and applications. This chapter also describes the objectives of the thesis.

Chapter 2 investigates the inhibitory effects of 2,4,5-T, 2,4-D and glyphosate on the activity of free and immobilized peroxidase. The pesticides inhibit the catalytic activity of the free and immobilized enzymes by a competitive mechanism, following the order 2,4,5-T > 2,4-D > glyphosate according to Lineweaver-Burk kinetic analysis. Inhibitory effects of the pesticides on the free and immobilized enzymes are nearly the same according inhibition constants (K_i).

In **Chapter 3**, the inhibitory effects of 2,4,5-T, 2,4-D and glyphosate on the diphenolase activity of mushroom tyrosinase are studied. 2,4,5-T and 2,4-D were found to be competitive inhibitors, while glyphosate is a mixed inhibitor according to Lineweaver-Burk kinetic analysis. The inhibitory activity follows the order glyphosate > 2,4,5-T > 2,4-D. Interactions of the pesticides with the enzyme were demonstrated by fluorescence quenching and computational docking analysis.

In **Chapter 4**, carbon nano-onions were used as supports to immobilize ALP, HRP and GOX by amidation reactions. The CNO-enzyme conjugates were characterized TEM and Raman spectroscopy. Thermogravimetric analysis

revealed high enzyme loads. The conjugates retained the same optimum pH and temperature as compared with the native enzymes, with a slight improvement of their activities and are stable for longer periods of time after storage at 37°C.

Finally, in **Chapter 5** we have explored the possibility to use CNO-modified electrodes for the construction of amperometric enzyme biosensors based on cross-linked and covalent immobilization of enzymes with CNO and chitosan. This combination allowed the development of highly sensitive biosensors for glyphosate and 2,4,5-T based on the inhibition of tyrosinase and HRP activities, respectively. Our results demonstrate the feasibility of using chitosan/CNO/enzyme composites for the development of sensitive biosensors based on activity inhibition.

This thesis is thus a contribution to a rapidly growing field related with the development of new classes of nanomaterial-based detection systems applied, in our case, to solve a challenging environmental problem of present times.

Chapter 1

Introduction

1.1 Global challenges associated to pesticide use

Today the World's population continues to grow albeit more slowly than in the recent past. Ten years ago, the global population was growing by 1.24% per year. Nowadays the growth rate is 1.10% per year, yielding an additional 83 million people annually. The World's population is projected to increase by slightly more than one billion people over the next 13 years, reaching 8.6 billion in 2030, and to increase further to 9.8 billion in 2050 and 11.2 billion by 2100. More than one half of the anticipated growth in global population between now and 2050 is expected to occur in Africa. Of the additional 2.2 billion people to be born between 2017 and 2050, 1.3 billion will be natural of African countries. Asia is expected to be the second largest contributor to this future growth, adding just over 750 million people between 2017 and 2050. Africa and Asia will be followed by Latin America and the Caribbean, North America and Oceania, where growth is projected to be much more modest. In the medium-variant projection, Europe is the only region with a smaller population in 2050 than in 2017 and beyond 2050, Africa will be the main contributor to global population growth.

Although the World's population is expected to continue growing until the end of the 21st century, the rate at which this growth will occur is expected to continue to fall. In recent years, the population of Africa has had the fastest growth among all regions, increasing at a rate of 2.6 per cent annually in 2010-2015, however, this rate is beginning to fall and is projected to reach 1.8% in 2045-2050 and 0.66% in 2095-2100 (1).

More disturbingly, the Food and Agriculture Organization of the United Nations (FAO) estimates for 2016 indicated that the global prevalence of undernourishment in 2016 may have actually risen to 11%, implying a return to the level reached in 2012 and suggesting a possible reversal of the downward trend sustained over recent decades. Sub-Saharan Africa also remains the region with the highest Prevalence of Undernourishment (PoU), affecting an alarming 22.7% of the population in 2016. The situation is especially urgent in Eastern Africa, where PoU increased from 31.1% in 2015 to 33.9% in 2016. The Caribbean and Asia continue to show a high PoU of 17.7% and 11.7%, respectively, while PoU levels remain relatively low in Latin America (2).

The absolute number of people in the world affected by chronic food deprivation began to rise in 2014 going from 775 million to 777 million people in 2015 and is now estimated to have increased further, to 815 million in 2016. Although progress continues in the fight against hunger, yet an unacceptably large number of people still lack the food they need for an active and healthy life. Globally, 108 million people in 2016 were reported to be facing crisis level food insecurity or worse. This represents 35% increase compared to 2015 when the figure was almost 80 million. Natural disasters and extreme weather events were also a primary driver of food insecurity in 2016, particularly for countries with inadequate capacities to respond to shocks and with populations characterized by low resilience (3).

A possibility to counteract the current undernourishment of many populations and feed global population growth is to increase the agricultural production per capita which could be obtained by several means such as increasing the area of agricultural land, enhancing the yielding of crops through the use of agrochemicals, organic fertilizers, biological controls, and an improved soil and water management.

To increase the area of agriculture land does not look like an easy task due to the decrease of agricultural land (hectares per inhabitant) in all regions of the globe which is partly due to population growth. There is also a net loss of agricultural land due to erosion, reduction of fertility, salinization and desertification of soils. However, the land should be found only at the cost of sacrificing the forest areas, most of them classified as ecological reserves and natural parks (4). Accordingly, an immediate response to the need for increasing production of food seem to be a more intensive use of agrochemicals. The chemical fertilizers are one of agrochemicals which have been used increasingly in recent years to fertilize the soil and control agricultural productivity and quality, specially to increase the yield of agricultural production. With excessive use, fertilizers contaminate the environment, especially water resources (5).

Pesticides are another group of agrochemicals covering a wide range of compounds others produced globally (Figure 1.1). They have been an integral part of the process by reducing losses due to weeds, diseases, insects and other natural factors that can damage the amount of harvestable production and agricultural product qualities. However, only a very small percentage of the administered pesticides reach their actual targets with the rest being dispersed into the environment, making them harmful for the ecosystems including human beings (Figure 1.2).

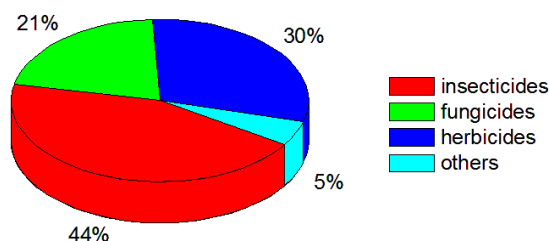


Figure 1.1. Types of pesticides and percentage of production in 2016.

Pesticides can produce a direct impact on humans when the people are exposed to them (Figure 2). Low-dose exposure is increasingly linked to human health effects such as immune suppression, hormone disruption, diminished intelligence, reproductive abnormalities and cancer. Food stuffs can be contaminated by pesticides, then transferred to people and animals. The contamination by pesticides of surface water (rivers, lakes, etc.) is mainly through runoff from treated fields, while ground water contamination comes from leaching of the pesticide through the soil. In India, for example, a study showed that 58% of drinking water samples drawn from various hand pumps and wells were contaminated by pesticides. On the other hand, pesticides not only contaminate soil but also cause a decline in populations of beneficial microorganisms producing negative effects on soil fertility by disrupting mineralization of the nutrients. Lastly, pesticides can directly hit non-target vegetation and wild fauna including the intoxication of birds, fish, freshwater animals, beneficial insects and other animals who use the treated fields as their dairy habitat (6).

A logical consequence of the increase of pesticide use for agricultural production is an increase in environmental contamination so the hazard of pesticide utilization makes essential to have accurate and reliable methods of monitoring their levels for safety purposes.

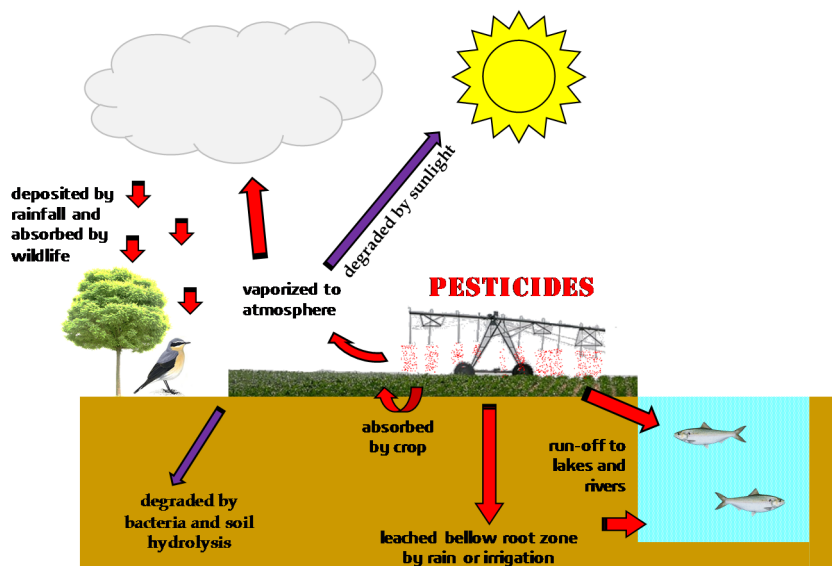


Figure 1.2. The pesticide cycle: main absorption and degradation pathways.

1.2 Pesticide definition and classification

According to FAO, pesticides are defined as *substances intended for preventing, destroying, attracting, repelling or controlling any pest, included unwanted species of plants or animals, during the production, storage, transport, distribution and processing of food, agricultural commodities or animal feeds, for use as a plant growth regulator, defoliant, desiccant, fruit thinning agent or sprouting inhibitor and substances applied as the components of a formulation responsible*. The active molecules, defined as the components of a formulation responsible for the direct or indirect biological activity against pests and diseases, or in regulating metabolism, growth etc. (7)

The pesticides can be classified in different ways (8). The main classification is as follows:

- **by chemical nature:** auxins, carbamates, organochlorine and organophosphorous compounds, phosphoramides, and many others.
- **by target species:** insecticides, acaricides, herbicides, fungicides, miticides, molluscicides, nematocides and others.
- **by hazard:** divided into 4 groups including Ia (extremely hazardous), Ib (highly hazardous), II (moderately hazardous) and III (slightly hazardous) and U (unlikely to present acute hazard) (9).

Another important classification is **by mode of action (MoA)**, that is, how the pesticides affect a specific target site within an organism. For example: The Insecticide Resistance Action Committee (IRAC) classified the insecticides into the 4 main groups and each group has its subgroups such as nerve and muscle target group (i.e. acetylcholinesterase inhibitors), growth and development target group (i.e. hormone receptor agonists), non-specific (multi-site) inhibitors and unknown or uncertain MoA group (10). Herbicides are also divided by their mode of action into many groups such as acetyl coenzyme A carboxylase (ACCase) inhibitors, root growth inhibitors, plant growth regulators, etc. Finally, according to (11), the classification of fungicides by MoA was never attempted before so he classified the fungicides based on their effects on the organisms such as effects on the synthesis of lipids, sterol, and other membrane components, effects on amino acids and protein synthesis, effects on signal transduction, etc.

These classifications are mainly useful for biochemists studying the biochemical consequences of pesticide action upon their targets and environment.

1.2 Methods for pesticide detection

According to (12), the main methods for pesticide detection include:

- chromatographic techniques such as thin layer chromatography, liquid chromatography and gas chromatography

- flow injection analysis
- capillary electrophoresis
- enzyme linked immunosorbent assay and other bioassays for pesticide detection
- spectrophotometry
- electroanalytical techniques like potentiometry, conductometry and voltammetry
- biosensors

Chromatographic techniques were the first implemented and validated of all of the above mentioned techniques. Flow injection analysis and capillary electrophoresis are also useful alternatives for use by regulatory authorities. These techniques are sensitive and reliable, however, they have limitations like complex procedures, time consuming sample treatment, need of highly trained technicians, inability to perform on site detection, requirement of expensive equipment etc. Thus, researchers have been investigating alternative methods of detection and screening that are cheaper, easier and more user friendly.

1.3 Biosensors for pesticide detection

Biosensors have emerged as field deployable analytical methods being able to provide simple, rapid, sensitive, selective, low cost and reliable detection of pesticide at low concentrations (7) and (13).

A biosensor can be defined as a *self-contained integrated device, which is capable of providing specific quantitative or semi-quantitative analytical information using biological recognition element (biochemical receptor) which is retained in direct spatial contact with a physico-chemical transduction element*. The biochemical receptor is responsible for recognizing the analyte by biological reaction which detected by the transducer, converted into a signal and

transferred to the detection system. The result is an electronic response which is proportional to a single analyte or a group of analytes (Figure 1.3). Depending on the specificity on the analytes, the biological recognition element can be an enzyme, a nucleic acid, a tissue, a cell, antibody or microorganism (14).

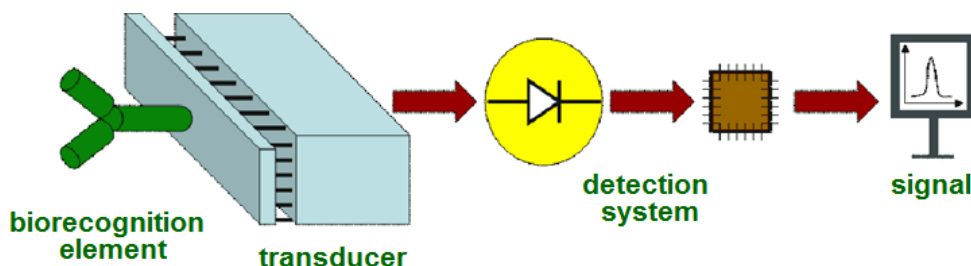


Figure 1.3. Main components of a biosensor.

Biosensors may be divided in two groups based on the interaction and reaction of their biological recognition elements with analytes. *Bio-affinity* sensors use antibodies or DNA as bioreceptors, while *bio-catalytic* sensors use enzymes. In both cases the specific recognition of an analyte by the biorecognition receptor is vital to develop a biosensor.

Hence, the specific biochemical targets of the pesticides can be used as the biorecognition receptor. Several biological recognition elements such as enzymes, antibodies, nucleic acids, etc. have been used in developing biosensors to detect pesticides in different mediums (15-17).

1.3.1 Main types of biosensor transducer technologies

The transducer is responsible for converting the information of the biological interaction between the analyte and the biological receptor into a signal (Figure 1.4). Therefore, transducer selection is very important in order to have a sensitive, robust, and cost-effective system (18-19).

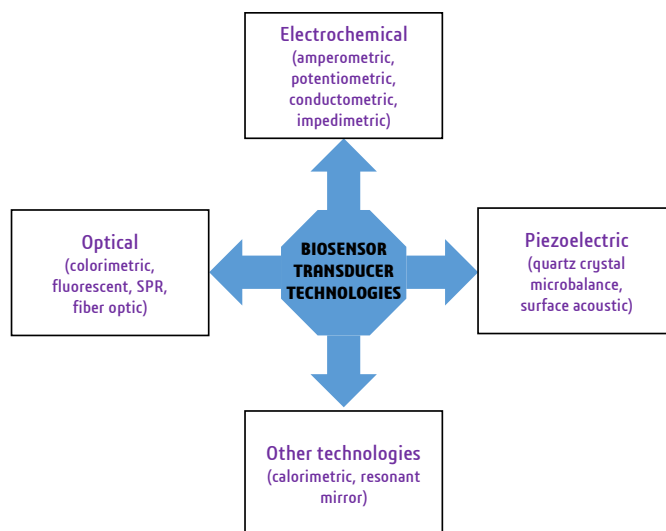


Figure 1.4. Main transducer technologies in biosensing.

1.3.1.1 Electrochemical transducers

Electrochemical biosensors are based on changes in the electrical properties of the transducer. The biological reaction would either generate a measurable current (amperometry), a potential change or charge accumulation (potentiometry) or alter the conductivity of a medium between electrodes (conductimetry). Other electrochemical detection techniques are also usable, such as impedimetric, which measures impedance (resistance) variations and field-effect transistor, which uses transistor technology to measure current as a result of a potential change at the gate of a semiconductor electrode (20). These type of biosensors are typically highly sensitive, cheap and easy to fabricate and miniaturize, which makes them very attractive for many applications, including pesticide detection (21-29).

1.3.1.2 Optical transducers

In optical biosensors, an optical signal is generated either as a result of the formation of biorecognition component-analyte complex (as in surface plasmon

resonance biosensors) or, most commonly, due to a reaction that produces a color or fluorescent signal from a chromophore or fluorophore present in the medium. The biological recognition element is immobilized onto the surface of the transducer and optical signals are collected by a photodetector and converted into electrical signals by the electronic device (30-31).

These biosensors usually involve a relatively complex instrumentation but have the advantage of possessing a high sensitivity. Apart from classical biomedical applications, there have been many recent advances in applications related to pesticide detection such as food quality and safety assurance (32-33).

1.3.1.3 Piezoelectric transducers

Piezoelectric transducers, also called mass-sensitive transducers, are capable of transforming the mass change at a specially modified surface into the change of a property of the support material. Quartz crystals are utilized as materials that resonate under the application of an external alternating electrical field. The mass changes caused by the formation of analyte-bioreceptor complex can be measured by means of piezoelectric transducers such as quartz crystal microbalances (QCM) and micro-cantilevers (34). Although less sensitive than electrochemical and optical biosensors, piezoelectric transducers have the advantage of direct detection in real time output and can be designed without the need of expensive or hazardous labels. Organophosphate and carbamate pesticides have been detected using this technique (35).

1.3.2 Biomolecule immobilization strategies

Immobilization of biological recognition element onto the transducer is a key step for achieving a biosensor with high sensitivity and stability. The activity and specificity of the biological recognition elements can be retained depending on the appropriate immobilization method after their binding to a transducer (Figure

1.5). Physical adsorption, covalent attachment and bio-affinity methods are the most useful for the development of biosensors based on either enzymes, antibodies, DNA or aptamers (36-38).

Physical methods such as adsorption or entrapment in a tridimensional matrix involve weak interactions such as electrostatic forces, hydrogen bonding and hydrophobic interaction between the biomolecule and the support. They are simple and easy to accomplish, and reversible but sometimes could lack stability. It is suited for enzymatic biosensor development due to the robustness of these biocatalysts.

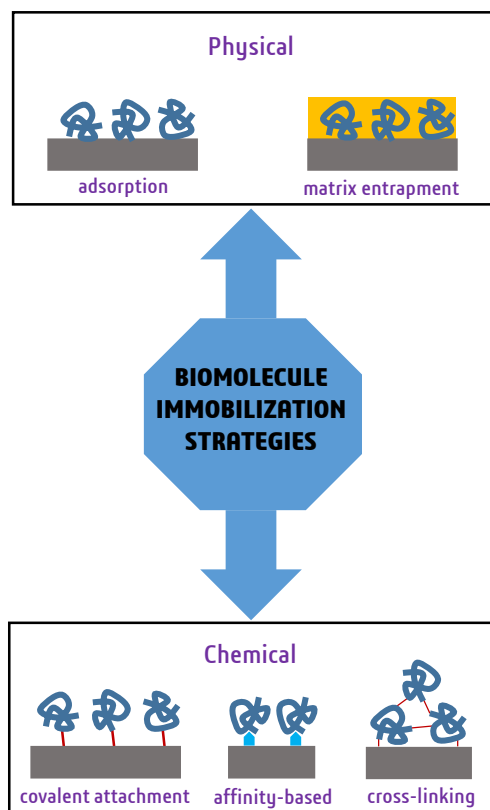


Figure 1.5. Some biomolecule immobilization strategies in biosensing.

Covalent immobilization refers to the binding of the biological recognition element on the transducer surface by initial activation of the surface using multifunctional reagents. Cross-linking is usually utilized to immobilize enzymes in which the biomolecules are randomly cross-linked with each other or in the presence of a functionally inert protein such as albumin. Affinity immobilization utilizes additional molecules to orient the biological recognition elements on the transducers to promote site-directed biological recognition elements. The biotin/(strept)avidin and protein A systems are the best known examples.

The versatility of these methods is evidenced in the development of acetylcholinesterase-based biosensors utilizing physical adsorption (39), cross-linking (40), covalent immobilization (41), entrapment (42), and affinity (43), as immobilization methods for pesticide detection.

These methods have also been widely used in pesticide immunosensing. For example, (44) developed an amperometric competitive immunosensor for 2,4-D detection in which the analyte was covalently immobilized on a silanized surface, while (45) relied on a high density aminodextran matrix to immobilize antibodies against the same analyte at the transducer surface with fluorescent detection. Affinity immobilization based on using protein A for antibody for atrazine detection has also been reported (46).

1.4 Enzymes as biorecognition element for pesticide detection

1.4.1 Overview of enzyme kinetics

Enzyme are biological catalysts which increase the rate of a reaction without itself being consumed by the process. The reactant and product concentrations are usually higher than the enzyme concentration in typical enzyme-catalyzed reactions. Consequently, each enzyme molecule catalyzes the conversion to product of many reactant molecules which are commonly known as substrates.

Enzyme mechanisms can be explained considering the dependence of the initial rate of enzyme-catalyzed reactions on substrate concentration (Michaelis-Menten kinetics). This analysis gives a series of kinetic parameters such as the initial rate (V_0), substrate concentration at half maximum rate (K_M), maximum rate (V_{max}), and catalytic constant of the enzyme k_{cat} (Equation 1, Figure 1.6).

$$V_0 = \frac{V_{max}[S]}{K_M + [S]} = \frac{k_{cat}[E][S]}{K_M + [S]} \quad \text{Equation (1)}$$

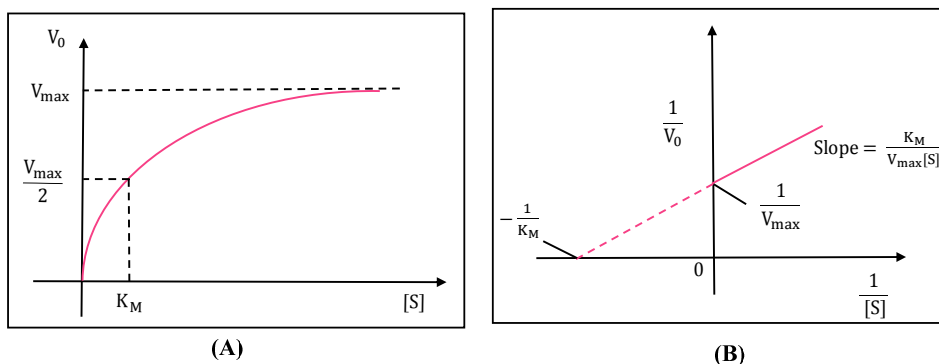


Figure 1.6. (A) Typical Michaelis-Menten plot (graphical analysis of reaction rate V_0 versus substrate concentration $[S]$). (B) Lineweaver-Burk plot of $1/V_0$ versus $1/[S]$

In practice the plot of V_0 versus $[S]$ is not very useful in determining the value of V_{max} because locating the asymptotic value V_{max} at very high substrate concentration is often difficult (Figure 1.6a). A more satisfactory approach, suggested by the American biochemists Lineweaver and Burk, employ the double-reciprocal plot of $1/V_0$ versus $1/[S]$ (Figure 1.6b). Equation 1 can thus be written as:

$$\frac{1}{V_0} = \frac{K_M}{V_{max}[S]} + \frac{1}{V_{max}} \quad \text{Equation (2)}$$

In this case, the substrate concentration is much larger than enzyme concentration which makes enzymes saturated. The period in which the enzymes remain saturated is called steady state ($V_0 = V_{\max}$).

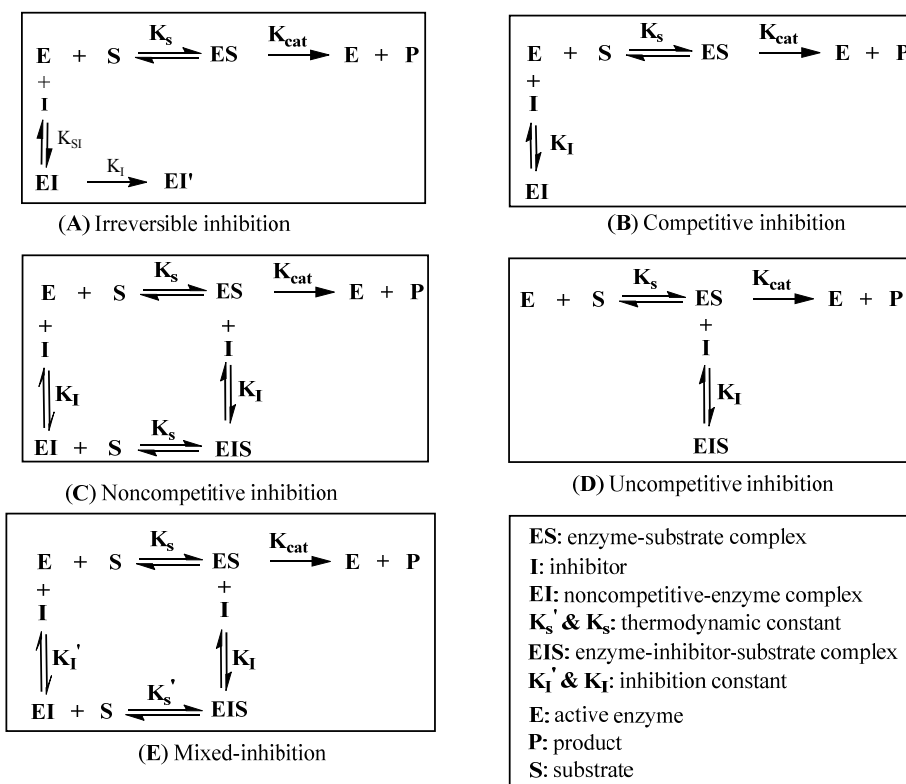
1.4.2 Kinetics of enzyme inhibition

Several substances might cause reduction of catalytic rate of enzyme-catalyzed reaction such as cyanide, heavy metals, polychlorinated bisphenols and other well-known inhibitors. The inhibitors can cause the enzymes inactivated reversibly and irreversibly. Pesticides are very important enzyme inhibitors, both in vitro and in vivo, and, as we will present later, they are the subject of intensive research.

Irreversible inhibitors cause an inactivating, covalent modification of enzyme structure. The irreversible inhibitors start forming a reversible non-covalent complex with the enzyme (EI) and then continue reacting to produce the covalently modified “dead-end complex” (EI') (Scheme 1A).

In *reversible inhibitors*, the enzyme activity is regenerated when the inhibitor concentration drops. The EI complex is created only by the similarity of enzyme and inhibitor shapes without chemical modification and the inhibitor maintains a reversible equilibrium with the enzyme. Reversible inhibitors might be divided into *competitive*, *non-competitive*, *uncompetitive* and *mixed* inhibitors. In **competitive inhibition** both the substrate and inhibitor compete for the same active site (Scheme 1B). The EI complex does not react with S to form a product. Increasing substrate concentration can displace all competitive inhibitors bound to active sites and consequently, V_{\max} is unchanged. **Non-competitive inhibition** takes place when the inhibitor binds to the enzyme at a site distinct from the active site so it can bind to both the free enzyme and the ES complex. This has no effect on the substrate binding, and vice versa (Scheme 1C). Neither EI nor EIS

complexes form a product thus inhibition might not be reversed by increasing the substrate concentration. In **uncompetitive inhibition** the inhibitor does not bind to the free enzyme but to the ES complex to form an inactive EIS complex (Scheme 1D). The EIS complex does not form a product. The inhibitor does not interfere with the formation of ES and uncompetitive inhibition cannot be reversed by increasing the substrate concentration. Finally, **mixed-type inhibition** is similar to non-competitive inhibition but the EI and EIS affinities are different.



Scheme 1. Types of enzymatic inhibition mechanisms.

In practice, the type of reversible inhibition can be easily identified by constructing Lineweaver-Burk plots at different inhibitor concentrations. Thus, competitive inhibition has graphics with a common intercept in the y-axis (Figure 1.7A), non-competitive inhibition has graphics with a common intercept in the x-

axis (Figure 1.7B), uncompetitive inhibition gives a series of parallel lines (Figure 1.7C) and mixed inhibition is, as the name indicates, an intermediate case between competitive and non-competitive mechanisms (Figure 1.7D).

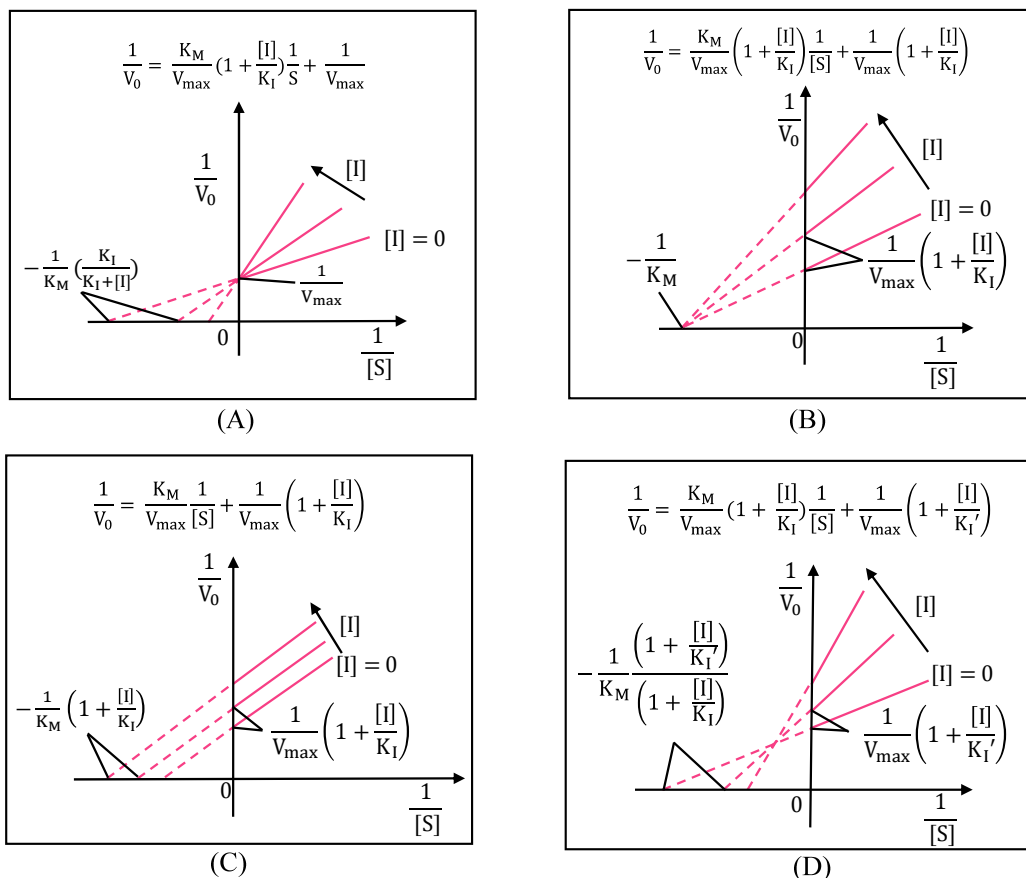


Figure 1.7. Lineweaver-Burk plots of (A) competitive inhibition, (B) non-competitive inhibition, (C) uncompetitive inhibition and (D) mixed inhibition

1.4.3 Pesticide biosensors based on enzyme activity inhibition

As mentioned above in the mode of action of pesticides, most of the pesticides have inhibition effects on enzymatic targets. In biosensors based on enzyme inhibition, the measurement of the target analyte is carried out by measuring the enzyme activity before and after exposure of the biosensor at the target analyte.

The percentage of inhibition is correlated to the concentration of target analyte, so it is possible to evaluate the unknown concentration analyte (18). The percentage of inhibition can be calculated by the following equation:

$$I\% = \frac{(A_0 - A_i) * 100}{A_0}$$

I% percentage of inhibition
 A₀ Enzyme activities before exposure at the analyte
 A_i Enzyme activities after exposure at the analyte

These biosensors can operate in two main ways (Figure 1.8). In the first case, the inhibitor is added to the same solution of substrate after measuring the initial activity for a period of time. This protocol is useful when the interaction is very fast. In the second protocol, the sensor is removed after measuring A₀, incubated with the pesticide and rinsed, and then A_i is measured.

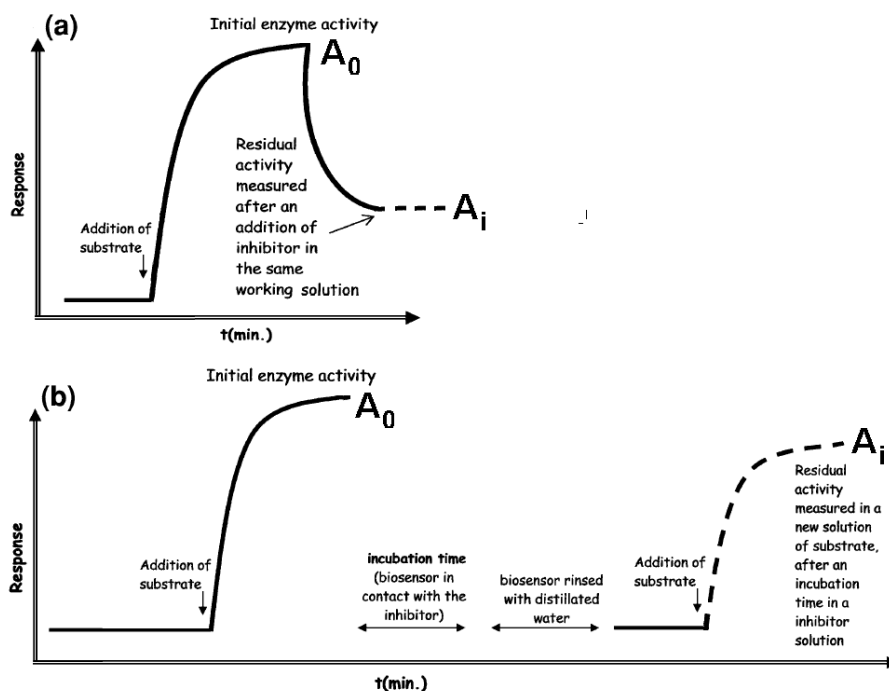
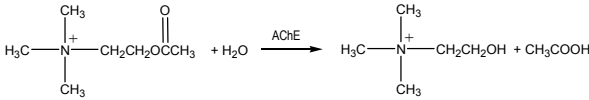
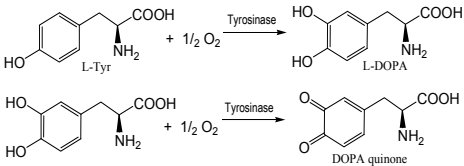
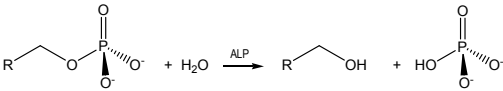


Figure 1.8. One-step (a) and two-step (b) protocols for biosensors based on enzyme inhibition.

There are several examples in the literature of biosensors based on enzyme inhibition. Table 1 collects the main enzymes used, their reaction mechanism and the most used methods for activity measurement (colorimetric and electrochemical).

Table 1. Example of enzymes used in pesticide detection.

Enzyme	Enzymatic reaction	Main methods for activity measurement
Acetylcholinesterase	 $\text{H}_3\text{C}-\text{N}^+(\text{CH}_3)_3-\text{CH}_2\text{CH}_2\text{OC}(=\text{O})\text{CH}_3 + \text{H}_2\text{O} \xrightarrow{\text{AChE}} \text{H}_3\text{C}-\text{N}^+(\text{CH}_3)_3-\text{CH}_2\text{CH}_2\text{OH} + \text{CH}_3\text{COOH}$	C: Ellman's reagent with thiocholine as substrate EC: potentiometric (pH sensor)
Tyrosinase	 $\text{L-Tyr} + \frac{1}{2} \text{O}_2 \xrightarrow{\text{Tyrosinase}} \text{L-DOPA}$ $\text{L-DOPA} + \frac{1}{2} \text{O}_2 \xrightarrow{\text{Tyrosinase}} \text{DOPA quinone}$	C: Detection of DOPA quinone at 475 nm EC: Amperometric detection of DOPA quinone.
Peroxidase	$\text{S}_{\text{red}} + \text{H}_2\text{O}_2 \xrightarrow{\text{peroxidase}} \text{S}_{\text{ox}} + \text{H}_2\text{O}$	C: Detection of oxidised TMB at 650 nm EC: Amperometric detection of oxidised TMB.
Alkaline phosphatase	 $\text{R-O-PO}_3^{2-} + \text{H}_2\text{O} \xrightarrow{\text{ALP}} \text{R-OH} + \text{HO-PO}_3^{2-}$	C: Detection of p-nitrophenolate at 405 nm. EC: Amperometric detection of p-aminophenol.

C: colorimetric, EC: electrochemical.

Acetylcholinesterase (AChE, EC 3.1.1.7) is the most used enzyme for pesticide detection. Its main biological role is the termination of the impulse transmission at cholinergic synapses by rapid hydrolysis of the neurotransmitter acetylcholine. AChE is typically synthesized in nerve, muscle and certain hematopoietic cells. Targeting on this enzyme, organophosphorus and carbamate insecticides were synthesized to eradicate insects in agricultural fields because of their powerful irreversible inhibition on the AChE catalytic activity. As result of the AChE inhibition acetylcholine neurotransmitter accumulates in the body which interferes with the muscular responses and leads to respiratory problems and finally produces insect death. Consequently, AChE and other cholinesterases have been used as biological recognition elements to develop biosensors for carbamate and organophosphorus insecticides (47-54).

Peroxidase (EC 1.11.1.7) is a heme-containing enzyme that utilizes peroxides such as hydrogen peroxide to oxidize a wide variety of organic and inorganic compounds such as phenolic compounds and its activity has been identified in plants, microorganisms and animals. On the basis of MoA of pesticides, peroxidase has not been reported as a target of any pesticide. However, several biosensors for pesticide detection based on peroxidase inhibition have been reported to detect glyphosate and glufosinate (55), glyphosate (56-57) and Thiocarb (58).

Tyrosinase (EC 1.14.18.1), is a multifunctional copper containing enzyme belonging to the oxidase family, distributed in microorganisms, animals, plants and humans. The enzyme plays a crucial role in melanogenesis by catalyzing two important steps of the synthesis of melanin. Several tyrosinase inhibitors have been discovered and synthesized to control the overproduction of melanin, which causes skin disorders (59). Research on biosensor development for pesticide detection has also been based on tyrosinase inhibition to detect, for

example, chlorophenol, dithiocarbamate and atrazine (60), dichlorvos (61), methyl parathion, carbofuran, diazinon and carbaryl (62), dimethyl- and diethyldithiocarbamates (63), thiocarb (64), diuron and atrazine (65), triazine pesticides (66), phenolic compounds (67), carbamate pesticides (68).

Finally, alkaline phosphatases (EC 3.1.3.1) are plasma membrane-bound glycoproteins widely distributed in nature, including prokaryotes and higher eukaryotes with exception of some higher plants. Its function is to hydrolyze various monophosphate esters at high pH with release of inorganic phosphate with the following reaction (69). Inhibition of ALP activity by different compounds has been reported and thus the enzyme has been used as bioreceptor to detect the inhibitors in several cases. Mazzei et al reported about successful development of biosensor using ALP to detect malathion and 2,4-dichlorophenoxyacid (2,4-D) using phenyl phosphate and ascorbate-2-phosphate as substrates (70). Paraoxon and methyl parathion have also been detected using phenyl phosphate (71). Sánchez et al found that ALP is inhibited by tetradifon, metham-sodium and fenitrothion during the enzyme catalysis of 1-naphthyl phosphate. A bienzymatic biosensor for 2,4-D detection was developed using ALP as biosensing element coupled with glucose oxidase (72). ALP catalyzes glucose-6-phosphate releasing glucose and then this product is oxidized by glucose oxidase (73). This biosensor mechanism was also developed by Mazzei (74) using acid phosphatase instead of alkaline phosphatase to detect methyl parathion, paraoxon, malathion and aldicarb.

Other enzymes have been also used as biological recognition element such as lipase to detect methyl-parathion and tributyrin (75), urease to detect atrazine (76), aldehyde dehydrogenase to detect dithiocarbamate fungicides by coupling this enzyme with diaphorase (77), acetolactate synthase to detect sulfonylurea

herbicides (78), ascorbate oxidase to detect ethyl paraoxon (79) and glucose oxidase to detect atrazine (80).

1.5 Carbon nano-onions: a class of carbon nanomaterials

Carbon atoms, with their unique ability to form long chains, give rise to molecules capable of creating new materials or even life through Mother Nature. Diamond and graphite are produced by natural reactions (81) and together with amorphous carbon were considered for a long time as the only allotropes of carbon available. With the advent of nanotechnology, scientists turned their attention to the possibility to produce carbon-based nanostructures. The first of these nanomaterials, called nanodiamond, was produced in the laboratory by detonation and its properties and applications have been recently reviewed (82). The research for other carbon nanomaterials became of wider interest after the discovery of new carbon forms such as fullerenes, carbon nanotubes (CNT), graphene and carbon nano-onions (CNOs) (81) and (83). These materials possess carbon atoms linked through sp_2 hybrid bonds and are, in a way, structurally derived from graphite (Figure 1.9).

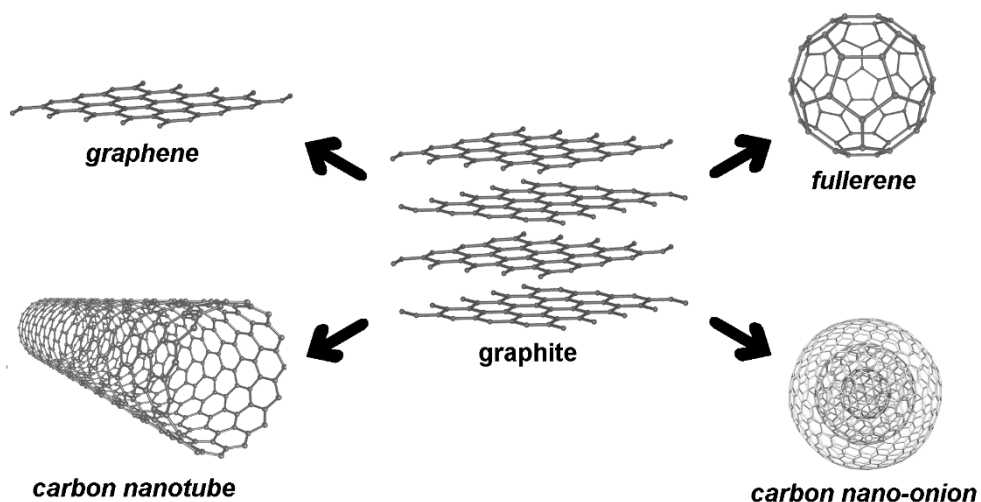


Figure 1.9. Carbon nanomaterials structurally derived from graphite.

Graphene is formed by a single graphitic layer and holds unique two-dimensional structure and properties including a zero-gap band structure, high electron mobility, and high electrical and thermal conductivity (84). Due to its high conductivity and surface area respect to volume ratio, graphene has been applied in high-speed electronic devices and sensor respectively (85). Fullerene have the form of spherical or semi-spherical carbon clusters, while CNTs are cylindrical structures that can be formed by one of more graphitic layers. Both materials also have interesting structural and properties and have been applied in many fields such as biological and environmental technology, electronics, optoelectrics and chemical sensors (86-89).

1.5.1 Synthesis and properties of carbon nano-onions

Carbon nano-onions were first discovered by Ugarte in 1992, by exposing an electron beam on amorphous carbon, which graphitized and curled up to form a spherical cluster (90). Four years later, Qin and his group followed this method to synthesize CNOs using a different substrate, i. e. diamond crystals (91-92). Afterwards, other methods for their synthesis have been reported. Arc-discharge was used by Sano and his group (93) to synthesize CNOs in water and obtaining high-quality spherical CNOs in large quantity. CNO synthesis was also achieved in different media such as distilled water and liquid nitrogen using this method (94). Heat treatment can also be used to synthesize CNO by converting nanodiamonds into graphitic CNOs (95-96).

Borghain et al. optimized arc-discharge method for CNO production by designing an in-house automated underwater apparatus to control the arc plasma which produce homogeneous CNOs, followed by efficient purification method. CNO growth and purification were investigated using thermogravimetric

analysis (TGA), high resolution transmission electron microscopy (HRTEM), Raman spectroscopy and X-ray diffraction (XRD). The electrochemical properties of the synthesized CNO were also tested by cyclic voltammetry based on the redox peak separations and heterogeneous electron transfer rate of the electroactive species. Faster and higher electrochemical performance were found in comparison with the bare electrode (97).

Chemical vapor deposition was also able to synthesize CNOs using precursor gases and a metallic substrate (Fe, Co, Ni and/or their combination) as catalyst. The produced materials contained catalyst metals encapsulated inside (98) and (99). Lately, this method was optimized with some modifications to synthesize hollow CNOs with controllable size (100). Carbon ion implantation was utilized to prepare large size CNOs with diameters close to the micrometer (101). The same author tried to optimize this method to reduce the CNO size (3-30 nm) by varying the synthesis conditions (102-104), demonstrating the versatility of the method.

Radio frequency and microwave plasma were reported as the technique for CNO synthesis. The CNOs synthesized by microwave plasma from C_2H_2 , carbon black and ferrocene displayed a clear polyhedral or spherical morphology with cores and waving layers (105). This technique was also used to synthesize hollow CNOs with high purity and 10-35 nm diameter from coal (106).

Thermolysis is also a heating technique which was developed for CNO synthesis without catalyst participation. The process was based on a thermolysis of a NaN_3 - C_6Cl_6 mixture and the obtained nanoparticles displayed a diameter from 30 to 100 nm (107). Thermal reduction of a mixture of glycerin and magnesium was also used to produce CNOs with a diameter of 60-90 nm (108). A large quantity of CNOs were easily produced by continuous explosion of naphthalene with a diameter of 50-56 nm (109).

Recently, our group successfully synthesized CNOs by annealing of commercially available nanodiamond and further functionalization with a radio frequency Ar/O₂ plasma was explored. Under heat treatment at 1200°C, nanodiamonds were transformed into a small spherical carbon nano-onions particles of 3-4 nm diameter and 5-6 graphitic shells. Synthesized CNOs were characterized using HRTEM, XRD, Raman spectroscopy (110).

1.5.2 Characterization carbon nano-onions

High-Resolution Transmission Electron Microscopy (HRTEM) has been employed to characterize the produced CNOs, which is able to visualize their structural properties and follow their formation (Figure 1.10a). Raman spectroscopy is a technique to distinguish the graphitic structure of CNOs (Figure 1.10b). The presence of the D-band at around 1350 cm⁻¹ indicates the structural disorder on the surface the particle due to the presence of sp³ carbons and the presence of the G-band at around 1580 cm⁻¹ indicates the presence of the graphitic layer of the surface or sp²-hybridized carbon networks (111-112). X-ray diffraction (XRD) is another technique to study the gradual transformation of diamond nanoparticles with sp₃ bonds into spherical CNOs (113)(110).

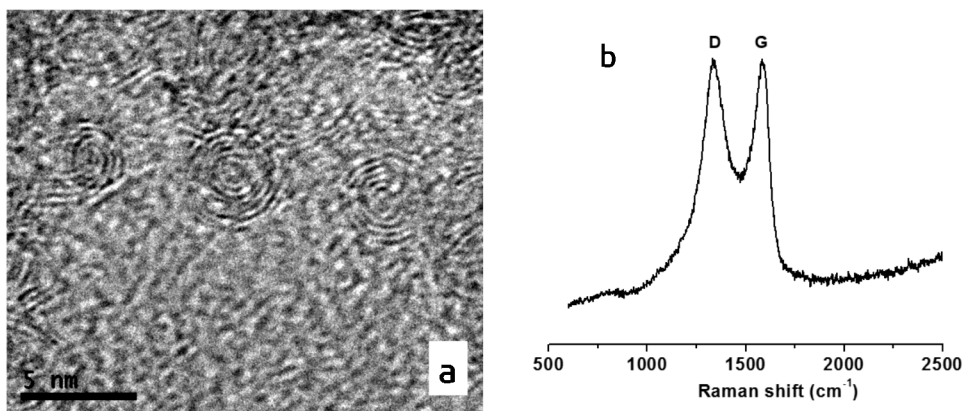


Figure 1.10. a) HRTEM image of CNOs obtained by nanodiamond annealing. b) Raman spectrum of the CNOs shown in a). (110).

The electrical properties of CNOs have been found to be between those of graphite and single-shell fullerenes using ultrahigh vacuum atomic force microscopy and scanning tunneling microscopy (114). The electronic structure of CNOs was investigated by core-level and valence-band photoemission spectroscopy by intercalation of CNOs with potassium (115). In addition, the optical properties have been analyzed by several techniques (116-119).

1.5.3 Functionalization of CNOs.

Due to the aggregation promoted by strong intermolecular interactions such as van-der Waals forces, CNOs are highly hydrophobic like any other carbon nanomaterial and insoluble in most solvents, which hinders many applications of these materials (120). To overcome this problem, surface functionalization is the method of choice to increase the solubility and improve other properties (Figure 1.11).

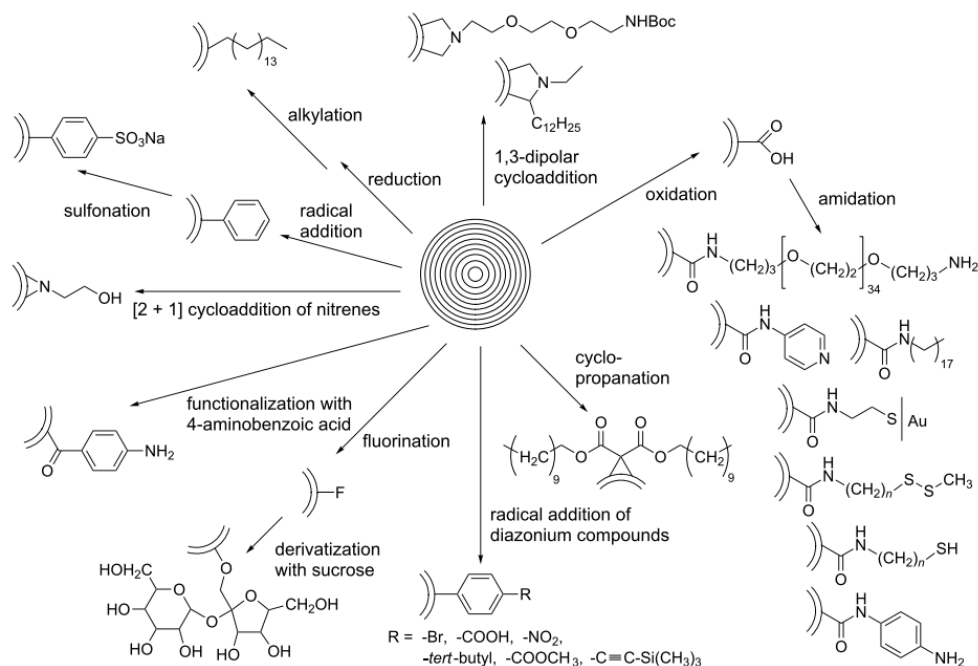


Figure 1.11. Covalent functionalization of CNOs (120)

A decade after their discovery, the first functionalization of CNOs was reported in which arc-discharge produced CNO was heated with an amino acid and paraformaldehyde in toluene. NMR spectroscopy, MALDI mass spectroscopy and UV-vis-NIR spectroscopy were used to analyze the successful functionalization of CNOs with N-alkyl groups. The functionalized CNOs was soluble in common organic solvents (121). Three years later, other CNO functionalization strategies were reported such as the 1,3-dipolar cycloaddition using a reaction mixture of purified CNOs, N-ethylglycine and dodecanal under heating. The other two types of functionalization started with oxidation of purified CNOs by heating under reflux in HNO₃ solution followed by reactions of the introduced carboxylate groups with diamine-terminated poly(ethyleneglycol) and octadecylamine, respectively (122). The reactivity of A-CNOs (15-20nm) and N-CNOs (5 nm) prepared from arc-discharge and annealing, respectively, was compared. [2+1] Bingel-Hirsch cyclopropanation, free-radical addition using benzoyl peroxide as radical source and oxidation in different acid solutions was successful only in smaller N-CNOs. A-CNOs could only be oxidized using the very strong oxidizing mixture of H₂SO₄/HNO₃ (50/50 v/v) while N-CNOs were destroyed. The authors concluded that the smaller CNOs are much more reactive for covalent functionalization, presumably due to the higher curvature of the surface (123).

[2+1] cycloaddition reactions on CNOs have been reported using different nitrene derivatives. CNOs were reacted with 2-azidoethanol, producing OH-functionalized CNOs (CNO-OH) while 2-bromo-2-methylpropanoate yielded Br-functionalized CNOs (CNO-Br). Both functionalized CNOs were characterized using TGA, XPS, TEM and Raman spectroscopy. Interestingly, CNO-OH emitted fluorescence while CNO-Br did not. The functionalized CNOs were further decorated with different polymer additions (124).

CNOs were covalently reacted with in situ generated diazonium compounds and thus introducing a variety of functional groups, such as bromides, benzoic acids, tert-butyl groups, nitro groups, methyl esters and trimethylsilyl (TMS) acetylene. In next step, the use of “click” chemistry was proposed in which the CNO-TMS acetylide composite was first deprotected and then coupled with zinc triphenyl azidophenyl porphyrin (125), fluoresceinamide-based fluorophores (126) or NIR-emitting aza-boron-dipyrromethenes (127-128)). Using an in situ chemical oxidative polymerization, polyaniline (PANI) was attached on the surface of benzoic acid/CNO (129). Fluorination on the surface of CNOs was carried out in a custom-built reactor at different temperatures. The fluorinate CNOs were characterized using FTIR, SEM/EDX, XRD, XPS, TGA, TEM, Raman and UV-Vis spectroscopy (130). Oxidation of CNOs using ozonolysis was investigated, the ozonized CNOs displayed high hydrophilicity, conductivity, and wettability (131). Finally, CNOs have also been functionalized via amidation reaction aminothiols to attach $-\text{CONH}-(\text{CH}_2)_n-\text{SH}$ and the electric conductivity properties of the product were investigated (132).

Alkylation is another important reaction tested on CNOs. Reduction of CNOs with a solution of Na-K alloy in 1,2-dimethoxyethane (DME) followed by alkylation with the addition of 1-bromohexadecane has been reported. The synthesized CNO-C₁₆ showed high solubility in organic solvents and was analyzed by ¹H-NMR. To support the successful functionalization, the product was characterized using FTIR, HRTEM and Raman spectroscopy (133).

Non-covalent functionalization is also a useful method to incorporate CNOs in composite materials to explore their inherent properties in the solid state and their possible applications. Kuzhir and his group studied the electromagnetic absorbing properties in microwave frequency range of a CNO composite made using binding matrices such as polymethylmetacrylate (PMMA) and

polydimethylsiloxane (PDMS) (134). Preparation of composites made of CNOs with poly (diallyldimethylammonium chloride) (PDMA) or chitosan (Chit) was reported and their mechanical and electrochemical properties were investigated (135). Other polymers used to fabricate CNO-based composites include poly(3,4-ethylenedioxythiophene):poly(styrene sulfonate) (136), conductive polymers such as polyaniline (137-139). These materials showed interesting capacitive properties and may be used in energy storage devices such as batteries and supercapacitors.

Our group recently made progress in this area by preparing highly solubilized cyclodextrin-modified CNOs by supramolecular interactions in aqueous solution. After oxidation of CNOs followed by amidation with aminated β -cyclodextrin a CNO/ β -CD derivative was prepared and self-assembled with a ferrocene-appended dextran (Fc-Dex) polymer by host-guest interactions. The resulting dispersion was stable for several weeks in water (140).

1.5.4 Applications of CNOs

The modification and incorporation of moieties on the surface of CNOs enable strategies for their application in different fields such as materials chemistry, environmental technology, energy storage devices and analytical applications (Figure 1.12).

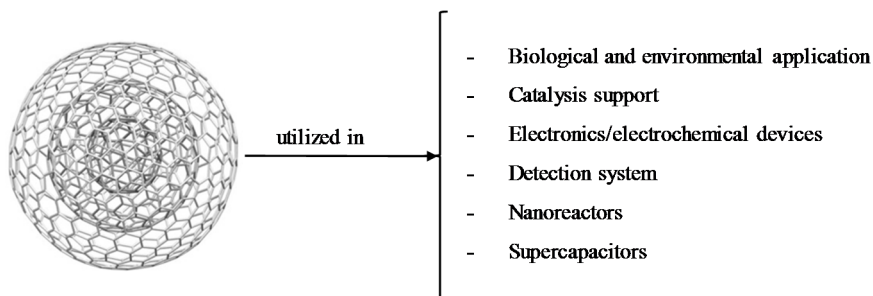


Figure 1.12. Main applications of CNOs.

1.5.4.1 Biological applications

To verify toxicity and biocompatibility of this carbon nanomaterial, several biological applications were reported. Carboxylated CNOs prepared by pyrolysis of wood were used for imaging the life cycle of *Drosophila melanogaster*. The combination of carboxylic groups with the defective nature of these polygonal CNOs displayed fluorescence property which were observed in the visible and NIR (141). Fluorescent CNOs were also employed to study *E. coli* and *C. elegans* (142). Boron difluoride azadipyrromethene fluorophores covalently attached to CNOs was utilized for cellular imaging and they found low cytotoxicity (143-144).

CNOs produced from arc-discharged showed less adverse effects on human skin fibroblast as compared with MWCNTs (145). Afterwards, CNOs synthesized by the same method were tested for potential toxic effects on cardiovascular system. On the basis of the experimental results, unmodified CNOs can induce DNA damage and apoptosis in human umbilical vein endothelial cells due to the generation of reactive oxygen species (146). Small CNOs, produced by annealing of nanodiamonds, were covalently modified with biomolecules. Biocompatibility tests of oxidized CNOs and biomolecule-CNO composites (PEGylated CNOs) on fibroblasts showed that no cytotoxic effect of these carbon nanomaterials (147).

1.5.4.2 Electronic/electrochemical applications

Due to their structure and high electric conductivity CNOs are good candidates for electronic applications. The first study on using CNOs as electrode materials in electrical double layer capacitors (EDLC) with an organic electrolyte indicate excellent capacitance retention and high discharge rate of the CNO-modified devices due to increase in conductivity. Therefore, small resistance and the modification steps that cause defects in the surface of CNOs improved the ion transport and capacitance (148). Bushueva and his group investigated the

electrochemical performance of CNO-modified capacitors with aqueous electrolyte. CNOs utilized to modify working electrodes were synthesized by vacuum annealing of nanodiamonds and polytetrafluoroethylene (PTFE). Charge-discharge measurements exhibited a dependence of the specific capacitance of CNOs on the degree of graphitization and defectness of particle surfaces (149). Afterward, micrometer-sized supercapacitors were developed by depositing CNOs on interdigital gold electrodes utilizing an electrophoretic deposition technique (EPD) which the CNO-based microsupercapacitors exhibited capacitance 4 times higher than that of electrocatalytic capacitors and the discharged rates 3 times higher than conventional supercapacitors (150).

The influencing factors on performance of supercapacitors like structure, physical and electrical properties of CNOs and nature of electrolytes were studied using molecular dynamics (MD) simulations of CNOs in organic electrolytes for better understanding of the interactions and migration of ions in the surface of CNOs. In general, CNOs capacitive performance is superior to other carbon nanomaterials at high charge/discharge rate (151).

A high surface porosity of CNOs is obtained by chemical activation using KOH, which increases the specific area for ion-accessible outer shells. The hydrophilicity of activated CNOs is also improved with a high charge/discharge rates as compared to non-activated CNOs (152). On other hand, composite of CNOs attached with RuO₂ are able to increase the capacitance of the electrodes as compared to the pure CNO materials (153). Furthermore, different composites were synthesized with CNOs as improved capacitance performance materials for application of rechargeable lithium batteries (154-157).

1.5.4.3 Detection systems

There are only a few reports on the use of CNOs in detection systems. The first report on the use of CNOs for the modification of sensor surfaces described the covalent attachment of oxidized CNOs (containing COOH groups) onto a self-assembled monolayer of cysteamine on gold by amidation, followed by biotin immobilization on the CNO surface to develop a complete layer of Au/thiol/ox-CNOs/biotin. This synthesized layer was utilized to monitor the interaction of immobilized biotin and avidin (158). Later a CNO/poly(diallyldimethylammonium chloride) (PDDA) composite was synthesized for dopamine detection. Electrochemical properties of the composite were examined and the results exhibited good selectivity and sensitivity for dopamine due to the combined effect of the CNOs and the cationic polymer (159).

Our research group recently utilized CNOs to modify electrodes for electrochemical detection of nitrite and ascorbic acid. Glassy carbon electrodes were first modified with small carbon nano-onions and functionalized either by electrografting ortho-aminophenol (oAP) groups or by physical adsorption of thionine to give electroactive surfaces which were able to electrochemically detect presence of nitrite and ascorbic acid with higher sensitivity and lower detection limit as compared to the non-CNO electrodes (160). We have also developed a DNA biosensor for detection of human papillomavirus oncogene based on surface modification with CNOs. The surface of glassy carbon electrodes was modified with small nano-onions and activated by electrografting of diazonium salts bearing terminal carboxylic acid and maleimide groups. DNA recognition sequences were immobilized by amidation or thiol-maleimide reactions and used in a sandwich-type assay to detect synthetic and PCR amplified HPV targets with enhanced sensibility (161).

In these examples, the presence of CNOs on the surface enhanced the sensitivity and lowered the limits of detection of amperometric assays with respect to the GC-only electrodes. This was explained considering the larger surface area achieved in the presence of CNO, which allows a much higher number of recognition units to be immobilized on the surface, and a faster electron transfer rate on the CNO-modified surface ascribed to the semi-metal properties and to the presence of structural defects on the CNOs that enhance electron transfer properties. Thus, the combination of the unique morphological and electronic properties provided by the CNOs opens the way for further applications of CNO-based surfaces in (bio)analytical devices.

1.6 Objectives of the thesis

As described in the preceding sections, there is currently a strong concern on the use of pesticides in agriculture and their possible side effects. This makes the development of sensitive and robust detection systems an important step in this direction. We have also seen that CNOs are very attractive and promising materials with defined structures and remarkable electrochemical properties that have been scarcely studied in biosensing.

The overall objective of this thesis is to study the interaction of different pesticides with peroxidase and tyrosinase with the aim to develop biosensors for pesticide detection based on CNO-modified electrodes (Figure 1.13).

To achieve this general objective, the following aspects have been focused on:

1. The inhibition of peroxidase and tyrosinase activities by three of the most used pesticides (2,4-D, 2,4,5-T and glyphosate) ⇒ **Chapters 2 and 3**
2. The use of oxidized CNOs as supports for the immobilization of enzymes and a study of the activity and stability of the immobilized enzymes ⇒ **Chapter 4**

3. The development of electrochemical biosensors for pesticide detection based on the prepared CNO-enzyme modified electrodes \Rightarrow **Chapter 5**.

This thesis is thus a contribution to a rapidly growing field related with the development of new classes of carbon nano-onion based nanomaterials that aims at expanding their current applications in the construction of novel detection systems with improved performances.

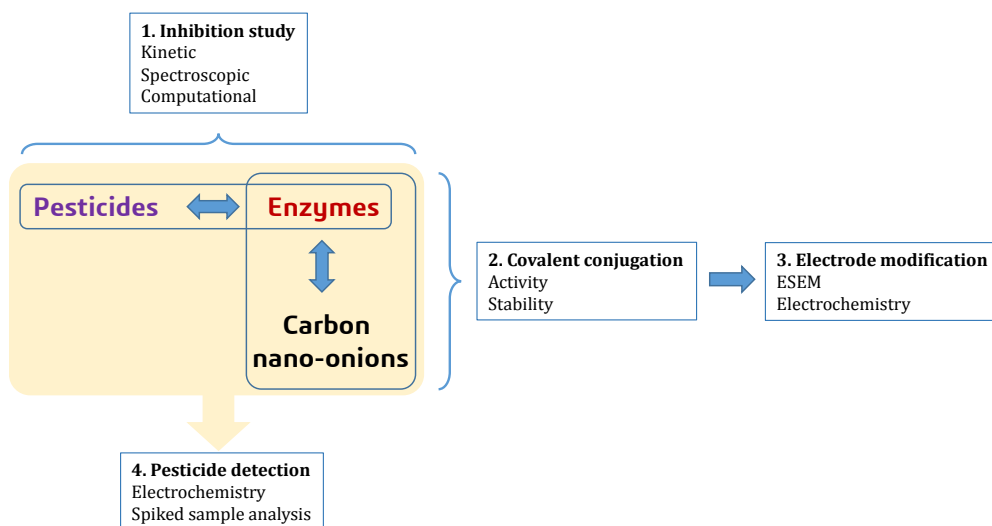


Figure 1.13. Conceptual map of the present thesis.

References

- 1-. UN. World Population Prospects, The 2017 revision. Department of economic and social affairs, population division. United Nations, 2017, New York.
- 2-. FAO, IFAD, UNICEF, WFP, WHO. The state of food security and nutrition in the world 2017. Building resilience for peace and food security. Food and Agriculture Organization of the United Nations, 2017, Rome.
- 3-. FSIN. Global report on food crises 2017. Food Security Information Network, 2017.

- 4-. N. Alexandratos. World food and agriculture: outlook for the medium and longer term. *Proc. Natl. Acad. Sci*, 1999. 96(11): pp. 5908-5914. DOI: <https://doi.org/10.1073/pnas.96.11.5908>.
- 5-. S. Savci. Investigation of effect of chemical fertilizers on environment. *APCBEE Procedia*, 2012. 1: pp. 287-292. DOI: <https://doi.org/10.1016/j.apcbee.2012.03.047>.
- 6-. M. W. Aktar, D. Sengupta, A. Chowdhury. Impact of pesticides use in agriculture: their benefits and hazards. *Interdisc Toxicol*, 2009. 2(1): pp. 1-12. DOI: 10.2478/v10102-009-0001-7.
- 7-. R. Rapini, G. Marrazza. Biosensor potential in pesticide monitoring. *Compr Anal Chem*, 2016. 74: pp. 1-29. DOI: <http://dx.doi.org/10.1016/bs.coac.2016.03.016>.
- 8-. Pesticide classifications and formulations cited on 20th, June 2018. http://westnile.ca.gov/special/category_a/?page=Chapter2.htm.
- 9-. WHO. Classification of pesticides by hazard and guidelines to classification 2009. World Health Organization, 2010, Geneva.
- 10-. T. C. Sparks, R. Nauen. IRAC: Mode of action classification and insecticide resistance management. *Pest Biochem Physiol*, 2014. 121: pp. 122-128. DOI: <https://doi.org/10.1016/j.pestbp.2014.11.014>.
- 11-. C. Yang, C. Hamel, V. Vujanovic, Y. Gan. Fungicide: mode of action and possible impact on nontarget microorganisms. *ISRN Ecology*, 2011. 2011: pp. 1-8. <http://dx.doi.org/10.5402/2011/130289>.
- 12-. R. Bhadekar, S. Pote, V. Tale, B. Nirichan. Developments in analytical methods for detection of pesticides in environmental samples. *Am J Analyt Chem*, 2011. 2: pp. 1-15. DOI: 10.4236/ajac.2011.228118.
- 13-. E. A. Songa, J. O. Okonkwo. Recent approaches to improving selectivity and sensitivity of enzyme-based biosensors for organosphorus pesticides: a review. *Talanta*, 2016. 155: pp. 289-304. DOI: <https://doi.org/10.1016/j.talanta.2016.04.046>.
- 14-. D. R. Thévenot, K. Toth, R. A. Durst, G. S. Wilson. Electrochemical biosensors: recommended definitions and classification. *Pure App. Che*, 1999. 71(12): pp. 2333-2348. DOI: [https://doi.org/10.1016/S0956-5663\(01\)00115-4](https://doi.org/10.1016/S0956-5663(01)00115-4).
- 15-. A. Sassolas, B. Prieto-Simón, J. Marty. Biosensors for pesticide detection: new trends. *Am J Analyst Chem*, 2012. 3(3): pp. 210-232. DOI: 10.4236/ajac.2012.33030.

- 16-. X. Jiang, D. Li, X. Xu, Y. Ying, Y. Li, Z. Ye, J. Wang. Immunosensors for detection of pesticide residues. *Biosens Bioelectron*, 2008. 23(11): pp. 1577-1587. DOI: <https://doi.org/10.1016/j.bios.2008.01.035>.
- 17-. C. I. L. Justino, A. C. Duarte, T. A. P. Rocha-Santos. Immunosensors in clinical laboratory diagnostics. *Adv Clin Chem*, 2016. 73: pp. 65-108. DOI: 10.1016/bs.acc.2015.10.004.
- 18-. F. Arduini, A. Amine. Biosensors based on enzyme inhibition. *Ad Biochem Eng Biotechnol*, 2014. 140: pp. 299-326. DOI: 10.1007/10_2013_224.
- 19-. M. Nirschl, F. Reuter, J. Vörös. Review of transducer principles for label-free biomolecular interaction analysis. *Biosensors*, 2011. 1(3): pp. 70-92. DOI: 10.3390/bios1030070.
- 20-. D. Grieshaber, R. MacKenzie, J. Vörös, E. Reimhult. Electrochemical Biosensors- Sensor Principles and Architectures. *Sensors*, 2008. 8(3): pp. 1400-1458. DOI: 10.3390/s80314000.
- 21-. S. Uniyal and R. K. Sharma. Technological advancement in electrochemical biosensor based detection of Organophosphate pesticide chlorpyrifos in the environment: A review of status and prospects. *Biosens Bioelectron*, 2018. 116: pp. 37-50. DOI: 10.1016/j.bios.2018.05.039.
- 22-. B. Liu, Y. Yang, Z. Wu, H. Wang, G. Shen, R. Yu. A potentiometric acetylcholinesterase biosensor based on plasma-polymerized film. *Sens. Actuator B-Chem*, 2005. 104(2): pp. 186-190. DOI: <https://doi.org/10.1016/j.snb.2004.04.093>.
- 23-. V. G. Andreou, Y. D. Clonis. A portable fiber-optic pesticide biosensor based on immobilized cholinesterase and sol-gel entrapped bromocresol purple for in-field use. *Biosens Bioelectron*, 2002. 17(1-2): pp. 61-69. DOI: [https://doi.org/10.1016/S0956-5663\(01\)00261-5](https://doi.org/10.1016/S0956-5663(01)00261-5).
- 24-. H. Tsai, R. Doong. Simultaneous determination of pH, urea, acetylcholine and heavy metals using array-based enzymatic optical biosensor. *Biosens Bioelectron*, 2005. 20(9): pp. 1796-1804. DOI: <https://doi.org/10.1016/j.bios.2004.07.008>.
- 25-. V. G. Andreou, Y. D. Clonis. Novel fiber-optic biosensor based on immobilized glutathione S transferase and sol-gel entrapped bromocresol green for the determination of atrazine. *Anal Chim Acta*, 2002. 460(2): pp. 151-161. DOI: [https://doi.org/10.1016/S0003-2670\(02\)00250-7](https://doi.org/10.1016/S0003-2670(02)00250-7).
- 26-. K. A. Joshi, J. Tang, R. Haddon, J. Wang, W. Chen, A. Mulchandani. A Disposable biosensor for organophosphorus nerve agents based on carbon nanotubes modified thick film strip electrode. *Electroanalysis*, 2005. 17(1): pp. 54-58. DOI: <https://doi.org/10.1002/elan.200403118>.

- 27-. N. Jaffrezic-Renault. New Trends in Biosensors for Organophosphorus Pesticides. *Sensors*, 2001. 1(2): pp. 60-74. DOI: <https://doi.org/10.3390/s10100060>.
- 28-. F. Mazzei, F. Botrè, S. Montilla, R. Pilloton, E. Podestà, C. Botrè. Alkaline phosphatase inhibition based electrochemical sensors for the detection of pesticides. *J Electroanal Chem*, 2004. 574(1): pp. 95-100. DOI: <https://doi.org/10.1016/j.jelechem.2004.08.004>.
- 29-. F. Mazzei, F. Botrè, C. Botrè. Acid phosphatase/glucose oxidase-based biosensors for the determination of pesticides. *Anal. Chim. Acta*, 1996. 336(1-3): pp. 67-75. DOI: [https://doi.org/10.1016/S0003-2670\(96\)00378-9](https://doi.org/10.1016/S0003-2670(96)00378-9).
- 30-. P. Damborský, J. Švitel, J. Katrlík. Optical biosensors. *Essays Biochem.*, 2016. 60(1): pp. 91-100. DOI: 10.1042/EBC20150010.
- 31-. L. M. Lechuga. Chapter 5 Optical biosensors. *Compr. Anal. Chem.*, 2005. 44: pp. 209-250. DOI: [https://doi.org/10.1016/S0166-526X\(05\)44005-2](https://doi.org/10.1016/S0166-526X(05)44005-2).
- 32-. K. Narsaiah, S. N. Jha, R. Bhardwaj, R. Sharma, R. Kumar. Optical biosensors for food quality and safety assurance- a review. *J. Food Sci. Technol.*, 2012. 49(4): pp. 383-406. DOI: 10.1007/s13197-011-0437-6.
- 33-. F. Ricci, G. Volpe, L. Micheli, G. Palleschi. A review on novel developments and applications of immunosensors in food analysis. *Anal. Chim. Acta*, 2007. 605(2): pp. 111-129. DOI: 10.1016/j.aca.2007.10.046.
- 34-. M. Farré, L. Kantiani, S. Pérez, D. Barceló. Sensors and biosensors in support of EU Directives. *Trends Analyt. Chem.*, 2009. 28(2): pp. 170-185. DOI: <https://doi.org/10.1016/j.trac.2008.09.018>.
- 35-. G. Marrazza. Piezoelectric biosensors for organophosphate and carbamate pesticides: a review. *Biosensors*, 2014. 4(3): pp. 301-317. DOI: 10.3390/bios4030301.
- 36-. A. Sassolas, L. J. Blum, B. D. Leca-Bouvier. Immobilization strategies to develop enzymatic biosensors. *Biotechnol. Adv.*, 2012. 30(3): pp. 489-511. DOI: <https://doi.org/10.1016/j.biotechadv.2011.09.003>.
- 37-. N. G. Welch, J. A. Scoble, B. W. Muir, P. J. Pigram. Orientation and characterization of immobilized antibodies for improved immunoassays (review). *Biointerphases*, 2017. 12(2): pp. 1559- 4106. DOI: 10.1116/1.4978435.
- 38-. A. Sassolas, L. Blum, B. D. Lecca-Bouvier. Optical detection systems using immobilized aptamers. *Biosens. Bioelectron.*, 2011. 26(9): pp. 3725-3736. DOI: 10.1016/j.bios.2011.02.031.

- 39-. C. Bonnet, S. Andreescu, J. Marty. Adsorption: an easy and efficient immobilisation of acetylcholinesterase on screen-printed electrodes. *Anal. Chim. Acta*, 2003. 481(2): pp. 209-211. DOI: 10.1016/S0003-2670(03)00122-3.
- 40-. X. Sun, X. Wang. Acetylcholinesterase biosensor based on prussian blue-modified electrode for detecting organophosphorous pesticides. *Biosens. Bioelectron.*, 2010. 25(12): pp. 2611-2614. DOI: 10.1016/j.bios.2010.04.028.
- 41-. A. Vakurov, C. E. Simpson, C. L. Daly, T. D. Gibson, P. A. Millner. Acetylcholinesterase-based biosensor electrodes for organophosphate pesticide detection: I. Modification of carbon surface for immobilization of acetylcholinesterase. *Biosens. Bioelectron.*, 2004. 20(6): pp. 1118-1125. DOI: <https://doi.org/10.1016/j.bios.2004.03.039>.
- 42-. M. Shi, J. Xu, S. Zhang, B. Liu, J. Kong. A mediator-free screen-printed amperometric biosensor for screening of organophosphorus pesticides with flow-injection analysis (FIA) system. *Talanta*, 2006. 68(4): pp. 1089-1095. DOI: 10.1016/j.talanta.2005.07.007.
- 43-. Y. Ivanov, I. Marinov, K. Gabrovska, N. Dimcheva, T. Godjevargova. Amperometric biosensor based on a site-specific immobilization of acetylcholinesterase via affinity bonds on a nanostructured polymer membrane with integrated multiwall carbon nanotubes. *J. Mol. Catal. B Enzym.*, 2010. 63(3-4): pp. 141-148. DOI: 10.1016/j.molcatb.2010.01.005.
- 44-. T. Kaláb, P. Skládal. A disposable amperometric immunosensor for 2,4-dichlorophenoxyacetic acid. *Anal. Chim. Acta*, 1995. 304(3): pp. 361-368. DOI: [https://doi.org/10.1016/0003-2670\(94\)00641-X](https://doi.org/10.1016/0003-2670(94)00641-X).
- 45-. A. Klotz, A. Brecht, C. Barzen, G. Gauglitz, R. D. Harris, G. R. Quigley, J. S. Wilkinson, R. A. Abuknesha. Immunofluorescence sensor for water analysis. *Sens. Actuators B Chem.*, 1998. 51(1-3): pp. 181- 187. DOI: [https://doi.org/10.1016/S0925-4005\(98\)00187-7](https://doi.org/10.1016/S0925-4005(98)00187-7).
- 46-. G. G. Guilbault, B. Hock, R. Schmid. A piezoelectric immunobiosensor for atrazine in drinking water. *Biosens. Bioelectron.*, 1992. 7(6): pp. 411- 419. DOI: [https://doi.org/10.1016/0956-5663\(92\)85040-H](https://doi.org/10.1016/0956-5663(92)85040-H).
- 47-. P. Taylor, S. Camp, Z. Radić. Acetylcholinesterase, in: *Encyclopedia of Neuroscience*. Academic Press, La Jolla, 2009. pp. 5-7. DOI: <https://doi.org/10.1016/B978-008045046-9.01132-3>.
- 48-. V. Dhull, A. Gahlaut, N. Dilbaghi, V. Hooda. Acetylcholinesterase Biosensors for Electrochemical Detection of Organophosphorus Compounds: A Review. *Biochem. Res. Int.*, 2013. 2013: pp. 1-18. DOI: <http://dx.doi.org/10.1155/2013/731501>.

- 49-. M. Pohanka. Biosensors containing acetylcholinesterase and butyrylcholinesterase as recognition tools for detection of various compounds. *Chem. Pap.*, 2015. 69(1): pp. 4-16. DOI: 10.2478/s11696-014-0542-x.
- 50-. C. S. Pundir, N. Chauhan. Acetylcholinesterase inhibition-based biosensors for pesticide determination: A review. *Anal. Biochem.*, 2012. 429(1): pp. 19- 31. DOI: <http://dx.doi.org/10.1016/j.ab.2012.06.025>.
- 51-. S. Hernandez, I. Palchetti, M. Mascini. Determination of anticholinesterase activity for pesticides monitoring using a thiocholine sensor. *Intern. J. Environ. Anal. Chem.*, 2000. 78(3-4): pp. 263-278. DOI: <https://doi.org/10.1080/03067310008041346>.
- 52-. C. La Rosa, R. Pariente, L. Hernández, E. Lorenzo. Determination of organophosphorus and carbamic pesticides with an acetylcholinesterase amperometric biosensor using 4-aminophenyl acetate as substrate. *Anal. Chim. Acta.*, 1994. 295(3): pp. 273- 282. DOI: [https://doi.org/10.1016/0003-2670\(94\)80232-7](https://doi.org/10.1016/0003-2670(94)80232-7).
- 53-. M. Khayyami, M. T. P. Pita, N. P. Garcia, G. Johansson, B. Danielsson, P. Larsson. Development of an amperometric biosensor based on acetylcholine esterase covalently bound to a new support material. *Talanta*, 1998. 45(3): pp. 557- 563. DOI: [https://doi.org/10.1016/S0039-9140\(97\)00182-3](https://doi.org/10.1016/S0039-9140(97)00182-3).
- 54-. G. Palleschi, M. Bernabei. Determination of organophosphorus insecticides with a choline electrochemical biosensor. *Sens. Actuators B Chem.*, 1992. 7(1-3): pp. 513- 517. DOI: [https://doi.org/10.1016/0925-4005\(92\)80355-2](https://doi.org/10.1016/0925-4005(92)80355-2).
- 55-. E. A. Songa, V. S. Somerset, T. Waryo, P. G. L. Baker, E. I. Iwuoha. Amperometric nanobiosensor for quantitative determination of glyphosate and glufosinate residues in corn samples. *Pure Appl. Chem.*, 2009. 81(1): pp. 123- 139. DOI: 10.1351/PAC-CON-08-01-15.
- 56-. Q. Zhang, G. Xu, L. Gong, H. Dai, S. Zhang, Y. Li, Y. Lin. An enzyme-assisted electrochemiluminescent biosensor developed on ordered mesoporous carbons substrate for ultrasensitive glyphosate sensing. *Electrochim. Acta*, 2015. 186: pp. 624- 630. DOI: <http://dx.doi.org/10.1016/j.electacta.2015.10.081>.
- 57-. G. C. Oliveira, S. K. Moccelini, M. Castilho, A. J. Terezo, J. Possavatz, M. R. L. Magalhães, E. G. C. Dore. Biosensor based on atemoya peroxidase immobilised on modified nanoclay for glyphosate biomonitoring. *Talanta*, 2012. 98: pp. 130-136. <https://doi.org/10.1016/j.talanta.2012.06.059>.
- 58-. S. K. Mocchelini, I. C. Vieira, F. D. Lima, B. G. Lucca, A. M. J. Barbosa, V. S. Ferreira. Determination of thiodicarb using a biosensor based on alfalfa sprout peroxidase immobilized in self-assembled monolayers. *Talanta*, 2010. 82(1): pp. 164- 170. DOI: <https://doi.org/10.1016/j.talanta.2010.04.015>.

- 59-. S. Ullah, S. Son, H. Y. Yun, D. H. Kim, P. Chun, H. R. Moon. Tyrosinase inhibitors: a patent review (2011-2015). *Expert. Opin. Ther. Pat.*, 2016. 26(3): pp. 347- 362. DOI: 10.1517/13543776.2016.1146253.
- 60-. J. Besombes, S. Cosnier, P. Labbé, G. Reverdy. A biosensor as warning device for the detection of cyanide, chlorophenols, atrazine and carbamate pesticides. *Anal. Chim. Acta*, 1995. 311(3): pp. 255- 263. DOI: [https://doi.org/10.1016/0003-2670\(94\)00686-G](https://doi.org/10.1016/0003-2670(94)00686-G).
- 61-. J. C. Vidal, S. Esteban, J. Gil, J. R. Castillo. A comparative study of immobilization methods of a tyrosinase enzyme on electrodes and their application to the detection of dichlorvos organophosphorus insecticide. *Talanta*, 2006. 68(3): pp. 791-799. DOI: 10.1016/j.talanta.2005.06.038.
- 62-. Y. D. Tanimoto de Albuquerque, L. F. Ferreira. Amperometric biosensing of carbamate and organophosphate pesticides utilizing screen-printed tyrosinase-modified electrodes. *Anal. Chim. Acta*, 2007. 596(2): pp. 210- 221. DOI: 10.1016/j.aca.2007.06.013.
- 63-. M. T. P. Pita, A. J. Reviejo, F. J. Manuel de Villena, J. M. Pingarrón. Amperometric selective biosensing of dimethyl- and diethyldithiocarbamates based on inhibition processes in a medium of reversed micelles. *Anal. Chim. Acta*, 1997. 340(1-3): pp. 89-97. DOI: [https://doi.org/10.1016/S0003-2670\(96\)00552-1](https://doi.org/10.1016/S0003-2670(96)00552-1).
- 64-. F. D. Lima, B. G. Lucca, A. M. J. Barbosa, V. S. Ferreira, S. K. Moccelini, A. C. Franzoi, I. C. Vieira. Biosensor based on pequi polyphenol oxidase immobilized on chitosan crosslinked with cyanuric chloride for thiodicarb determination. *Enzyme Microb. Technol.*, 2010. 47(4): pp. 153- 158. DOI: 10.1016/j.enzmictec.2010.05.006.
- 65-. T. M. Anh, S. V. Dzyadevych, M. C. Van, N. J. Renault, C. N. Duc, J. Chovelon. Conductometric tyrosinase biosensor for the detection of diuron, atrazine and its main metabolites. *Talanta*, 2004. 63(2): pp. 365- 370. DOI: 10.1016/j.talanta.2003.11.008.
- 66-. L. Campanella, A. Bonanni, E. Martini, N. Todini, M. Tomassetti. Determination of triazine pesticides using a new enzyme inhibition tyrosinase OPEE operating in chloroform. *Sens. Actuators B Chem.*, 2005. (111- 112): pp. 505- 514. DOI: <https://doi.org/10.1016/j.snb.2005.03.082>.
- 67-. Y. Guan, L. Liu, C. Chen, X. Kang, Q. Xie. Effective Immobilization of Tyrosinase via Enzyme Catalytic Polymerization of L-DOPA for Highly Sensitive Phenol and Atrazine Sensing. *Talanta*, 2016. 160: pp. 125- 132. DOI: <https://doi.org/10.1016/j.talanta.2016.07.003>.

- 68-. L. Campanella, D. Lelo, E. Martini, M. Tomassetti. Organophosphorus and carbamate pesticide analysis using an inhibition tyrosinase organic phase enzyme sensor; comparison by butyrylcholinesterase + choline oxidase opee and application to natural waters. *Anal. Chim. Acta*, 2007. 587(1): pp. 22- 32. DOI: 10.1016/j.aca.2007.01.023.
- 69-. U. Sharma, D. Pal, R. Prasad. Alkaline phosphatase: an overview. *Ind J Clin Biochem*, 2014. 29(3): pp. 269- 278. DOI: 10.1007/s12291-013-0408-y.
- 70-. F. Mazzei, F. Botrè, S. Montilla, R. Pilloton, E. Podestrà, C. Botrè. Alkaline phosphatase inhibition based electrochemical sensors for the detection of pesticides. *J. Electroanal. Chem.*, 2004. 574(1): pp. 95- 100. DOI: 10.1016/j.jelechem.2004.08.004.
- 71-. M. S. Ayyagari, S. Kamtekar, R. Pande, K. A. Marx, J. Kumar, S. K. Tripathy, D. L. Kaplan. Biosensors for pesticide detection based on alkaline phosphatase catalyzed chemiluminescence. *Mater. Sci. Eng. C*, 1995. 2(4): pp. 191- 196. DOI: [https://doi.org/10.1016/0928-4931\(95\)00077-1](https://doi.org/10.1016/0928-4931(95)00077-1).
- 72-. F. G. Sánchez, A. N. Díaz, M. C. R. Peinado, C. Belledone. Free and sol-gel immobilized alkaline phosphatase-based biosensor for the determination of pesticides and inorganic compounds. *Anal. Chim. Acta*, 2003. 484(1): pp. 45- 51. DOI: 10.1016/S0003-2670(03)00310-6.
- 73-. C. Botrè, F. Botrè, F. Mazzei, E. Podestrà. Inhibition-based biosensors for the detection of environmental contaminants: determination of 2,4-dichlorophenoxyacetic acid. *Environ. Toxicol. Chem.*, 2000. 19(12): pp. 2876-2881. DOI: <https://doi.org/10.1002/etc.5620191204>.
- 74-. F. Mazzei, F. Botrè, C. Botrè. Acid phosphatase/glucose oxidase-based biosensors for the determination of pesticides. *Anal. Chim. Acta*, 1996. 336(1-3): pp. 67-75. DOI: [https://doi.org/10.1016/S0003-2670\(96\)00378-9](https://doi.org/10.1016/S0003-2670(96)00378-9).
- 75-. F. Kartal, A. KilinÇ, S. Timur. Lipase biosensor for tributyrin and pesticide detection. *Intern. J. Environ. Anal. Chem.*, 2007. 87(10): pp. 715- 722. DOI: 10.1080/03067310701327741.
- 76-. Y. Braham, H. Barhoumi, A. Maaref. Urease capacitive biosensors using functionalized magnetic nanoparticles for atrazine pesticide detection in environmental samples. *Anal. Methods*, 2013. 5(18): pp. 4898- 4904. DOI: 10.1039/C3AY40579F.
- 77-. T. Noguier, J. Marty. High sensitive bienzymic sensor for the dithiocarbamate fungicides. *Anal. Chim. Acta*, 1997. 347(1-2): pp. 63- 70. DOI: [https://doi.org/10.1016/S0003-2670\(97\)00127-X](https://doi.org/10.1016/S0003-2670(97)00127-X).

- 78-. A. Seki, F. Ortéga, J. Marty. Enzyme sensor for the detection of herbicides inhibiting acetolactate synthase. *Anal. Lett.*, 1996. 29(8): pp. 1259- 1271. DOI: <https://doi.org/10.1080/00032719608001479>.
- 79-. K. Rekha, M. D. Gouda, M. S. Thakur, N. G. Karanth. Ascorbate oxidase based amperometric biosensor for organophosphorus pesticide monitoring. *Biosens. Bioelectron.*, 2000. 15(9-10): pp. 499- 502. DOI: 10.1016/S0956-5663(00)00077-4.
- 80-. Q. Yang, Y. Qu, Y. Bo, Y. Wen, S. Huang. Biosensor for atrazin based on aligned carbon nanotubes modified with glucose oxidase. *Microchim. Acta*, 2010. 168(3-4): pp. 197- 203. DOI: 10.1007/s00604-009-0272-x.
- 81-. J. L. Delgado, M. A. Herranz, N. Martín. The nano-forms of carbon. *J. Mater. Chem.*, 2008. 18(13): pp. 1417- 1426. DOI: 10.1039/B717218D.
- 82-. V. N. Mochalin, O. Shenderova, D. Ho, Y. Gogotsi. The properties and applications of nanodiamonds. *Nat. Nanotechnol.*, 2012. 7(1): pp. 11-23. DOI: 10.1038/NNANO.2011.209.
- 83-. S. Liu, X. Guo. Carbon nanomaterials field-effect-transistor-based biosensors. *NPG Asia Mater.*, 2012. 4: pp. e23. DOI: 10.1038/am.2012.42.
- 84-. G. Zhao, X. Li, M. Huang, Z. Zhen, Y. Zhong, Q. Chen, X. Zhao, Y. He, R. Hu, T. Yang, R. Zhang, C. Li, J. Kong, J. Xu, R. Ruoff, H. Zu. The physics and chemistry of graphene-on-surfaces. *Chem. Soc. Rev.*, 2017. 46(15): pp. 4417- 4449. DOI: 10.1039/c7cs00256d.
- 85-. M. J. Allen, V. C. Tung, R. B. Kaner. Honeycomb carbon: a review of graphene. *Chem. Rev.*, 2010. 110(1): pp. 132- 145. DOI: 10.1021/cr900070d.
- 86-. D. M. Guldi. Carbon nanotubes: science and application. *Angew. Chem. Int. Ed*, 2006. 45(5): pp. 694- 695. DOI: <https://doi.org/10.1002/anie.200585355>.
- 87-. W. Yang, K. R. Ratinac, S. P. Ringer, P. Thordarson, J. J. Gooding, F. Braet. Carbon nanomaterials in biosensors: should you use nanotubes or graphene? *Angew. Chem. Int. Ed.*, 2010. 49(12): pp. 2114- 2138. DOI: 10.1002/anie.200903463.
- 88-. R. Chen, Y. Li, K. Huo, P. K. Chu. Microelectrode arrays based on carbon nanomaterials: emerging electrochemical sensors for biological and Environmental applications. *RSC Adv.*, 2013. 3(41): p. 18698- 18715. DOI: 10.1039/C3RA43033B.
- 89-. D. Jariwala, V. K. Sangwan, L. J. Lauhon, T. J. Marks, M. C. Hersam. Carbon nanomaterials for electronics, optoelectronics, photovoltaics, and sensing. *Chem. Soc. Rev.*, 2013. 42(7): pp. 2824- 2860. DOI: 10.1039/c2cs35335k.

- 90-. D. Ugarte. Curling and closure of graphitic networks under electron-beam irradiation. *Nature*, 1992. 359(6397): pp. 707- 709. DOI: 10.1038/359707a0.
- 91-. L. Qin, S. Iijima. Onion-like graphitic particles produced from diamond. *Chem. Phys. Lett.*, 1996. 262(3-4): pp. 252- 258. DOI: [https://doi.org/10.1016/0009-2614\(96\)01037-8](https://doi.org/10.1016/0009-2614(96)01037-8).
- 92-. B. S. Xu, S. I. Tanaka. Formation of giant onion-like fullerenes under A1 nanoparticles by electron irradiation. *Acta mater.*, 1998. 46(15): pp. 5249- 5257. DOI: [https://doi.org/10.1016/S1359-6454\(98\)00221-3](https://doi.org/10.1016/S1359-6454(98)00221-3).
- 93-. N. Sano, H. Wang, M. Chhowalla, I. Alexandrou, G. A. J. Amaratunga. Synthesis of carbon 'onions' in water. *Nature*, 2001. 414(6863): pp. 506- 507. DOI: 10.1038/35107141.
- 94-. I. Alexandrou, H. Wang, N. Sano, G. A. Amaratunga. Structure of carbon onions and nanotubes formed by arc in liquids. *J. Chem. Phys.*, 2004. 120(2): pp. 1055- 1058. DOI: 10.1063/1.1629274.
- 95-. V. L. Kuznetsov, A. L. Chuvilin, Y. V. Butenko, I. Y. Mal'kov, V. M. Titov. Onion-like carbon from ultra-disperse diamond. *Chem. Phys. Lett.*, 1994. 222(4): p. 343- 348. DOI: [https://doi.org/10.1016/0009-2614\(94\)87072-1](https://doi.org/10.1016/0009-2614(94)87072-1).
- 96-. S. Tomita, T. Sakurai, H. Ohta. Structure and electronic properties of carbon onions. *J. Chem. Phys.*, 2001. 114(17): p. 7477- 7482. DOI: <https://doi.org/10.1063/1.1360197>.
- 97-. R. Borgohain, J. Yang, J. P. Selegue, D. Y. Kim. Controlled synthesis, efficient purification, and electrochemical characterization of arc-discharge carbon nano-onions. *Carbon*, 2014. 66: pp. 272- 284. DOI: <https://doi.org/10.1016/j.carbon.2013.09.001>.
- 98-. X. Wang, B. Xu, X. Liu, J. Guo, H. Ichinose. Synthesis of Fe-included onion-like Fullerenes by chemical vapor deposition. *Diamond Relat. Mater.*, 2006. 15(1): pp. 147- 150. DOI: <https://doi.org/10.1016/j.diamond.2005.09.005>.
- 99-. Y. Yang, X. Liu, Y. Han, W. Ren, B. Xu. Ferromagnetic Property and Synthesis of Onion-Like Fullerenes by Chemical Vapor Deposition Using Fe and Co Catalysts Supported on NaCl. *J. Nanomater.*, 2011. 2011: pp. 1-6. DOI: <http://dx.doi.org/10.1155/2011/720937>.
- 100-. C. Zhang, J. Li, E. Liu, C. He, C. Shi, X. Du, R. H. Hauge, N. Zhao. Synthesis of hollow carbon nano-onions and their use for electrochemical hydrogen storage. *Carbon*, 2012. 50(10): pp. 3513- 3521. DOI: <https://doi.org/10.1016/j.carbon.2012.03.019>.
- 101-. T. Cabio'h, J. P. Riviere, J. Delafond. A new technique for fullerene onion formation. *J. Mater. Sci.*, 1995. 30(19): pp. 4787-4792. DOI: 10.1007/BF01154486.

- 102-. T. Cabio'h, M. Jaouen, M. F. Denanot, P. Bechet. Influence of the implantation parameters on the microstructure of carbon onions produced by carbon ion implantation. *App. Phys. Lett.*, 1998. 73(21): pp. 3096- 3098. DOI: <https://doi.org/10.1063/1.122684>.
- 103-. T. Cabio'h, E. Thune, M. Jaouen. Carbon-onion thin-film synthesis onto silica substrates. *Chem. Phys. Lett.*, 2000. 320(1-2): pp. 202- 205. DOI: [https://doi.org/10.1016/S0009-2614\(00\)00212-8](https://doi.org/10.1016/S0009-2614(00)00212-8).
- 104-. T. Cabio'h, E. Thune, J. P. Rivière, S. Camelio, J. C. Girard, P. Guérin, M. Jaouen, L. Henrard, P. Lambin. Structure and properties of carbon onion layers deposited onto various substrates. *J. App. Phys.*, 2002. 91(3): pp. 1560- 1567. DOI: 10.1063/1.1421222.
- 105-. F. Dong-Ju, L. Xu-Guang, D. Ai-Bing, H. Pei-De, J. Hu-Sheng, X. Bing-She. Synthesis of nano-structured onion-like fullerenes by MW plasma. *J. Inorg. Mater.*, 2006. 21(3): pp. 577- 582.
- 106-. A. B. Du, X. G. Liu, D. J. Fu, P. D. Han, B. S. Xu. Onion-like fullerenes synthesis from coal. *Fuel*, 2007. 86(1-2): pp. 294- 298. DOI: <https://doi.org/10.1016/j.fuel.2006.05.031>.
- 107-. M. Bystrzejewski, M. H. Rummeli, T. Gemming, H. Lange, A. Huczko. Catalyst-free synthesis of onion-like carbon nanoparticles. *New Carbon Mater.*, 2010. 25(1): pp. 1- 8. DOI: [https://doi.org/10.1016/S1872-5805\(09\)60011-1](https://doi.org/10.1016/S1872-5805(09)60011-1).
- 108-. J. Du, Z. Liu, Z. Li, B. Han, Z. Sun, Y. Huang. Carbon onions synthesized via thermal reduction of glycerin with magnesium. *Mater. Chem. Phys.*, 2005, 93(1): pp. 178- 180. DOI: <https://doi.org/10.1016/j.matchemphys.2005.03.012>.
- 109-. M. Choucair, J. A. Stride. The gram-scale synthesis of carbon onions. *Carbon*, 2012. 50(3): pp. 1109- 1115. DOI: <https://doi.org/10.1016/j.carbon.2011.10.023>.
- 110-. J. P. Bartolome, A. Fragoso. Preparation and characterization of carbon nano-onions by nanodiamond annealing and functionalization by radio-frequency Ar/O₂ plasma. *Fullerenes, Nanotubes, Carbon Nanostruct.*, 2017. 25(5): pp. 327-334. DOI: <https://doi.org/10.1080/1536383X.2017.1303604>.
- 111-. D. Roy, M. Chhowalla, H. Wang, N. Sano, I. Alexandrou, T. W. Clyne, G. A. J. Amaratunga. Characterization of carbon nano-onions using Raman spectroscopy. *Chem. Phys. Lett.*, 2003. 373(1-2): pp. 52-56. DOI: [https://doi.org/10.1016/S0009-2614\(03\)00523-2](https://doi.org/10.1016/S0009-2614(03)00523-2).
- 112-. S. Tomita, T. Sakurai, H. Ohta, M. Fujii, S. Hayashi. Structure and electronic properties of carbon onions. *J. Chem. Phys.*, 2001. 114(17): pp. 7477-7482. DOI: <https://doi.org/10.1063/1.1360197>.
- 113-. S. Tomita, A. Burian, J. C. Dorre, D. LeBolloch, M. Fujii, S. Hayashi. Diamond nanoparticles to carbon onions transformation: X-ray diffraction studies. *Carbon*,

2002. 40(9): pp. 1469-1474. DOI: [https://doi.org/10.1016/S0008-6223\(01\)00311-6](https://doi.org/10.1016/S0008-6223(01)00311-6).

114-. S. M. Hou, C. G. Tao, G. M. Zhang, X. Y. Zhao, Z. Q. Xue, Z. J. Shi, Z. N. Gu. Ultrahigh vacuum scanning probe microscopy studies of carbon onions. *Physica E*, 2001. 9(2): pp. 300-304. DOI: [https://doi.org/10.1016/S1386-9477\(00\)00273-3](https://doi.org/10.1016/S1386-9477(00)00273-3).

115-. M. Montalti, S. Krishnamurthy, Y. Chao, Y. V. Butenko, V. L. Kuznetsov, V. R. Dhanak, M. R. C. Hunt, L. Siller. Photoemission spectroscopy of clean and potassium-intercalated carbon onions. *Phys. Rev. B*, 2003. 67(11): pp. 113401-4. DOI: <https://doi.org/10.1103/PhysRevB.67.113401>.

116-. A. Ruiz, J. Bretón, J. M. G. Llorente. A theoretical model of the photoabsorption spectra of carbon buckyonions. *J. Chem. Phys.*, 2004. 120(13): pp. 6163- 6172. DOI: <http://dx.doi.org/10.1063/1.1651061>.

117-. S. Tomita, M. Fujii, S. Hayashi. Optical extinction properties of carbon onions prepared from diamond nanoparticles. *Phys. Rev. B.*, 2002. 66(24): pp. 245424-245430. DOI: [10.1103/PhysRevB.66.245424](https://doi.org/10.1103/PhysRevB.66.245424).

118-. E. Koudoumas, O. Kokkinaki, M. Konstantaki, S. Couris, S. Korovin, P. Detkov, V. Kuznetsov, S. Pimenov, V. Pustovoi. Onion-like carbon and diamond nanoparticles for optical limiting. *Chem. Phys. Lett.*, 2002. 357(5-6): pp. 336-340. DOI: [https://doi.org/10.1016/S0009-2614\(02\)00557-2](https://doi.org/10.1016/S0009-2614(02)00557-2).

119-. S. Tomita, S. Hayashi, Y. Tsukuda, M. Fujii. Ultraviolet-visible absorption spectroscopy of carbon onions. *Phys. Solid State*, 2002. 44(3): pp. 450-453. DOI: <https://doi.org/10.1134/1.1462669>.

120-. J. Bartelmess, S. Giordani. Carbon nano-onions (multi-layer fullerenes): chemistry and applications. *Beilstein J. Nanotechnol.*, 2014. 5: pp. 1980-1998. DOI: [10.3762/bjnano.5.207](https://doi.org/10.3762/bjnano.5.207).

121-. V. Georgakilas, D. M. Guldi, R. Signorini, R. Bozio, M. Prato. Organic functionalization and optical properties of carbon onions. *J. Am. Chem. Soc.*, 2003. 125(47): pp. 14268- 14269. DOI: [10.1021/ja0342805](https://doi.org/10.1021/ja0342805).

122-. A. S. Rettenbacher, B. Elliot, J. S. Hudson, A. Amirkhaniyan, L. Echegoyen. Preparation and functionalization of multilayer fullerenes (carbon nano-onions). *Chem. Eur. J.*, 2006. 12(2): pp. 376- 387. DOI: [10.1002/chem.200500517](https://doi.org/10.1002/chem.200500517).

123-. A. Palkar, F. Melin, C. M. Cardona, B. Elliott, A. K. Naskar, D. D. Edie, A. Kumbhar, L. Echegoyen. Reactivity differences between carbon nano onions (CNOs) prepared by different methods. *Chem. Asian J.*, 2007. 2(5): pp. 625- 633. DOI: [10.1002/asia.200600426](https://doi.org/10.1002/asia.200600426).

124-. L. Zhou, C. Gao, D. Zhu, W. Xu, F. F. Chen, A. Palkar, L. Echegoyen, E. S. Kong. Facile functionalization of multilayer fullerenes (carbon nano-onions) by nitrene

chemistry and “grafting from” strategy. *Chem. Eur. J.*, 2009. 15(6): pp. 1389-1396. DOI: 10.1002/chem.200801642.

125-. K. Flavin, M. N. Chaur, L. Echegoyen, S. Giordani. Functionalization of multilayer fullerenes (carbon nano-onions) using diazonium compounds and “click” chemistry. *Org. Lett.*, 2010. 12(4): pp. 840-843. DOI: 10.1021/ol902939f.

126-. M. Yang, K. Flavin, I. Kopf, G. Radics, C. H. A. Hearnden, G. J. McManus, B. Moran, A. Villalta-Cerdas, L. A. Echegoyen, S. Giordani, E. C. Lavelle. *Small*, 2013. 9(24): pp. 4194-4206. DOI: <https://doi.org/10.1002/sml.201300481>.

127-. S. Giordani, J. Bartelmess, M. Frasconi, I. Biondi, S. Cheung, M. Grossi, D. Wu, L. Echegoyen, D. F. O’Shea. NIR fluorescence labelled carbon nano-onions: synthesis, analysis and cellular imaging. *J. Mater. Chem. B*, 2014. 2(42): pp. 7459-7463. DOI: 10.1039/c4tb01087f.

128-. J. Bartelmess, E. D. Luca, A. Signorelli, M. Baldrighi, M. Becce, R. Brescia, V. Nardone, E. Parisini, L. Echegoyen, P. P. Pompa, S. Giordani. Boron dipyrromethene (BODIPY) functionalized carbon nano-onions for high resolution cellular imaging. *Nanoscale*, 2014. 6(22): pp. 13761-13769. DOI: 10.1039/C4NR04533E.

129-. A. Łapiński, A. T. Dubis, M. E. Plonska-Brzezinska, J. Mazurczyk, J. Breczko, L. Echegoyen. Vibrational spectroscopic study of carbon nano-onions coated with polyaniline. *Phys. Status Solidi C*, 2012. 9(5): p. 1210-1212. DOI: 10.1002/pssc.201100782.

130-. Y. Liu, R. L. V. Wal, V. N. Khabashesku. Functionalization of carbon nano-onions by direct fluorination. *Chem. Mater.*, 2007. 19(4): pp. 778-786. DOI: 10.1021/cm062177j.

131-. M. E. Plonska-Brzezinska, A. Lapinski, A. Z. Wilczewska, A. T. Dubis, A. Villalta-Cerdas, K. Winkler, L. Echegoyen. *Carbon*, 2011. 49(15): pp. 5079-5089. DOI: <https://doi.org/10.1016/j.carbon.2011.07.027>.

132-. S. Sek, J. Breczko, M. E. Plonska-Brzezinska, A. Z. Wilczewska, L. Echegoyen. STM-based molecular junction of carbon nano-onion. *Chemphyschem*, 2013. 14(1): pp. 96-100. DOI: 10.1002/cphc.201200624.

133-. A. Molina-Ontoria, M. N. Chaur, M. E. Plonska-Brzezinska, L. Echegoyen. Preparation and characterization of soluble carbon nano-onions by covalent functionalization, employing a Na-K alloy. *Chem. Commun.*, 2013. 49(24): pp. 2406-2408. DOI: 10.1039/C3CC39077B.

134-. P. P. Kuzhir, D. S. Bychanok, S. A. Maksimenko, A. V. Gusinski, O. V. Ruhavets, V. L. Kuznetsov, S. I. Moseenkov, C. Jones, O. Shenderova, P. Lambin. Onion-like carbon based polymer composite films in microwaves. *Solid State Sci.*, 2009. 11(10): pp. 1762-1767. DOI: 10.1016/j.solidstatesciences.2008.12.003.

- 135-. J. Breczko, K. Winkler, M. E. Plonska-Brzezinska, A. Villalta-Cerdas, L. Echegoyen. Electrochemical properties of composites containing small carbon nano-onions and solid polyelectrolytes. *J. Mater. Chem.*, 2010. 20(36): pp. 7761-7768. DOI: 10.1039/C0JM01213K.
- 136-. M. E. Plonska-Brzezinska, J. Mazurczyk, B. Palys, J. Breczko, A. Lapinski, A. T. Dubis, L. Echegoyen. Preparation and characterization of composites that contain small carbon nano-onions and conducting polyaniline. *Chem. Eur. J.*, 2012. 18(9): pp. 2600-2608. DOI: 10.1002/chem.201102175.
- 137-. M. E. Plonska-Brzezinska, M. Lewandowski, M. Błaszyk, A. Molina-Ontoria, T. Luciński, L. Echegoyen. Preparation and characterization of carbon nano-onion/PEDOT:PSS composites. *Chemphyschem.*, 2012. 13(18): pp. 4134-4141. DOI: 10.1002/cphc.201200789.
- 138-. M. E. Plonska-Brzezinska, D. M. Brus, J. Breczko, L. Echegoyen. Carbon nano-onions and biocompatible polymers for flavonoid incorporation. *Chem. Eur. J.*, 2013. 19(16): pp. 5019-5024. DOI: 10.1002/chem.201300009.
- 139-. R. Borgohain, J. Li, J. P. Selegue, Y. T. Cheng. Electrochemical study of functionalized carbon nano-onions for high-performance supercapacitor electrodes. *J. Phys. Chem. C*, 2012. 116(28): pp. 115068-15075. DOI: 10.1021/jp301642s.
- 140-. E. Wajs, A. Molina-Ontoria, T. T. Nielsen, L. Echegoyen, A. Frago. Supramolecular solubilization of cyclodextrin-modified carbon nano-onions by host-guest interactions. *Langmuir*, 2015. 31(1): pp. 535-541. DOI: 10.1021/la504065r.
- 141-. M. Ghosh, S. K. Sonkar, M. Saxena, S. Sarkar. Carbon nano-onions for imaging the life cycle of *Drosophila Melanogaster*. *Small*, 2011. 7(11): pp. 3170-3177. DOI: 10.1002/smll.201101158.
- 142-. S. K. Sonkar, M. Ghosh, M. Roy, A. Begum, S. Sarkar. High-fluorescence bioimaging agent in food chain- an in vivo study from unicellular *E. coli* to multicellular *C. elegans*. *Mater Express*, 2012. 2(2): pp. 105-114. DOI: <https://doi.org/10.1166/mex.2012.1064>.
- 143-. S. Giordani, J. Bartelmess, M. Frasconi, I. Biondi, S. Cheung, M. Grossi, D. Wu, L. Echegoyen, D. O'Shea. NIR fluorescence labelled carbon nano-onions: synthesis, analysis and cellular imaging. *J. Mater. Chem. B*, 2014. 2(42): pp. 7459-7463. DOI: 10.1039/c4tb01087f.
- 144-. J. Bartelmess, E. D. Luca, A. Signorelli, M. Baldrighi, M. Becce, R. Brescia, V. Nardone, E. Parisini, L. Echegoyen, P. P. Pompa, S. Giordani. Boron dipyrromethene (BODIPY) functionalized carbon nano-onions for high resolution

cellular imaging. *Nanoscale*, 2014. 6(22): pp. 13761-13769. DOI: 10.1039/C4NR04533E.

145-. L. Ding, J. Stilwell, T. Zhang, O. Elboudwarej, H. Jiang, J. P. Selegue, P. A. Cookie, J. W. Gray, F. F. Chen. Molecular Characterization of the cytotoxic mechanism of multiwall carbon nanotubes and nano-onions on human skin fibroblast. *Nano Lett.*, 2005. 5(12): pp. 2448-2464. DOI: 10.1021/nl051748o.

146-. Y. Xu, S. Wang, J. Yang, X. Gu, J. Zhang, Y. Zheng, J. Yang, L. Xu, X. Zhu. Multiwall carbon nano-onions induce DNA damage and apoptosis in human umbilical vein endothelial cells. *Environ Toxicol.*, 2013. 28(8): pp. 442-450. DOI: 10.1002/tox.20736.

147-. C. M. Sayes, J. D. Fortner, W. Guo, D. Lyon, A. M. Boyd, K. D. Ausman, Y. J. Tao, B. Sitharaman, L. J. Wilson, J. B. Hughes, J. L. West, V. L. Colvin. The differential cytotoxicity of water-soluble fullerenes. *Nano Lett.*, 2004. 4(10): pp. 1881-1887. DOI: 10.1021/nl0489586.

148-. C. Portet, G. Yushin, Y. Gogotsi. Electrochemical performance of carbon onions, nanodiamonds, carbon black and multiwalled nanotubes in electrical double layer capacitors. *Carbon*, 2007. 45(13): pp. 2511-2518. DOI: <https://doi.org/10.1016/j.carbon.2007.08.024>.

149-. E. G. Bushueva, P. S. Galkin, A. V. Okotrub, L. G. Bulusheva, N. N. Gavrillov, V. L. Kuznetsov, S. I. Moiseev. Double layer supercapacitor properties of onion-like carbon materials. *phys. stat. sol. (b)*, 2008. 245(10): pp. 2296-2299. DOI: 10.1002/pssb.200879608.

150-. D. Pech, M. Brunet, H. Durou, P. Huang, V. Mochalin, Y. Gogotsi, P. Taberna, P. Simon. Ultrahigh-power micrometer-sized supercapacitors based on onion-like carbon. *Nat Nanotechnol*, 2010. 5(9): pp. 651-654. DOI: 10.1038/nnano.2010.162.

151-. J. K. McDonough, A. I. Frolov, V. Presser, J. Niu, C. H. Miller, T. Ubieto, M. V. Fedorow, Y. Gogotsi. Influence of the structure of carbon onions on their electrochemical performance in supercapacitor electrodes. *Carbon*, 2012. 50(9): pp. 3298-3309. DOI: <https://doi.org/10.1016/j.carbon.2011.12.022>.

152-. Y. Gao, Y. S. Zhou, M. Qian, X. N. He, J. Redepenning, P. Goodman, H. M. Li, L. Jiang, Y. F. Lu. Chemical activation of carbon nano-onions for high-rate supercapacitor electrodes. *Carbon*, 2013. 51: pp. 52-58. DOI: <https://doi.org/10.1016/j.carbon.2012.08.009>.

153-. R. Borgohain, J. Li, J. P. Selegue, Y. T. Cheng. Electrochemical study functionalized carbon nano-onions for high-performance supercapacitor electrodes. *J. Phys. Chem. C*, 2012. 116(28): pp. 15068-15075. DOI: 10.1021/jp301642s.

- 154-. F. Han, B. Yao, Y. Bai. Preparation of carbon nano-onions and their application as anode materials for rechargeable lithium-ion batteries. *J. Phys. Chem. C*, 2011. 115(18): pp. 8923-8927. DOI: [dx.doi.org/10.1021/jp2007599](https://doi.org/10.1021/jp2007599).
- 155-. Y. Wang, F. Yan, S. W. Liu, A. Y. S. Tan, H. Song, X. W. Sun, H. Y. Yang. Onion-like carbon matrix supported Co₃O₄ nanocomposites: a highly reversible anode material for lithium ion batteries with excellent cycling stability. *J. Mater. Chem. A*, 2013. 1(17): pp. 5212-5216. DOI: [10.1039/C3TA10559H](https://doi.org/10.1039/C3TA10559H).
- 156-. Y. Wang, S. F. Yu, C. Y. Sun, T. J. Zhu, H. Y. Yang. MnO₂/onion-like carbon nanocomposites for pseudocapacitors. *J. Mater. Chem.*, 2012. 22(34): pp. 17584-17588. DOI: [10.1039/c2jm33558a](https://doi.org/10.1039/c2jm33558a).
- 157-. Y. Wang, Z. J. Han, S. F. Yu, R. R. Song, H. H. Song, K. Ostrikov, H. Y. Yang. Core-leaf onion-like carbon/MnO₂ hybrid nano-urchins for rechargeable lithium-ion batteries. *Carbon*, 2013. 64: pp. 230-236. DOI: <https://doi.org/10.1016/j.carbon.2013.07.057>.
- 158-. J. Luszczyn, M. E. Plonska-Brzezinska, A. Palkar, A. T. Dubis, A. Simionescu, D. T. Simionescu, B. Kalska-Szostko, R. Winkler, L. Echegoyen. *Chem. Eur. J.*, 2010, 16(16): pp. 4870-4880. DOI: <https://doi.org/10.1002/chem.200903277>.
- 159-. J. Breczko, M. E. Plonska-Brzezinska, L. Echegoyen. Electrochemical oxidation and determination of dopamine in the presence of uric and ascorbic acids using a carbon nano-onion and poly(diallyldimethylammonium chloride) composite. *Electrochim. Acta*, 2012. 72: pp. 61-67. DOI: <http://dx.doi.org/10.1016/j.electacta.2012.03.177>.
- 160-. J. P. Bartolome, A. Fragoso. Electrochemical detection of nitrite and ascorbic acid at glassy carbon electrodes modified with carbon nano-onions bearing electroactive moieties. *Inorganica Chim. Acta*, 2017. 468: pp. 223-231. DOI: <https://doi.org/10.1016/j.ica.2017.06.024>.
- 161-. J. P. Bartolome, L. Echegoyen, A. Fragoso. Reactive carbon nano-onion modified glassy carbon surfaces as DNA sensors for human Papillomavirus oncogene detection with enhanced sensitivity. *Anal. Chem.*, 2015. 87(13): pp. 6744-6751. DOI: [10.1021/acs.analchem.5b00924](https://doi.org/10.1021/acs.analchem.5b00924).

Chapter 2

Enzyme kinetics study on the inhibition of free and immobilized horseradish peroxidase by 2,4,5-T, 2,4-D and glyphosate

Abstract

The inhibitory effect of 2,4,5-T, 2,4-D, glyphosate and paraquat on H_2O_2 -catalyzed activity of free and immobilized horseradish peroxidase for oxidation of 3,3',5,5'-Tetramethylbenzidine (TMB) has been investigated by kinetic measurements using spectrophotometry analysis. 2,4,5-T, 2,4-D and glyphosate inhibit the H_2O_2 -catalyzed activity of the enzyme following a competitive mechanism, while paraquat does not have effect according to Lineweaver-Burk kinetic analysis. The inhibitory effect on free horseradish peroxidase follows the order 2,4,5-T > 2,4-D > glyphosate with K_i values of 211, 555 and 889 μM , while on immobilized horseradish peroxidase follow the same order with nearly the same of K_i values of 213, 558 and 890 respectively. The result suggests that these pesticides interact with the active site of the enzyme competing with substrate H_2O_2 and inhibiting the enzyme activity even after being immobilized.

Keywords: peroxidase; herbicides; enzyme inhibition; spectroscopy.

2.1. Introduction

As described in Chapter 1, agricultural pesticides are defined as substances intended for controlling any pest, including unwanted plant or animal species during the production, distribution and processing of agricultural products or animal feeds. These substances are components of a formulation responsible for some direct or indirect biological activity against pests and diseases or for regulating the metabolism and/or growth of crops [1]. Pesticides are toxic substances that affect ecosystems and can cause several health problems such as neurological and bone marrow disorders, immunological diseases, etc. when they enter the food chain.

Among the many existing pesticides, 2,4,5-trichlorophenoxyacetic acid (2,4,5-T), 2,4-dichlorophenoxyacetic acid (2,4-D) and N-(phosphonomethyl)glycine (glyphosate) are some of the most common herbicides used in the agricultural industry. The phenoxy herbicides, either as acid, amine salt or ester, are used as weed control to defoliate broad-leafed plants [2]. On the other hand, glyphosate is an organophosphorous compound that blocks the activity of the enzyme enolpyruvylshikimate-3-phosphate synthase and is the most frequently used herbicide worldwide to date [3].

Peroxidases (EC 1.11.1.X) are hydrogen peroxide (H_2O_2) catalyzing enzymes naturally associated with the oxidation of wide range of phenolic as well as non-phenolic substrates. These enzymes found in all living organisms including bacteria, fungi, algae, plants and animals. The plant peroxidases, belonging to the class III peroxidase, are involved in various vital processes of plant growth and development throughout the plant life cycle including cell wall metabolism, lignification, suberization, reactive oxygen species metabolism, auxin metabolism, fruit growth and ripening, defense against pathogens etc. Peroxidases have used in several applications such as development of analytical

and diagnostic kits, de-colorization of industrial dyes, bioremediation of phenolic compounds, pulp and paper industry, hair dyeing, immunoassays, organic polymer synthesis and grafting, elimination of odorous compounds and biosensor. In biosensor application, peroxidases were also used as biorecognition element and labeling enzyme for biosensor development [4,5].

Sensing of peroxidases toward analytes can rely on catalysis of the analytes by the enzyme and inhibitory effect of the analytes on the catalytic activity of the enzyme. Based on analyte catalysis, peroxidase from horseradish has been widely used for developing enzymatic biosensors [6,7] to detect a wide variety of catalyzable compounds such as phenol and related aromatic compounds [8], antioxidants (butylated hydroxyanisole and propyl gallate) [9] and polyphenol [10], and inhibitors such as glyphosate [11-15], copper (II) ions [16], nitric oxide [17], sulfide [18], zinc ions [19] and thiodicarb [20]. Glyphosate was found to be non-competitive inhibitor on horseradish peroxidase immobilized electrochemically on sulfonated polymer matrix using H_2O_2 as substrate [11].

In this chapter, we compare the inhibitory effects of 2,4,5-T, 2,4-D, paraquat and glyphosate (Figure 2.1) on the reaction reduction activity of free and immobilized HRP using H_2O_2 and fixed TMB as substrates. The kinetic parameters and inhibition constants were measured, and an inhibition mechanism is proposed on the basis of the kinetic results.

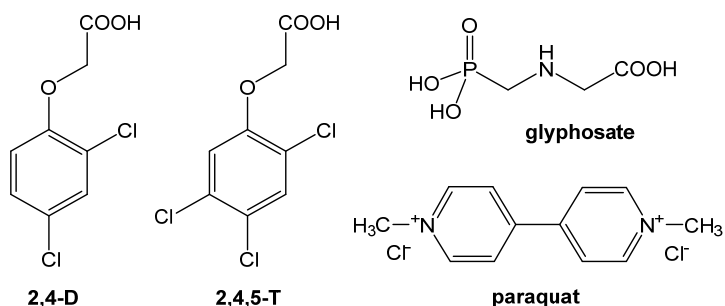


Figure 2.1. Structures of the studied pesticides.

2.2. Experimental

2.2.1 Materials

All chemicals were used as received without any further purification. Peroxidase from Horseradish (442.5 mg containing 113 purpurogallin units/mg), viologen dichloride hydrate (paraquat), glyphosate, 2,4-D, tyrosinase from mushroom (9.3 mg containing 2687 units/mg), biotinamidocaproyl labeled peroxidase (prepared from type VI horseradish peroxidase containing biotin content 2.6 mol/mol and 250 units/mg of protein), Phosphate Buffered Saline (containing 0.138 M NaCl and 0.0027 M KCl), 3,3',5,5'-tetramethylbenzidine (>99% for assay in 100 mg glass bottle) and 3,3',5,5'- tetramethylbenzidine (TMB) Liquid Substrate System for ELISA were purchased from Sigma-Aldrich. 2,4,5-T was purchased from Tokyo Chemical Industry Co. Ltd. (TCI).

96-well microtiter plates (flat form, individually wrapped) and Thermo Scientific™ Pierce™ High Binding Streptavidin Coated Plates were purchased from Fisher Scientific. Water was purified using a Milli-Q water purification system (Millipore) to a resistivity of 18.2 MΩ·cm.

2.2.2 Immobilization of biotinylated peroxidase on Streptavidin Coated Plates

Biotinylated peroxidase was immobilized on streptavidin coated plates based on affinity interaction of labeling biotin on the enzyme molecules with streptavidin immobilized on the coated plates (see Scheme 2.1) using a similar method as previously reported [21]. 100 μL of solution of biotinylated HRP (1 mg/ml) in 0.01 M Phosphate Buffered Saline (PBS) were added into every well of streptavidin coated plate for 3 hours of incubation. After recovering the biotinylated HRP solution, the wells were washed with PBS Tween 4 times, then stored in the fridge when not in use.

2.2.3 HRP activity and pesticide inhibition assays

Absorbances were recorded spectrophotometrically on a SpectraMax 340PC Microplate Reader at 650 nm on 96-well microplates at 25°C. All measurements were performed in 4 replicates in 0.01 M phosphate buffer pH 6.5 containing 0.138 M NaCl and 0.0027 M KCl.

HRP activities were measured at 650 nm based on the change of solution color of *oxidized TMB* for 2 min at 10 s intervals employing 0.07 mM and 0.9 mM of TMB:H₂O₂ (1:1) for free HRP and immobilized HRP, respectively, in the absence and presence of different concentrations of pesticides at different incubation times. The final concentrations of free and immobilized enzymes were 0.22583 nM and 0.25078 nM, respectively. Each well was estimated to have 0.06 pmol of immobilized enzyme. All measurements were done in triplicate.

To study the inhibition mechanism, HRP concentrations were varied from 0.0415 to 0.167 µg/mL. The kinetic parameters such as the Michaelis-Menten constant (K_m) and maximal velocity (V_{max}) of each pesticide were determined through Lineweaver-Burk plot analysis using various concentrations of H₂O₂ (0.0225 - 0.05 mM) and fixed TMB (0.08 mM) as substrates. The inhibition constants (K_i , K_{IS}) were determined from the slope of the linear dependence of the slopes and intercepts, respectively, of the Lineweaver-Burk plots versus the pesticide concentration (the so-called 'secondary plots', see Figures 2.5 and 2.7 for free and immobilized HRP, respectively).

2.3. Results and Discussion

2.3.1 Concentration effect of pesticides on the activity of free HRP

Figure 2.2 shows the effects of 2,4,5-T, 2,4-D, glyphosate and paraquat in range of concentrations from 0 µM to 0.4 mM on the redox reaction of horseradish

peroxidase after 1 and 30 minutes of incubation, respectively. From both figures, it can be seen that paraquat has no effect on the enzyme activity of peroxidase with the employed substrate, even after 1 hour of incubation. In contrast, 2,4,5-T, 2,4-D and glyphosate have a strong inhibitory effect on the enzyme activity that increases with incubation time. The percentage of inhibition increases with increasing concentrations of the pesticides. It can be seen from the figure, 2,4,5-T is the most potent inhibitor of the studied pesticides and the only one reached IC_{50} with 211 μ M. This result is the first report of comparison of inhibitory effects of these most used herbicides on the catalytic activity of HRP.

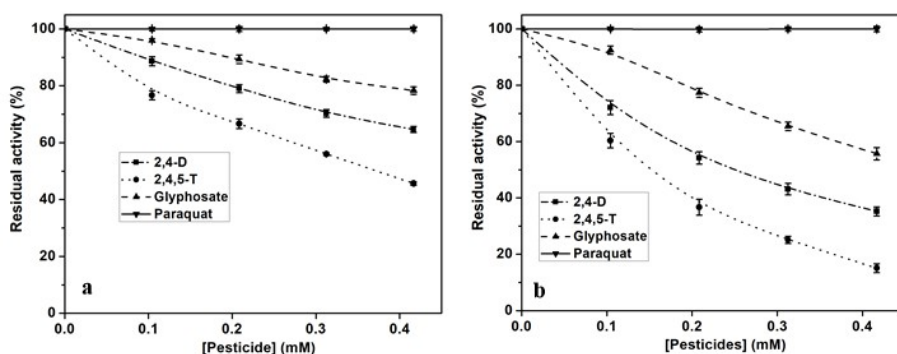
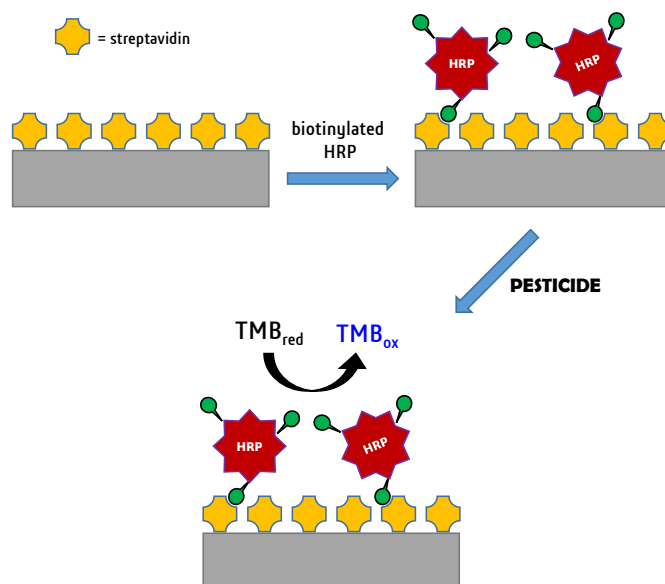


Figure 2.2. Effects of 2,4,5-T, 2,4-D, glyphosate and paraquat on the activity of free horseradish peroxidase a) after 1 min incubation, b) after 30 min of incubation. Conditions: 10 mM phosphate buffered saline pH 6.5, 25°C.

2.3.2 Concentration effect of pesticides on the activity of immobilized HRP

To study the inhibition of immobilized HRP, the biotinylated enzyme was immobilized on streptavidin-coated microtiter plates. After incubation with the pesticide inhibitor, the activity was measured using TMB (Scheme 2.1)



Scheme 2.1. Schematic representation of affinity immobilization of biotinylated HRP on streptavidin-coated plates.

Figure 2.3 shows the effect of 2,4,5-T, 2,4-D, glyphosate and paraquat in range of concentrations from 0 μM to 0.4 mM on the activity of immobilized horseradish peroxidase after 1 and 30 minutes of incubation, respectively. From both figures, it can be seen that paraquat has also no effect on the enzyme activity of peroxidase with the employed substrate, even after 1 hour of incubation. In contrast, 2,4,5-T, 2,4-D and glyphosate have a strong inhibitory effect on the enzyme activity that increases with incubation time. The percentage of inhibition increases with increasing concentrations of the pesticides. It can be seen from the figure, 2,4,5-T is the most potent inhibitor of the studied pesticides. However, none of these herbicides reached the IC_{50} , the difference of inhibition degree between free and immobilized horseradish peroxidase might be caused by several factors, such as heterogeneity of the enzyme/inhibitor interface, substrate concentrations and enzyme concentrations.

According to Arduini [22], in the case of reversible inhibition using free enzyme in solution, the enzyme concentration does not affect the degree of inhibition if the enzyme concentration is lower than the concentration of the inhibitor. The free enzyme in solution is well distributed in the solution compared to the immobilized enzyme which is attached to the microplate in a way that its contact with the solution environment is notably less efficient than for the free enzyme in solution. Other factors should be employed to accelerate contact between enzyme and inhibition including stirring. On the other hand, substrate concentration is another factor which affects the inhibition degree and the highest inhibition can be obtained using substrate at a concentration lower than that of the inhibitor. It can also be seen in the formula of the figure 1.7A that the inhibition degree decreases with increased concentration of substrate for the same concentration of the enzyme. The above results thus suggest the occurrence of competitive inhibition, which was verified in the next step.

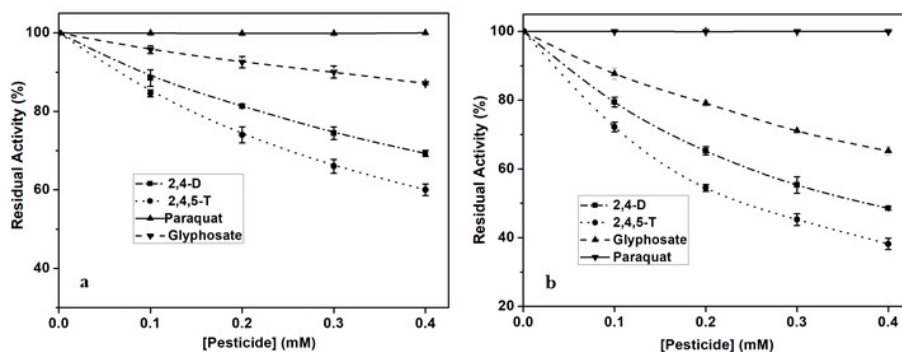


Figure 2.3. Effects of 2,4,5-T, 2,4-D, glyphosate and paraquat on the activity of the immobilized horseradish peroxidase for redox reactions of TMB:H₂O₂ (1:1) a) after 1 min incubation, b) after 30 min of incubation. Condition 10 mM phosphate buffered saline pH 6.5, 25°C.

2.3.3 Inhibition mechanism of 2,4,5-T, 2,4-D and glyphosate on the activity of free HRP

Reversible inhibitors bind noncovalently to the enzyme, while irreversible inhibitors commonly form covalent bonds with the enzyme or react with residues involved in catalysis to modify chemically the active site, as explained in Chapter 1. To investigate the inhibition mechanism, the dependence of the enzyme activity versus enzyme concentration in the presence of increasing concentrations of the pesticides was determined, in which a family of straight lines were obtained as seen in Figure 2.4. As a consequence of the inhibition, a decrease in the slope of the straight line with increasing of concentration of pesticides was observed, which suggested that the enzyme undergoes a reversible inhibition [23].

The reversible inhibitors can be classified in 4 groups (competitive, uncompetitive, noncompetitive and mixed-type inhibitors) [24]. The kinetic behavior of horseradish peroxidase during the catalysis of TMB:H₂O₂ in the presence of the pesticides was studied using the Lineweaver-Burk plots (Figure 2.5) to identify the type of inhibitor to which each pesticide belongs to and the corresponding inhibition parameters. As can be seen, 2,4,5-T, 2,4-D, and glyphosate gave a family of lines with different slopes and the same intercept, indicating a competitive inhibition mechanism. This means that the three studied pesticides are bound to the free enzyme but not to the enzyme-substrate complex. This results in an increase of K_m of peroxidase without changing V_{max} .

The inhibitor constant (K_i) for the binding of these pesticides with the free enzyme were estimated from the slope of the of apparent Michaelis-Menten constant (K_m^{app}) versus inhibitor concentration to be 0.889, 0.555 and 0.211 mM for glyphosate, 2,4-D and 2,4,5-T, respectively (Figure 2.5, insets).

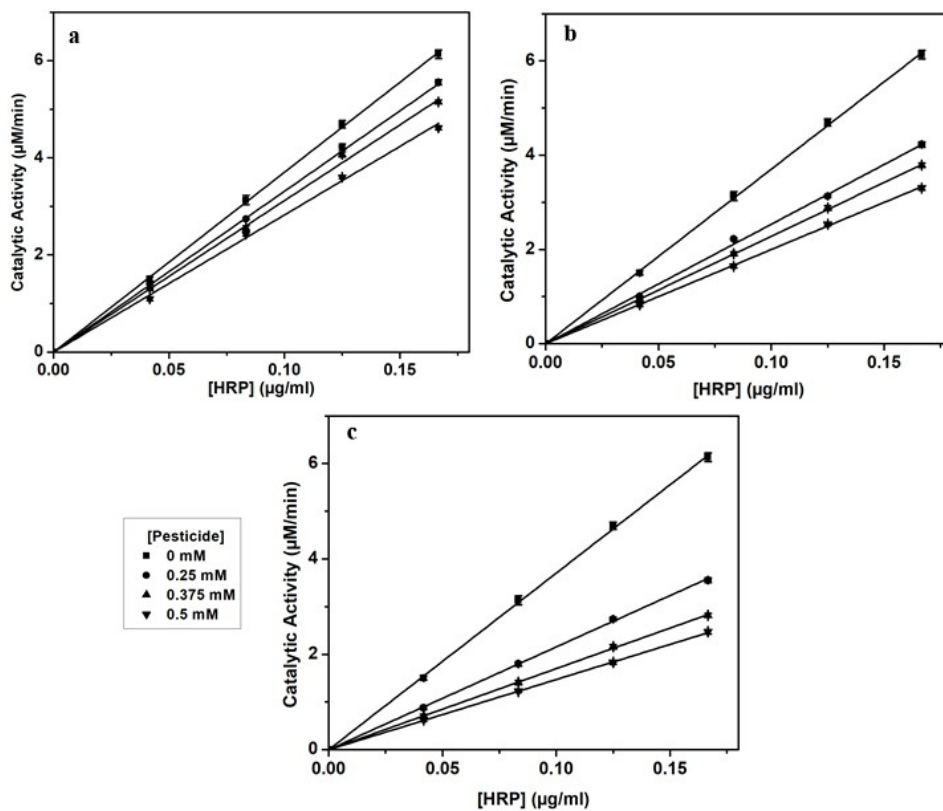


Figure 2.4. Effect of glyphosate (a), 2,4-D (b) and 2,4,5-T (c) on the activity of Horseradish peroxidase at different enzyme concentrations. Condition: 10 mM phosphate buffered saline pH 6.5, 25°C.

This inhibition constant corresponds to the degree of dissociation of the enzyme-inhibitor complex and the affinity of the inhibitors for the enzyme at 50% of inhibition so the smaller K_i the more potent the inhibitor is. Consequently, the inhibitory affinity of the studied pesticides follows the order 2,4,5-T > 2,4-D > glyphosate.

Based on the inhibitory effect of the pesticides, horseradish peroxidase biosensor is more sensitive toward 2,4,5-T comparison to 2,4-D and glyphosate.

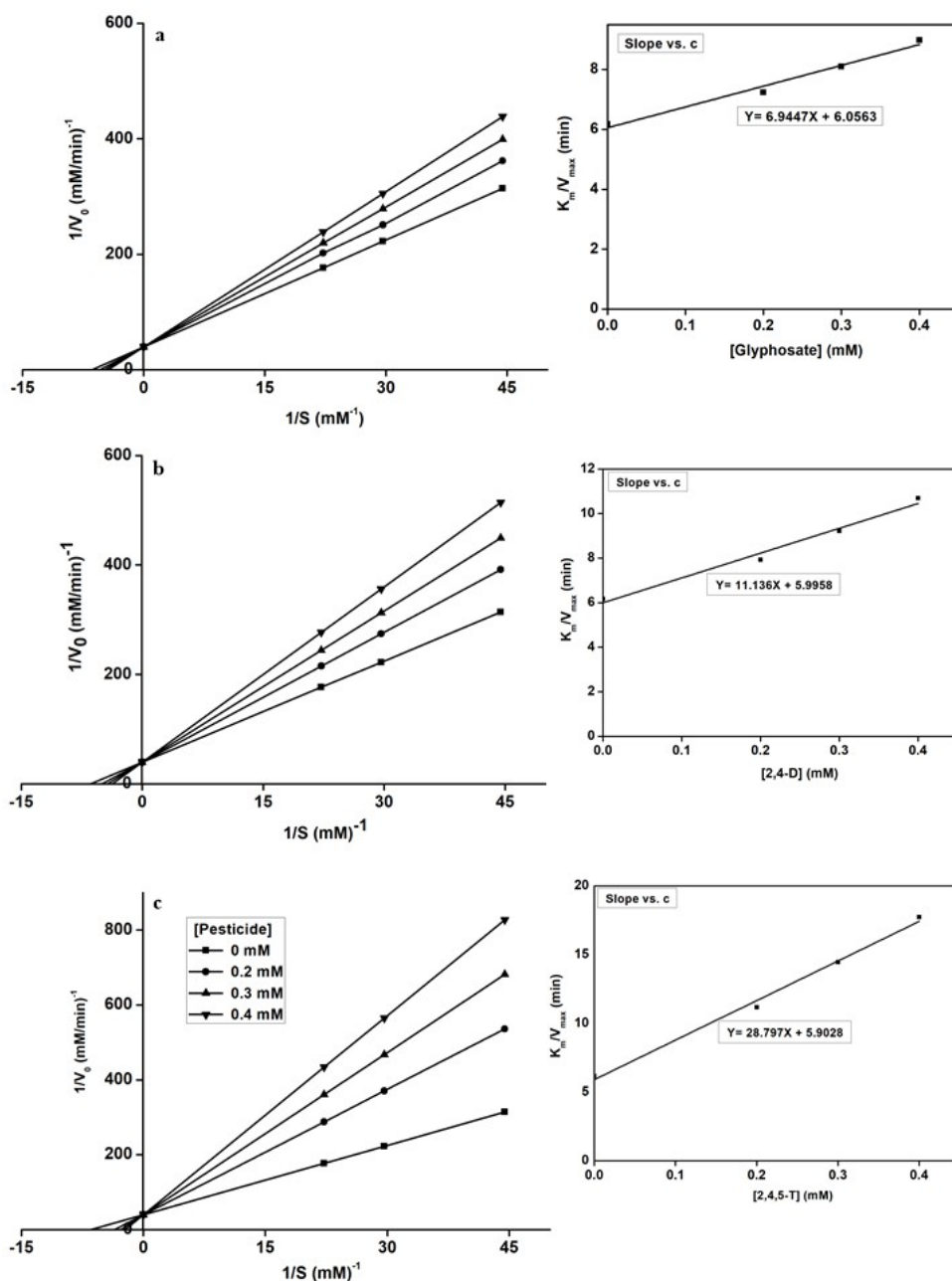


Figure 2.5. Lineweaver-Burk plots for the inhibition of glyphosate (a), 2,4-D and 2,4,5-T on horseradish peroxidase at different concentrations of pesticides. Insets: secondary plots (slope vs. concentration) used for the determination of inhibition constants. Condition phosphate buffered saline pH 6.5, 25°C.

2.3.4 Inhibition mechanism of 2,4,5-T, 2,4-D and glyphosate on the activity of immobilized HRP

The kinetic behavior of immobilized horseradish peroxidase during the catalysis of TMB:H₂O₂ in the presence of the pesticides was studied using the Michaelis-Burk plots (Figure 2.6) to identify type of inhibitor which each pesticide belongs to and degree of its inhibition on the enzyme activity.

As can be seen, 2,4,5-T, 2,4-D, and glyphosate gave a family of lines with different slopes and the same intercept indicating a competitive inhibition mechanism meaning that the 3 studied pesticides are also bound to active site of the immobilized enzyme but not to the enzyme-substrate complex. This results in an increase of K_m of peroxidase without changing V_{max} . The inhibitor constant (K_i) for the binding of these pesticides with the immobilized enzyme were estimated from the slope of the of apparent Michaelis-Menten constant (K_m^{app}) versus inhibitor concentration to be 0.890, 0.558 and 0.214 mM for glyphosate, 2,4-D and 2,4,5-T respectively (Figure 2.7, inset and table 1).

Based on this result, the HRP immobilization via affinity binding between biotin linked with enzyme and streptavidin coated plate does not change significantly the conformation of the enzyme structure, and, consequently, the kinetic parameters. This follows the principle of affinity binding exploits for application in enzyme immobilization in which the remarkable selectivity of the interaction, control orientation of immobilized enzyme and minimal conformational changes caused by this type [25].

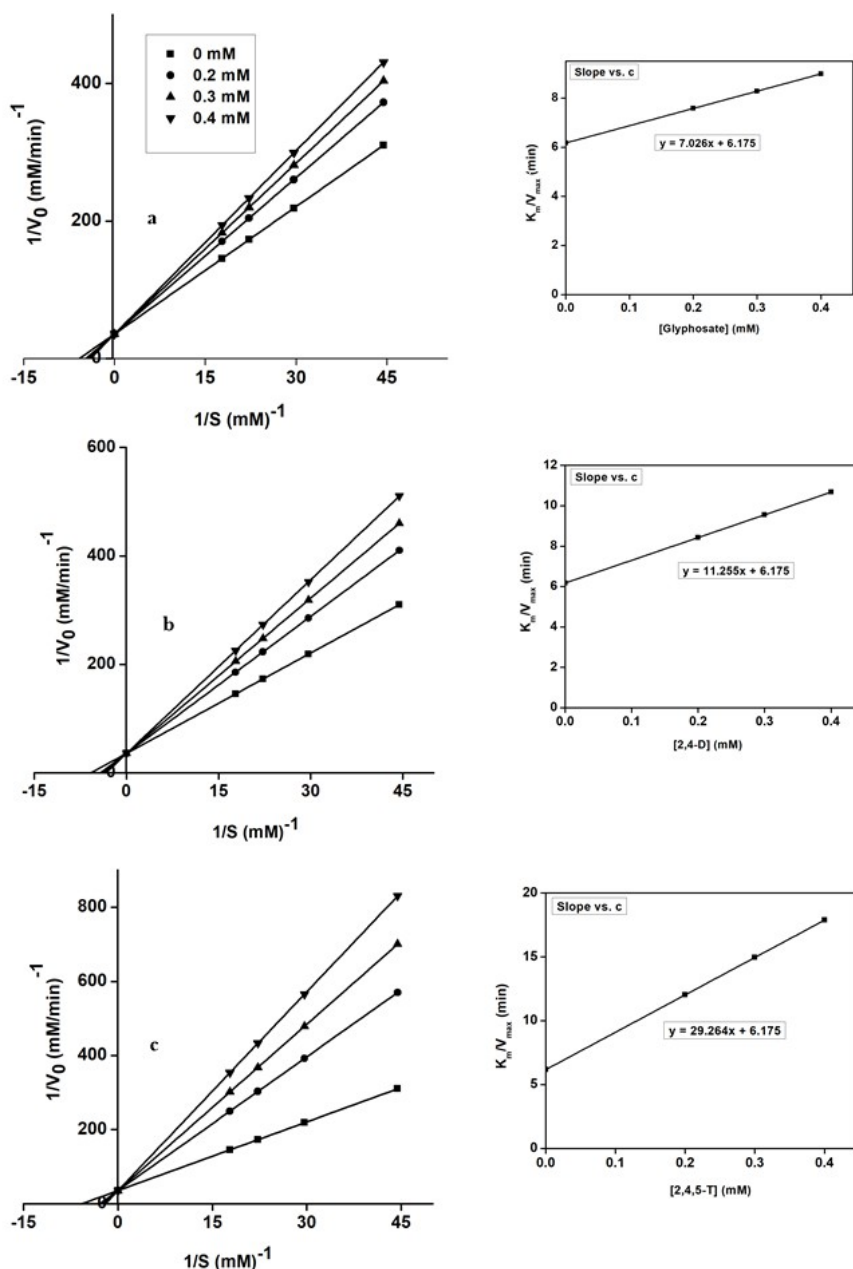


Figure 2.6. Lineweaver-Burk plots for the inhibition of glyphosate (a), 2,4-D and 2,4,5-T on immobilized horseradish peroxidase at different concentrations of pesticides. Insets: secondary plots (slope vs. concentration) used for the determination of inhibition constants. Condition phosphate buffered saline pH 6.5, 25°C.

Table.2.1. Constants and mechanism of inhibition of the studied pesticides on catalytic activity of free and immobilized HRP.

Pesticide	K_i (μM)		Inhibition mechanism	
	Free HRP	Immobilized HRP	Free HRP	Immobilized HRP
<i>2,4,5-T</i>	211 \pm 3	214 \pm 4	Competitive	Competitive
<i>2,4-D</i>	555 \pm 4	558 \pm 5	Competitive	Competitive
<i>Glyphosate</i>	889 \pm 7	890 \pm 2	Competitive	Competitive

2.5 Conclusions

In this Chapter we have studied for the first-time comparison of the inhibitory activity of 2,4,5-T, 2,4-D and glyphosate on the activity of free and immobilized horseradish peroxidase. The results illustrate that 2,4,5-T, 2,4-D and glyphosate inhibit both free and immobilized enzyme following a competitive mechanism according to Lineweaver-Burk kinetic analysis.

The inhibitory effect follows the order 2,4,5-T > 2,4-D > glyphosate for both enzyme forms. The results suggest that these pesticides interact with the active site of the enzyme, hindering the access of the substrate to the active site even after being immobilized. The fact that the inhibition of immobilized HRP does not reach 100% may hinder the sensitivity of a pesticide biodetection system. However, this possible disadvantage could be overcome using innovative immobilization strategies. Work in this direction will be presented in Chapter 5.

References

- [1] C. D. S. Tomlin (Ed.), *The pesticide manual: a world compendium*, 15th ed. British Crop Protection Council, 2009.
- [2] E. Kennepohl, I. C. Munro, J. S. Bus, *Phenoxy Herbicides*, in: *Hayes' Handbook of Pesticide Toxicology (Third Edition)*. Krieger R., Ed. Academic Press, New York, 2010, Chapter 84, pp. 1829-1847.
- [3] D. Farmer, *Inhibitors of Aromatic Acid Biosynthesis*, in: *Hayes' Handbook of Pesticide Toxicology (Third Edition)*. Krieger R., Ed. Academic Press, New York, 2010, Chapter 92, pp. 1967-1972.
- [4] V. P. Pandey, M. Awasthi, S. Singh, S. Tiwari, U. N. Dwivedi. A comprehensive review on function and application of plant peroxidase. *Biochem. Anal. Biochem.*, 2017. 6(1). DOI: 10.4172/2161-1009.1000308.
- [5] M. Hamid, K. Rehman. Potential application of peroxidase. *Food Chemistry*, 2009. 115(4): pp. 1177-1186. DOI: <https://doi.org/10.1016/j.foodchem.2009.02.035>.
- [6] G. V. Presnova, M. Y. Rybcova, A. M. Egorov. Electrochemical biosensors based on horseradish peroxidase. *Russ. J. Gen. Chem.*, 2008. 78(12): pp. 2482-2488.
- [7] E. E. Ferapontova. Direct peroxidase bioelectrocatalysis on a variety of electrode materials. *Electroanalysis*, 2004. 16(13-14): pp. 1101-1112. DOI: <https://doi.org/10.1002/elan.200403003>.
- [8] T. Ruzgas, J. Emnéus, L. Gorton, G. Marko-Varga. The development of a peroxidase biosensor for monitoring phenol and related aromatic compounds. *Anal. Chim. Acta*, 1995. 311(3): pp. 245-253. DOI: [https://doi.org/10.1016/0003-2670\(95\)00047-4](https://doi.org/10.1016/0003-2670(95)00047-4).
- [9] L. Wu, W. Yin, K. Tang, D. Li, K. Shao, Y. Zuo, J. Ma, J. Liu, H. Han. Enzymatic biosensor of horseradish peroxidase immobilized on Au-Pt nanotube/Au-graphene for the simultaneous determination of antioxidants. *Anal. Chim. Acta*, 2016. 933: pp. 89-96. DOI: <https://doi.org/10.1016/j.aca.2016.06.020>.
- [10] S. Imabayashi, Y. Kong, M. Watanabe. Amperometric biosensor for polyphenol based on horseradish peroxidase immobilized on gold electrodes. *Electroanalysis*, 2001. 13(5): pp. DOI: [https://doi.org/10.1002/1521-4109\(200104\)13:5<408::AID-ELAN408>3.0.CO;2-2](https://doi.org/10.1002/1521-4109(200104)13:5<408::AID-ELAN408>3.0.CO;2-2).
- [11] E. A. Songa, O. A. Arotiba, J. H. O. Owino, N. Jahed, P. G. L. Baker, E. I. Iwuoha. Electrochemical detection of glyphosate herbicide using horseradish peroxidase immobilized on sulfonated polymer matrix. *Bioelectrochemistry*, 2009. 75(2): pp. 117-123. DOI: <https://doi.org/10.1016/j.bioelechem.2009.02.007>.

- [12] E. A. Songa, T. Waryo, N. Jahed, P. G. L. Baker, B. V. Kgarebe, E. I. Iwuoha. Electrochemical nanobiosensor for glyphosate herbicide and its metabolite. *Electroanalysis*, 2009. 21(3-5): pp. 671-674. DOI: 10.1002/elan.200804452.
- [13] E. A. Songa, V. S. Somerset, T. Waryo, P. G. L. Baker, E. I. Iwuoha. Amperometric nanobiosensor for quantitative determination of glyphosate and glufosinate residues in corn samples. *Pure App. Chem.*, 2009. 81(1): pp. 123-139. DOI: 10.1351/PAC-CON-08-01-15.
- [14] Q. Zhang, G. Xu, L. Gong, H. Dai, S. Zhang, Y. Li, Y. Lin. An enzyme-assisted electrochemiluminescent biosensor developed on ordered mesoporous carbon substrate for ultrasensitive glyphosate sensing. *Electrochim. Acta*, 2015. 186: pp. 624-630. DOI: <https://doi.org/10.1016/j.electacta.2015.10.081>.
- [15] G. C. Oliveira, S. K. Moccelini, M. Castilho, A. J. Terezo, J. Possavatz, M. R. L. Magalhães, E. F. G. C. Dores. Biosensor based on atemoya peroxidase immobilised on modified nanoclay for glyphosate biomonitoring. *Talanta*, 2012. 98 pp. 130-136. DOI: <https://doi.org/10.1016/j.talanta.2012.06.059>.
- [16] M. Moyo, J. O. Okonkwo, N. M. Agyei. Optimization of horseradish peroxidase immobilization on glassy carbon electrode based on maize tassel-multiwalled carbon nanotubes for sensitive copper(II) ion detection. *Int. J. Electrochem. Sci.*, 2014. 9: pp. 1439-1453.
- [17] E. Casero, M. Darder, F. Pariente, E. Lorenzo. Peroxidase enzyme electrodes as nitric oxide biosensors. *Anal. Chim. Acta*, 2000. 403(1-2): pp. 1-9. DOI: [https://doi.org/10.1016/S0003-2670\(99\)00555-3](https://doi.org/10.1016/S0003-2670(99)00555-3).
- [18] H. Sun, Z. Liu, C. Wu, P. Xu, X. Wang. Amperometric inhibitive biosensor based on horseradish peroxidase-nanoporous gold for sulfide determination. *Sci. Rep.*, 2016. 6: 30905. DOI: 10.1038/srep30905.
- [19] M. Moyo. Horseradish peroxidase biosensor to detection zinc ions in aqueous solutions. *Open Journal of Applied Biosensor*, 2014. 3(1): pp. 1-7. DOI: 10.4236/ojab.2014.31001 .
- [20] S. K. Moccelini, I. C. Vieira, F. D. Lima, B. G. Lucca, A. M. J. Barbosa, V. S. Ferreira. Determination of thiodicarb using a biosensor based on alfalfa sprout peroxidase immobilized in self-assembled monolayers. *Talanta*, 2010. 82(1): pp. 164-170. DOI: <https://doi.org/10.1016/j.talanta.2010.04.015>.
- [21] P. Ertl, S. R. Mikkelsen. Electrochemical biosensor array for the identification of microorganism based on lectin-lipopolysaccharide recognition. *Anal. Chem.*, 2001. 73(17): pp. 4241-4248. DOI: 10.1021/ac010324l.
- [22] F. Arduini, A. Amine. Biosensors based on enzyme inhibition. *Adv Biochem Eng Biotechnol*, 2014. 140: pp. 299-326. DOI: 10.1007/10_2013_224.

- [23] J. Yang, R. Chang, S. Ge, M. Zhao, C. Liang, L. Xiong, Q. Sun. The inhibition effect of starch nanoparticles on tyrosinase activity and its mechanism. *Food Funct.*, 2016. 7(12): pp. 4801-4815. DOI: 10.1039/C6FO01228K.
- [24] R. R. Ramsay, K. F. Tipton. Assessment of enzyme inhibition: A review with example from the development of monoamine oxidase and cholinesterase inhibitory drugs. *Molecules*, 2017. 22(7): pp. 1192. DOI: <https://doi.org/10.3390/molecules22071192>.
- [25] N. R. Mohamad, N. H. C. Marzuki, N. A. Buang, F. Huyop, R. A. Wahab. An overview of technologies for immobilization of enzymes and surface analysis techniques for immobilized enzymes. *Biotechnol. Biotechnol. Equip.*, 2015. 29(2): pp. 205-220. DOI: <http://dx.doi.org/10.1080/13102818.2015.1008192>.

Chapter 3

Kinetic, spectroscopic and computational docking study of the inhibitory effect of the pesticides 2,4,5-T, 2,4-D and glyphosate on the diphenolase activity of mushroom tyrosinase¹

Abstract

The inhibitory effect of 2,4,5-T, 2,4-D, glyphosate and paraquat on the diphenolase activity of mushroom tyrosinase for oxidation of L-DOPA has been investigated by kinetic measurements, fluorescence spectroscopy and computational docking analysis. 2,4,5-T and 2,4-D inhibit the diphenolase activity of the enzyme following a competitive mechanism, while glyphosate is a mixed inhibitor according to Lineweaver-Burk kinetic analysis. The inhibitory activity follows the order glyphosate > 2,4,5-T > 2,4-D with IC₅₀ values of 65, 90 and 106 μM, respectively. Intrinsic tyrosinase fluorescence quenching and computational docking analysis suggest that 2,4,5-T and 2,4-D interact with the active site of the enzyme through hydrophobic interactions, while glyphosate interacts with the external lysine and arginine residues of the enzyme by hydrogen bonding and hydrophilic interactions inducing conformational changes in the protein structure.

Keywords: tyrosinase; herbicides; enzyme inhibition; fluorescence spectroscopy; computational docking analysis

¹ Part of this Chapter has been published in V. Sok, A. Fragoso, *International Journal of Biological Macromolecules* **2018**, *48*, 136-143.

3.1. Introduction

As described in Chapter 1, agricultural pesticides are defined as substances intended for controlling any pest, including unwanted plant or animal species during the production, distribution and processing of agricultural products or animal feeds. These substances are components of a formulation responsible for some direct or indirect biological activity against pests and diseases or for regulating the metabolism and/or growth of crops [1]. Pesticides are toxic substances that affect ecosystems and can cause several health problems such as neurological and bone marrow disorders, immunological diseases, etc. when they enter the food chain.

Among the many existing pesticides, 2,4,5-trichlorophenoxyacetic acid (2,4,5-T), 2,4-dichlorophenoxyacetic acid (2,4-D) and N-(phosphonomethyl)glycine (glyphosate) are some of the most common herbicides used in the agricultural industry. The phenoxy herbicides, either as acid, amine salt or ester, are used as weed control to defoliate broad-leafed plants [2]. On the other hand, glyphosate is an organophosphorous compound that blocks the activity of the enzyme enolpyruvylshikimate-3-phosphate synthase and is the most frequently used herbicide worldwide to date [3].

Tyrosinase (EC. 1.14.18.1), is a multifunctional copper containing enzyme belonging to oxidase family, distributed in microorganisms, animals, plants and humans. This enzyme plays a crucial role in melanogenesis by catalyzing two important steps of the synthesis. First, it oxidizes monophenols by *o*-hydroxylation to a diphenol followed by oxidation of the corresponding product to *o*-quinone (diphenolase activity) [4,5]. Ultraviolet irradiation stimulates tyrosinase-catalyzed melanogenesis in the skin, which offer the opportunity for novel therapeutic approaches by minimizing acute and chronic photodamage in human skin [6]. Tyrosinase is also responsible for enzymatic browning of fresh

horticultural products following bruising, cutting or other damage to the cell [7]. Several families of compounds are known to effectively inhibit monophenolase and diphenolase tyrosinase activities such as kojic acid, polyphenols, flavonoids, benzaldehyde/benzoate derivatives, steroids, etc. [8] and there is an intense interest in the investigation of new tyrosinase inhibitors for biomedical [9], food [10] and cosmetic [11] industries.

The tyrosinase inhibitory effect of pesticides was first reported by Chen and Polatnick after studying the influence of glyphosate and 2,4-D on root induction in mung bean [12]. The growth inhibition was related with the effect of both herbicides on peroxidase and tyrosinase activities but the inhibition kinetics and mechanism were not reported. Since then, tyrosinase has been widely used as biorecognition element for developing enzymatic biosensors to detect a wide variety of pesticides [13] such as 2,4-D [14-16], atrazine [17-19] organophosphate [20] and carbamate pesticides [21,22]. Metal dithiocarbamates (Ziram®, Diram® and zinc diethyldithiocarbamate) were found to be competitive, mixed and non-competitive inhibitors, respectively, using phenol as substrate [22]. Inhibition of catechol oxidation by tyrosinase in the presence of atrazine is competitive [23] as well as in the presence of methyl-parathion and carbofuran [24] while diazinon and carbaryl are mixed inhibitors. The vast majority of these reports have focused mainly on the determination of analytical parameters and analysis of samples with very little emphasis on the mechanism of inhibition.

In this Chapter, we compare the inhibitory effects of 2,4,5-T, 2,4-D, paraquat and glyphosate (Figure 3.1) on the diphenolase activity of mushroom tyrosinase using L-DOPA as substrate. The kinetic parameters and inhibition constants were measured and a inhibition mechanism is proposed on the basis of intrinsic tyrosinase fluorescence measurements and computational docking analysis.

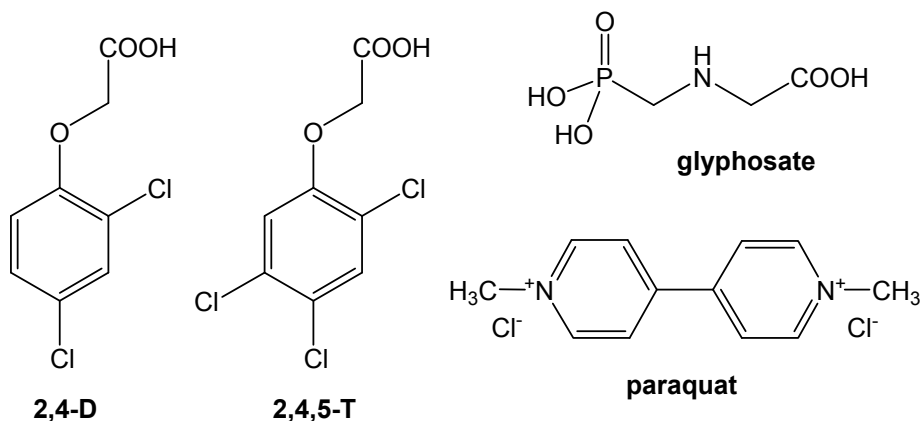


Figure 3.1. Structures of the studied pesticides.

3.2. Experimental

3.2.1 Materials

All chemicals were used as received without any further purification. Viologen dichloride hydrate (paraquat), glyphosate, 2,4-D, tyrosinase from mushroom (9.3 mg containing 2687 units/mg), Phosphate Buffered Saline (containing 0.138 M NaCl and 0.0027 M KCl) and 3,4-dihydroxy-L-phenylalanine (L-DOPA) were purchased from Sigma-Aldrich. 2,4,5-T was purchased from Tokyo Chemical Industry Co. Ltd. (TCI).

96-well microtiter plates (flat form, individually wrapped) were purchased from Fisher Scientific. Water was purified using a Milli-Q water purification system (Millipore) to a resistivity of 18.2 M Ω -cm.

3.2.2 Tyrosinase activity and pesticide inhibition assays

Absorbances were recorded spectrophotometrically on a SpectraMax 340PC Microplate Reader at 475 nm on 96-well microplates at 25°C. All measurements

were performed in 4 replicates in 0.01 M phosphate buffer pH 6.5 containing 0.138 M NaCl and 0.0027 M KCl.

Mushroom tyrosinase activities were measured at 475 nm based on the change of solution color of *oxidized L-DOPA* (1 mM) for 2 min at 2 s intervals in the absence and presence of different concentrations of pesticides at different incubation times. The final concentration of enzyme was 0.7 $\mu\text{g}/\text{mL}$. All measurements were done in triplicate.

To study the inhibition mechanism, tyrosinase concentrations were varied from 0.2 to 0.85 $\mu\text{g}/\text{mL}$. The kinetic parameters such as the Michaelis-Menten constant (K_m) and maximal velocity (V_{max}) of each pesticide were determined through Lineweaver-Burk plot analysis using various concentrations of L-DOPA (0.1 - 0.75 mM) as substrate. The inhibition constants (K_i , K_{is}) were determined from the slope of the linear dependence of the slopes and intercepts, respectively, of the Lineweaver-Burk plots versus the pesticide concentration (the so-called ‘secondary plots’, see Figure 3.4) [8]

3.2.3 Fluorescence studies

The fluorescence experiments were performed at 25°C and 37°C in a Cary Eclipse spectrofluorimeter equipped with a Peltier temperature control. The excitation wavelength was set at 280 nm. The spectra were recorded in 1-cm quartz cells in the wavelength interval of 290-400 nm at 1 nm intervals with excitation and emission slits of 10 nm and a scan rate of 240 nm/min. All measurements were carried out in triplicate and the average value of the fluorescence changes was used in the calculations. The total volume was corrected for the dilution effect due to the aliquot additions. The quartz cell was previously cleaned with concentrated nitric acid for 10 min, followed by extensive rinsing with ultrapure water and dried with nitrogen before the measurements. The enzyme

concentration used was 4 μM and measurements were made in the same buffer used for the kinetic studies, which was used to record the blank signal.

3.2.4 Computational docking study

The tyrosinase/pesticide structures were simulated using the crystal structure of *Agaricus bisporus* tyrosinase (PDB ID: 2Y9X) as .pdb file. Tropolone was removed from the active site and the enzyme was modeled using units A and E of the crystal structure in order to reduce the search area on the protein.

2,4,5-T and 2,4-D (deprotonated forms) were first energy-minimized at the PM3 level using Hyperchem 7.0 (Hypercube, Inc.), transformed to .mol2 files using Open Babel 2.4.1 [25] and used as input structures of the pesticides. Blind docking structures were generated using the free online tool MTiAutoDock 1.0 [26] that uses an AutoDock 4.2.6 algorithm to generate orientations/conformations of the protein/ligand structure [27].

For the docking of fully deprotonated glyphosate, the structure of the ligand was taken from the PDB structure with code 2AAY. A grid box of 40 \times 40 \times 40 points centered in the Cu1 atom with 0.375 Å spacing was used for the calculation. Protein/ligand interactions and structure visualization were carried out using BIOVIA Discovery Studio 2017 (Accelrys).

3.3. Results and Discussion

3.3.1 Concentration effect of pesticides on the diphenolase activity of tyrosinase

Figure 3.2 shows the effects of 2,4,5-T, 2,4-D, glyphosate and paraquat in range of concentrations from 0 μM to 200 μM on the oxidation of L-DOPA by mushroom tyrosinase after 1 and 30 minutes of incubation, respectively. From both figures, it can be seen that paraquat has no effect on the diphenolase activity of tyrosinase with the employed substrate, even after 1 hour of incubation. In

contrast, 2,4,5-T, 2,4-D and glyphosate have a strong inhibitory effect on the enzyme activity that increases with incubation time. The percentage of inhibition increases with increasing concentrations of the pesticides. As can be seen from Table 1, glyphosate is the most potent inhibitor of the studied pesticides with an IC_{50} of 65 μ M. This value is similar to that reported for kojic acid, an inhibitor commonly used as reference by many investigators [28].

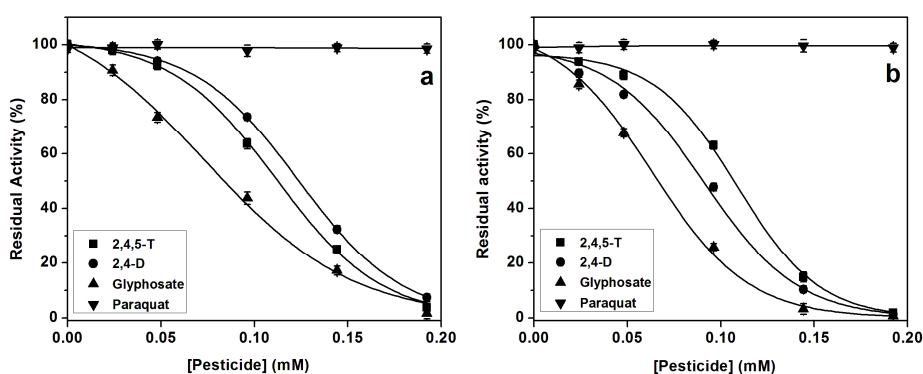


Figure 3.2. Effect of 2,4,5-T, 2,4-D, glyphosate and paraquat on the activity of mushroom tyrosinase for the oxidation of L-DOPA: a) after 1 min incubation, b) after 30 minutes of incubation. Conditions: 0.1 M phosphate buffer pH 6.5, 25°C.

3.3.2 Inhibition mechanism of 2,4,5-T, 2,4-D and glyphosate on the activity of tyrosinase

The dependence of the enzyme activity versus enzyme concentration in the presence of increasing concentrations of the pesticides gave a family of straight lines (Figure 3.3) with intercepts essentially equal to zero. This indicates a reversible inhibition since increasing inhibitor concentrations resulted in a decrease in the slopes of the lines.

The kinetic behavior of mushroom tyrosinase during the oxidation of L-DOPA in the presence of the pesticides was studied using the Michaelis-Menten formalism

by constructing double-reciprocal Lineweaver-Burk plots (Figure 3.4). As can be seen, 2,4,5-T and 2,4-D gave a family of lines with different slopes and the same intercept indicating a competitive inhibition mechanism meaning that they are bound to free enzyme but not to the enzyme-substrate complex. This results in an increase of K_m of tyrosinase without changing V_{max} . The inhibitor constant (K_i) for the binding of these pesticides with the free enzyme were estimated from the slope of the of apparent Michaelis-Menten constant ($K_{m\ app}$) versus inhibitor concentration to be 44 and 77 μM for 2,4,5-T and 2,4-D, respectively (Figure 3.4, inset and Table 3.1).

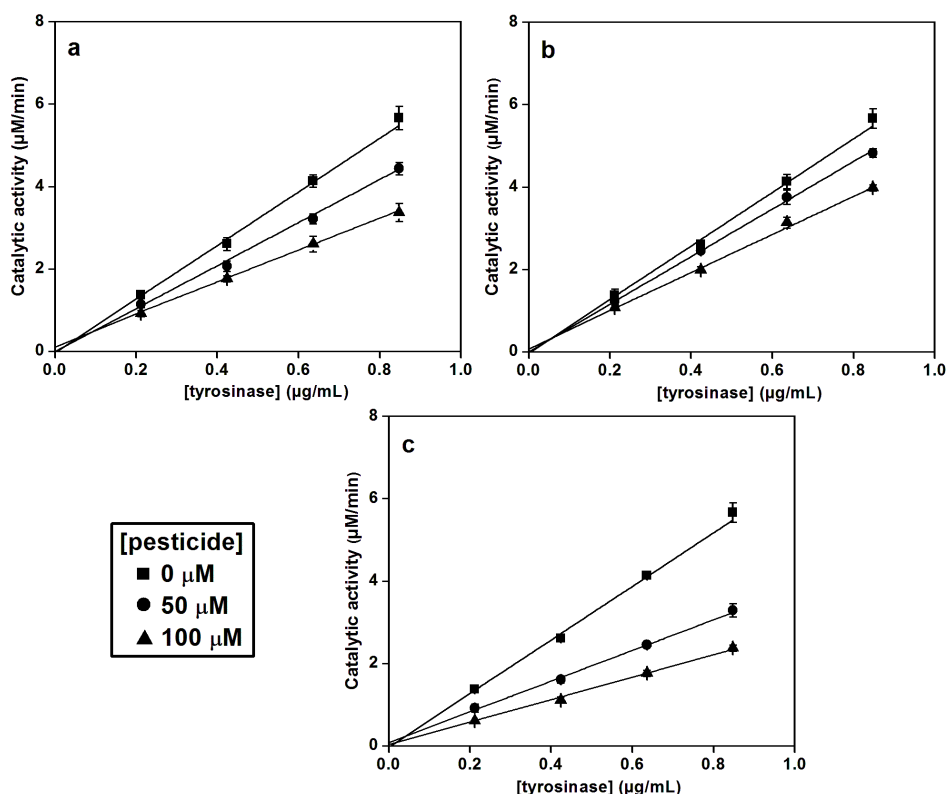


Figure 3.3. Effect of 2,4,5-T (a), 2,4-D (b) and glyphosate (c) on the activity of mushroom tyrosinase at different enzyme concentrations. Conditions: 0.1 M phosphate buffer pH 6.5, 25°C.

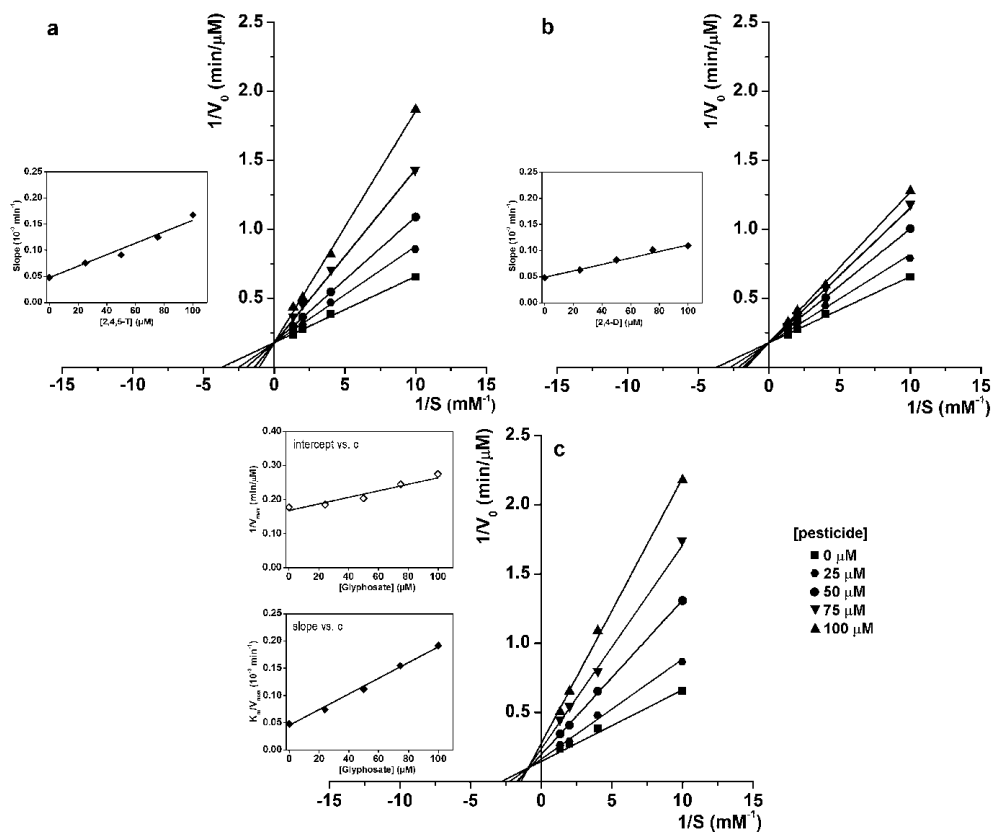


Figure 3.4. Lineweaver-Burk plots for the inhibition of 2,4,5-T (a), 2,4-D (b) and glyphosate (c) on mushroom tyrosinase at different concentrations of pesticide. Insets: Secondary plots (slope vs. concentration and intercept vs. concentration) used for the determination of inhibition constants. Conditions: 0.1 M phosphate buffer pH 6.5, 25°C.

Table 3.1. IC_{50} values and inhibition constants for the inhibition of mushroom tyrosinase by the studied pesticide.

Pesticide	IC_{50} (μM)	K_i (μM)	K_{is} (μM)	Inhibition mechanism
2,4,5-T	90 ± 4	40 ± 1	-	competitive
2,4-D	106 ± 7	77 ± 4	-	competitive
Glyphosate	65 ± 3	33 ± 2	183 ± 4	mixed

In the case of glyphosate, it can be seen that the Lineweaver-Burk plots gave a family of lines with different slopes and different Y-axis intercepts, indicating that glyphosate is a mixed-type inhibitor. This means that glyphosate not only binds with the free enzyme but also with the enzyme-substrate complex resulting in an increase of K_m and a decrease of V_{max} . The inhibitor constant (K_i) for glyphosate was $33 \mu\text{M}$ and the inhibitor constant of enzyme-substrate complex (K_{is}), obtained from the vertical intercepts versus glyphosate concentration, was found to be $183 \mu\text{M}$. This means that glyphosate interacts stronger with the free enzyme than with the enzyme-substrate complex. The K_i value is slightly lower than that recently reported for kojic acid ($36 \mu\text{M}$) [29] and demonstrates that glyphosate is a potent tyrosinase inhibitor.

3.3.3 Fluorescence studies

The kinetic results on the inhibitory activity of 2,4,5-T, 2,4-D and glyphosate on tyrosinase indicates that there is a direct interaction between the pesticides and the enzyme. Fluorescence quenching is a common method to study protein/ligand interactions since it is sensitive to conformational changes induced by the quencher [30]. In particular, tryptophan residues are responsible for the fluorescence of the enzyme at 330 nm when excited at 282 nm (Figure 3.5a). Addition of 2,4,5-T and 2,4-D in the concentration range of 0.5 to $20 \mu\text{M}$ induced a gradual quenching of the tyrosinase fluorescence with negligible changes in the peak maximum (see Figure 3.5b for 2,4,5-T). This suggests that these pesticides interact with tyrosinase but do not change the overall conformation of tyrosinase. Conversely, fluorescence quenching in the presence of glyphosate induced a 7 nm red shift in the emission maximum, indicating a slight change in the conformation of the enzyme (Figure 3.5c).

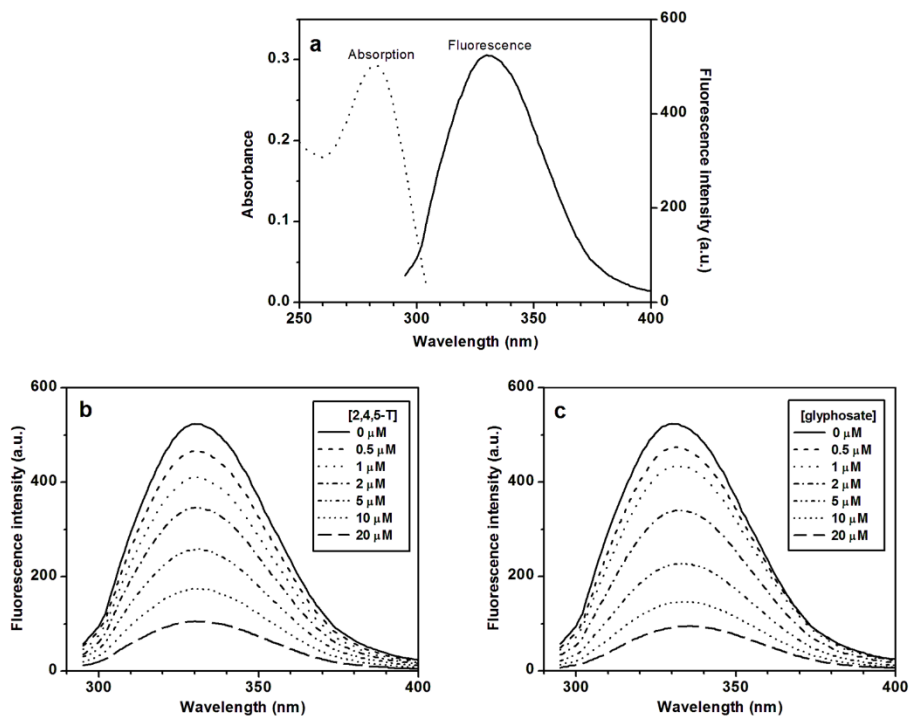


Figure 3.5: a) Absorption (·····) and emission (—) spectra of tyrosinase excited at 280 nm. b) Emission spectra of tyrosinase in the presence of different concentrations of 2,4,5-T. c) Emission spectra of tyrosinase in the presence of different concentrations of glyphosate. The spectra were recorded in phosphate buffer pH 6.5 at 25°C.

The fluorescence quenching was analyzed using the Stern-Volmer equation:

$$\frac{F_0}{F} = 1 + K_{SV}[Q] = 1 + \kappa_q \tau_0 [Q]$$

where F_0 and F are the fluorescence intensities before and after the addition of the pesticide (quencher), respectively, $[Q]$ is the molar concentration of the quencher, K_{SV} is the Stern-Volmer constant, κ_q is the intermolecular quenching rate constant and τ_0 is the fluorescence lifetime (10 ns for most biological macromolecules [31]). A linear dependence of F_0/F on the quencher

concentration was observed (Figure 3.6a), indicating that the tryptophan residues are equally accessible to interaction with the pesticide. The obtained K_{SV} constants were in the order of or close to 10^5 M^{-1} , indicating a strong intermolecular interaction (Table 3.2).

It is known that linear Stern-Volmer plots can be originated from dynamic or static quenching mechanisms. Dynamic quenching occurs by interaction of the quencher with the excited state of the fluorophore that causes no alteration in the conformation of the protein. On the other hand, a static quenching mechanism is an indication of the formation of a molecular complex between the protein and the quencher. The values of k_q were significantly higher than $2 \times 10^{10} \text{ M}^{-1} \text{ s}^{-1}$, which is considered the high-limit collisional quenching rate constant for biomolecules [31]. This indicates an essentially static quenching mechanism.

In the case of static quenching, the modified Stern-Volmer equation allows to calculate the number of binding sites (n) in the protein:

$$\log\left(\frac{F_0 - F}{F}\right) = \log K_a + n \log[Q]$$

where K_a is the static protein quencher association constant (Table 3.2). The values of n were close to 1 in all cases with high K_a values, indicating a strong static interaction of these pesticides with tyrosinase. Both K_{SV} and K_a values followed the trend glyphosate > 2,4,5-T > 2,4-D, in agreement with the inhibition kinetic results (Figure 3.6b).

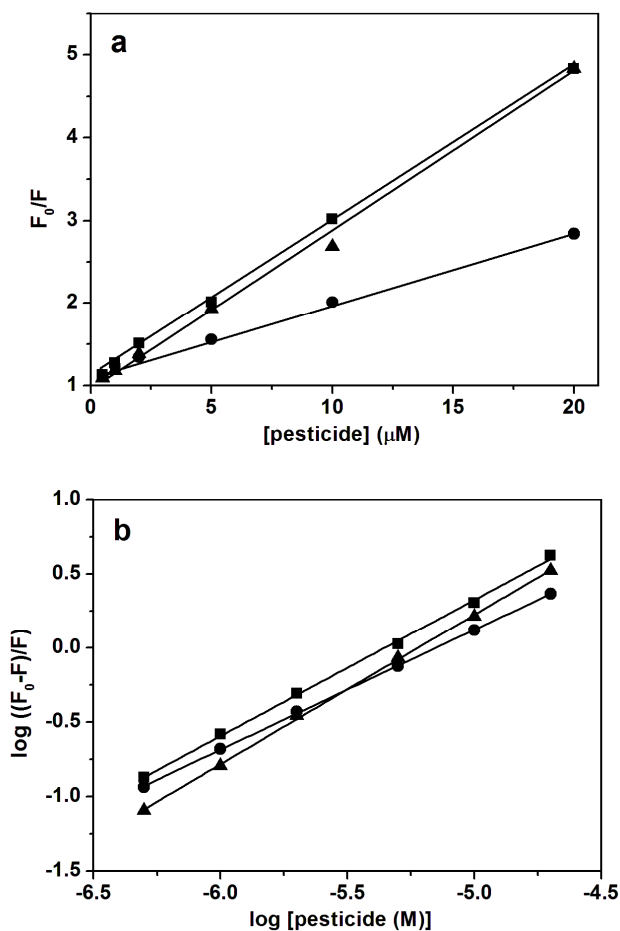


Figure 3.6: Stern-Volmer (a) and modified Stern-Volmer (b) plots for the tyrosinase fluorescence quenching caused by 2,4,5-T (■), 2,4-D (▲) and glyphosate (●).

Table 3.2. Stern-Volmer parameters for the quenching of tyrosinase fluorescence by the studied pesticides.

Pesticide	$K_{\text{SV}} (\text{M}^{-1})$	$\kappa_{\text{q}} (\text{M}^{-1} \text{s}^{-1})$	$K_{\text{a}} (\text{M}^{-1})$	n
2,4,5-T	1.9×10^5	1.9×10^{13}	8.1×10^4	0.94
2,4-D	8.6×10^4	8.6×10^{12}	1.5×10^4	0.90
Glyphosate	2.0×10^5	2.0×10^{13}	1.5×10^5	1.08

To further clarify the binding mechanism, the K_{SV} values were measured at higher temperature. At 37°C the K_{SV} for 2,4,5-T and 2,4-D increased slightly to 2.1×10^5 and $8.8 \times 10^4 \text{ M}^{-1}$, while K_{SV} for glyphosate decreased by almost 40% until $8.3 \times 10^4 \text{ M}^{-1}$. These results suggest that the interactions between the aromatic pesticides on one side, and glyphosate on the other seem to be of a different nature. 2,4,5-T and 2,4-D mainly interact through hydrophobic interactions while glyphosate, which is a dianion at the studied pH and is markedly hydrophilic, appears to interact via hydrogen bonds with polar residues in the protein.

3.3.4 Molecular docking analysis

To understand the inhibition mechanism of mushroom tyrosinase by 2,4,5-T, 2,4-D and glyphosate, the docking modes of the pesticides were examined using in the X-ray crystal structure of tyrosinase from *Agaricus bisporus* (PDB code 2Y9W) and fully deprotonated ligands.

With 2,4,5-T, the ligand is oriented with the carboxylate group pointing toward the inside of the cavity interacting with the pair of copper atoms of the active site (Figure 3.7a). There is a complex set of hydrophobic and π interactions involving a T-shaped π - π interaction between the 2-Cl atom and His-263, 4-Cl with His-244 and 5-Cl with Phe-264. There is also a favorable π - σ interaction between the aromatic ring of 2,4,5-T and Val-283. The ligand is deeply buried in the active site (Figure 3.7b), exposing the 4-Cl and 5-Cl atoms to the solvent.

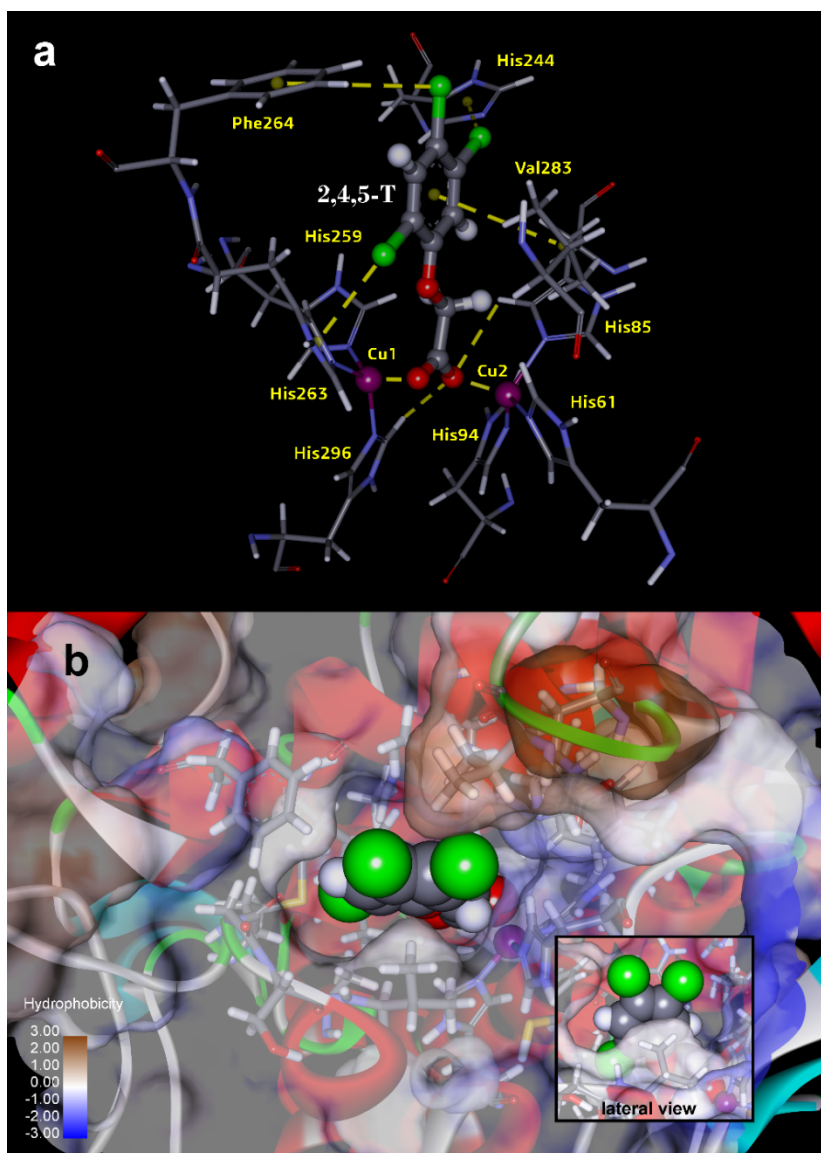


Figure 3.7: Docking study of 2,4,5-T with tyrosinase: a) Calculated 3D structure for the interaction of 2,4,5-T with the active site of tyrosinase. b) Tertiary structure of tyrosinase with 2,4,5-T bounded to the active site.

On the other hand, 2,4-D has a less complex interaction pattern with the active site of tyrosinase due to the presence of a smaller hydrogen atom in position 5

(Figure 3.8a). As in 2,4,5-T, the carboxylate group interacts with the copper atoms. The hydrophobic interactions involving the 2-Cl and 4-Cl atoms are similar to 2,4,5-T, as well as the π - σ interaction between the aromatic ring of 2,4-D and Val-283. This simpler interaction pattern is consistent with the lower inhibition constant of 2,4-D with respect to 2,4,5-T. In both cases, the carboxylate group acts as a bridge between the two copper atoms, each of which presents a distorted tetrahedral coordination geometry (Figure 3.8b).

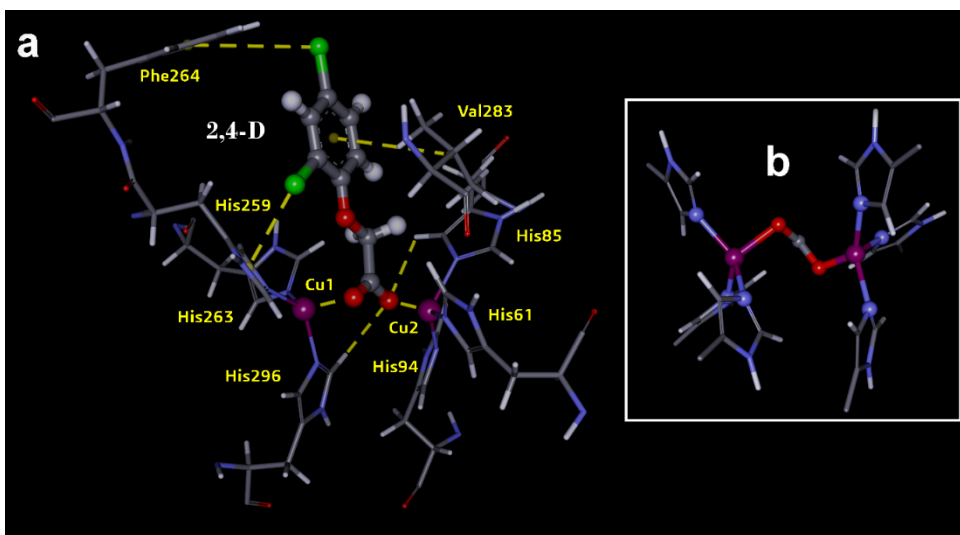


Figure 3.8: Docking study of 2,4,-D with tyrosinase: a) Calculated 3D structure for the interaction of 2,4-D with the active site of tyrosinase. b) Binding motif of the carboxylate group of 2,4,-D with the dicopper center of tyrosinase.

In the case of glyphosate, we found two poses with similar scoring functions. In one case, the ligand is located inside the active site in a geometry resembling that of 2,4,5-T with respect to the interaction of the carboxylate group with the dicopper center (Figure 3.9a). An oxygen atom of the phosphate group interacts via a σ - π bond with His-263, while the adjacent methylene group forms a CH- π bond with the C=O group of Asn-260. In this configuration, the phosphate group is exposed to the solvent (Figure 3.9b). In the other solution, the glyphosate

molecule resides outside the active site, twisted $\sim 90^\circ$ with respect to the previous configuration (Figure 3.9c). The structure is stabilized by interactions between the carboxylate and phosphate groups with His-244 and Asn-81, respectively. Although we could not simulate the interaction of glyphosate with a tyrosinase/L-DOPA complex, these results may explain the mixed inhibition mechanism of glyphosate, in which the pesticide can interact with both the free enzyme and the enzyme-substrate complex.

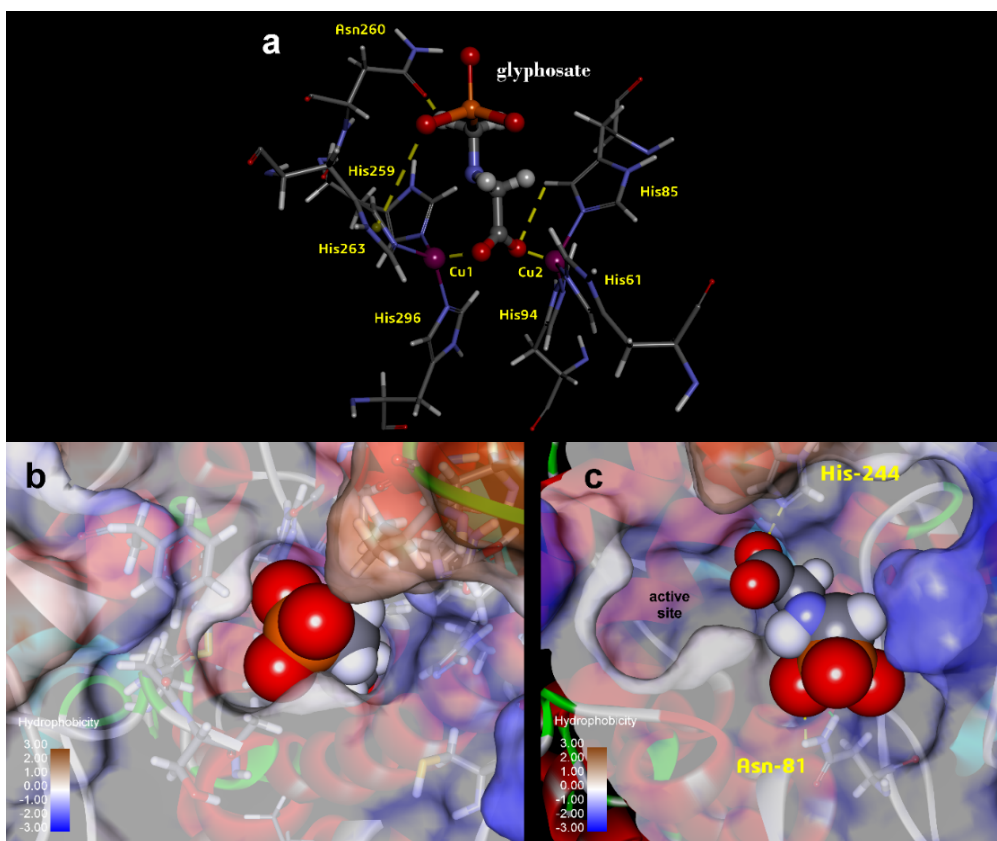


Figure 3.9: Docking study of glyphosate with tyrosinase: a) Calculated 3D structure for the interaction of glyphosate with the active site of tyrosinase. b) and c) Tertiary structure of tyrosinase with glyphosate inside (b) and outside (c) of the active site.

3.4 Conclusions

The inhibition of enzyme activity by pesticides is one of their most common mechanism of action as well as a strategy for constructing enzyme-based detection systems. In this chapter we have studied for the first time the inhibitory activity of 2,4,5-T, 2,4-D and glyphosate on the diphenolase activity of mushroom tyrosinase. Our results demonstrate that 2,4,5-T and 2,4-D inhibit the enzyme following a competitive mechanism, while glyphosate is a mixed inhibitor according to Lineweaver-Burk kinetic analysis. The inhibitory activity follows the order glyphosate > 2,4,5-T > 2,4-D. Intrinsic tyrosinase fluorescence quenching and computational docking analysis suggest that these pesticides interact with the active site of the enzyme, hindering the access of the substrate to the active site. These results could be useful in the construction of improved pesticide biodetection systems. In particular, the strong inhibition exhibited by glyphosate combined with the good stability of tyrosinase seems suitable for developing novel electrochemical biosensors for in-field use. This will be the subject of Chapter 5.

References

- [1] C. D. S. Tomlin (Ed.), *The pesticide manual: a world compendium*, 15th ed. British Crop Protection Council, 2009.
- [2] E. Kennepohl, I. C. Munro, J. S. Bus, Phenoxy Herbicides, in: *Hayes' Handbook of Pesticide Toxicology (Third Edition)*. Krieger R., Ed. Academic Press, New York, 2010, Chapter 84, pp. 1829-1847.
- [3] D. Farmer, Inhibitors of Aromatic Acid Biosynthesis, in: *Hayes' Handbook of Pesticide Toxicology (Third Edition)*. Krieger R., Ed. Academic Press, New York, 2010, Chapter 92, pp. 1967-1972.
- [4] S. Seo, V. K. Sharma, N. Sharma. Mushroom tyrosinase: recent prospects, *J. Agric. Food Chem.* 51 (2003) 2837-2853.

- [5] X. Lai, H. J. Wichers, M. Soler-Lopez, B. W. Dijkstra, Structure and function of human tyrosinase and tyrosinase-related proteins, *Chem. Eur. J.*, 24 (2018) 47-55.
- [6] B. A. Gilchrest, H. Park, M. S. Eller, M. Yaar, Mechanisms of ultraviolet light-induced pigmentation. *Photochem. Photobiol.* 63 (1996) 1-10.
- [7] M. V. Martinez, J. R. Whitaker. The biochemistry and control of enzymatic browning, *Trend. Food Sci. Technol.* 6 (1995) 195-200.
- [8] T. Chang, An updated review of tyrosinase inhibitors, *Int. J. Mol. Sci.* 10 (2009) 2440-2475.
- [9] Y. Manse, K. Ninomiya, R. Nishi, I. Kamei, Y. Katsuyama, T. Imagawa, S. Chaipech, O. Muraoka, T. Morikawa, Melanogenesis inhibitory activity of a 7-O-9'-linked neolignan from *Alpinia galanga* fruit, *Bioorg. Med. Chem.* 24 (2016) 6215-6224.
- [10] K. Chen, D. Zhao, Yu. Chen, X. Wei, Y. Li, L. Kong, R. C. Hider, T. Zhou, A novel inhibitor against mushroom tyrosinase with a double action mode and its application in controlling the browning of potato, *Food Bioproc. Technol.* 10 (2017) 2146-2155.
- [11] P. Burger, A. Landreau, S. Azoulay, T. Michel, X. Fernandez, Skin whitening cosmetics: feedback and challenges in the development of natural skin lighteners, *Cosmetics* 3 (2016) 36.
- [12] P. K. Chen, M. Polatnick. Comparative study on artemisinin, 2,4-D, and glyphosate, *J. Agric. Food Chem.* 39 (1991) 991-994.
- [13] N. Verma, A. Bhardwaj. Biosensor technology for pesticides - a review, *Appl. Biochem. Biotechnol.* 175 (2015) 3093-3119.
- [14] J. Wang, V. B. Nascimento, S. A. Kane, K. Rogers, M. R. Smyth, L. Angnes. Screen-printed tyrosinase-containing electrodes for the biosensing of enzyme inhibitors, *Talanta* 43 (1996) 1903-1907.
- [15] G. Kim, J. Shim, M. Kang, S. Moon. Preparation of a highly sensitive enzyme electrode using gold nanoparticles for measurement of pesticides at the ppt level, *J. Environ. Monit.*, 10 (2008) 632-637.
- [16] G. Kim, M. Kang, J. Shim, S. Moon. Substrate-bound tyrosinase electrode using gold nanoparticles anchored to pyrroloquinoline quinone for a pesticide biosensor, *Sens. Act. B* 133 (2008) 1-4.
- [17] F. A. McArdle, K. C. Persaud, Development of an enzyme-based biosensor for atrazine detection, *Analyst*, 118 (1993) 419-423.
- [18] T. M. Anh, S. V. Dzyadevych, M. C. Van, N. J. Renault, C. N. Duc, J. Chovelon. Conductometric tyrosinase biosensor for the detection of diuron, atrazine and its main metabolites, *Talanta* 63 (2004) 365-370.
- [19] C. Tortolini, P. Bollela, R. Antiochia, G. Favero, F. Mazzei, Inhibition-based biosensor for atrazine detection, *Sens. Act. B* 224 (2016) 552-558.

- [20] Y. D. Tanimoto de Albuquerque, L. F. Ferreira. Amperometric biosensing of carbamate and organophosphate pesticides utilizing screen-printed tyrosinase-modified electrodes, *Anal. Chim. Acta* 596 (2007) 210-221.
- [21] J. Besombes, S. Cosnier, P. Labbé, G. Reverdy. A biosensor as warning device for the detection of cyanide, chlorophenols, atrazine and carbamate pesticides. *Anal. Chim. Acta* 311 (1995) 255-263.
- [22] M. T. Pérez Pita, A. J. Reviejo, F. J. Manuel de Villena, J. M. Pingarrón. Amperometric selective biosensing of dimethyl- and diethyldithiocarbamates based on inhibition processes in a medium of reversed micelles, *Anal. Chim. Acta* 340 (1997) 89-97.
- [23] A. Hipólito-Moreno, M. E. León-González, L. V. Pérez-Arribas, L. M. Polo-Díez. Non-aqueous flow-injection determination of atrazine by inhibition of immobilized tyrosinase. *Anal. Chim. Acta* 362 (1998) 187-192.
- [24] J. C. Vidal, L. Bonel, J. R. Castillo. A modulated tyrosinase enzyme-based biosensor for application to the detection of dichlorvos and atrazine pesticides, *Electroanalysis* 20 (2008) 865-873.
- [25] N. M O'Boyle, M. Banck, C. A James, C. Morley, T. Vandermeersch, G. R. Hutchison, *Open Babel: An open chemical toolbox*, *J. Cheminf.* 3 (2011) 33
- [26] Ressource Parisienne en BioInformatique Structurale Web portal, MTiAutoDock 1.0. <http://mobyte.rpbs.univ-paris-diderot.fr/cgi-bin/portal.py#forms::MTiAutoDock>
- [27] C. M. Labbé, J. Rey, D. Lagorce, M. Vavruša, J. Becot, O. Sperandio, B. O. Villoutreix, P. Tufféry, M. A. Miteva, *MTiOpenScreen: a web server for structure-based virtual screening*, *Nucl. Acids Res.* 43, (2015) W448-W454.
- [28] E. Neeley, G. Fritch, A. Fuller, J. Wolfe, J. Wright, W. Flurkey, Variations in IC_{50} values with purity of mushroom tyrosinase, *Int. J. Mol. Sci.* 10 (2009) 3811-3823.
- [29] D. M. Liu, J. L. Yang, W. Ha, J. Chen, Y. P. Shi, Kinetics and inhibition study of tyrosinase by pressure mediated microanalysis, *Anal. Biochem.* 15 (2017) 54-59.
- [30] D. Kim, J. Park, J. Kim, C. Han, J. Yoon, N. Kim, J. Seo, C. Lee, Flavonoids as mushroom tyrosinase inhibitors: a fluorescence quenching study, *J. Agric. Food Chem.* 54 (2006) 935-941.
- [31] J. R. Lakowicz (Ed.) *Principles of Fluorescence Spectroscopy*, 3rd edition. Springer-Verlag, 2006, Chapter 17.

Chapter 4

Preparation and characterization of alkaline phosphatase, horseradish peroxidase and glucose oxidase conjugates with carboxylated carbon nano-onions²

Abstract

Carbon nanomaterials have emerged as suitable supports for enzyme immobilization and stabilization due to their inherently large surface area, high electrical conductivity, chemical stability and mechanical strength. In this paper, carbon nano-onions (CNOs) were used as supports to immobilize alkaline phosphatase, horseradish peroxidase and glucose oxidase. CNOs were first functionalized by oxidation to generate carboxylic groups on the surface followed by the covalent linking of the using a soluble carbodiimide as coupling agent. The CNO-enzyme conjugates were characterized by TEM and Raman spectroscopy. Thermogravimetric analysis revealed a specific enzyme load of ~0.5 mg of protein per milligram of CNO. The immobilized enzymes showed enhanced storage stability without altering the optimum pH and temperatures. These properties make the prepared nanobiocatalyst of potential interest in biosensing and other biotechnological applications.

² This chapter has been published in V. Sok, A. Fragoso, *Preparative Biochemistry and Biotechnology* **2018**, *48*, 136-143.

4.1 Introduction

Enzyme immobilization allows the reuse of the protein for an extended period of time and enables easier separation of the catalyst from the product. In most cases, immobilization improves many properties of the enzymes such as performance in organic solvents, pH tolerance, heat stability or functional stability, increasing the structural rigidity of the protein which prevents dissociation-related inactivation [1]. The improvement of enzyme properties by immobilization can be carried out using non-covalent or covalent techniques [2]. Covalent immobilization has some advantages over non-covalent immobilization, including enhanced stability and minimization of the leakage of the enzyme [3]. The selection of the optimum support material can affect the immobilization process whereby properties of both the enzyme and support material will determine the properties of the supported enzyme preparation [4].

Among the several existing supports, nanomaterials have been recently reported for enzyme immobilization and stabilization giving an inherently large surface area, which leads to high enzyme loading and consequently high volumetric enzyme activity [5]. This, combined with a high electrical conductivity, chemical stability and strong mechanical strength makes carbon nanomaterials excellent candidates for enzyme immobilization [6]. In particular, carbon nanotubes (CNTs) have been the most explored carbon nanomaterial for this application as they are readily available and can be easily functionalized. In this sense, examples of direct physical adsorption or assisted by polymers and/or surfactants, layer-by-layer deposition and covalent linking can be found in the literature [7].

Carbon nano-onions (CNOs) are a relatively unexplored form of carbon discovered by Ugarte in 1992 [8] and formed by concentric fullerene-like layers. Similarly to CNTs, CNOs are insoluble in organic and inorganic solvents and hence a number of reactions have been explored to improve their solubility and

biocompatibility such as cycloaddition, oxidation with mineral acids, cyclopropanation and radical addition, among others [9] Modified CNOs have also shown low cytotoxicity and biocompatibility [10] *in vitro* and *in vivo*. Other reported applications of CNOs include biological imaging, environmental remediation, etc. [11]

We have recently shown that CNOs can enhance the sensitivity of amperometric biosensors in DNA sensing [12]. The CNO layer can be used as support to immobilize a biorecognition element and, due to their large surface area and electronic properties, the resulting sensing platform shows enhanced performance as compared to systems not containing these nanomaterials. This has prompted us to study the immobilization of enzymes on CNOs with the aim to develop enzymatic biosensors for pesticides, an application that to the best of our knowledge has not been reported yet. For this, we have selected alkaline phosphatase (ALP, EC 3.1.3.1), horseradish peroxidase (HRP, EC 1.11.1.7) and glucose oxidase (GOX, EC 1.1.3.4). These enzymes are widely used in different fields such as immunoassays and electrochemical biosensors, biocatalysis and food industry, etc. [13]

4.2. Experimental Section

4.2.1 Materials

All chemicals and solvents were used as received. NaOH (2 M) was purchased from Scharlau. HCl (1 M) and GOX from *Aspergillus niger* (~200 U/mg) were purchased from Fluka. Tris(hydroxymethyl) aminomethane hydrochloride (Tris HCl), ALP from bovine intestinal mucosa (10 DEA units/mg), Alkaline Phosphatase Yellow (pNPP) Liquid Substrate System for ELISA, magnesium chloride, D-(+)-glucose, N-(3-dimethylaminopropyl)-N'-ethylcarbodiimide hydrochloride (EDC) and Phosphate Buffered Saline (0.138 M NaCl and 0.0027 M KCl) were purchased

from Sigma. 96-well microtiter plates were purchased from Fisher Scientific. *o*-Dianisidine dihydrochloride was purchased from Alfa Aesar. 2,2'-Azino-bis(3-ethylbenzthiazoline-6-sulfonic acid) (ABTS) purchased from Thermo Fisher Scientific. Horseradish Peroxidase Type IV (~60 U/mg) was purchased from Biolyse Laboratories. All solutions were prepared with water purified using a Milli-Q purification system (Millipore, 18.2 M Ω ·cm).

4.2.2 Instrumentation

Raman spectra were recorded in a RENISHAW inVia instrument equipped with a 514 nm excitation laser at 1 mW. A glass slide was used to hold the samples, which were lyophilized before analysis. The I_D/I_G ratio was calculated by dividing the areas of D-band and G-band peaks after background subtraction. Transmission Electron Microscopy images were recorded using an FEI TecnaiTM transmission electron microscope on Cu grids. Thermogravimetric analysis (TGA) was performed on a TGA/DSC analyzer from Mettler Toledo using a heating rate of 10°C/min until 1000°C. All samples (~ 1 mg) were measured in alumina crucibles. Samples were lyophilized in a Labconco NativeZone 1 Liter Benchtop Nativeze Dry system. Absorbances were recorded on a SpectraMax 340PC Microplate Reader on 96-well microplates at room temperature.

4.2.3 Preparation of oxidized CNOs

Small CNOs were obtained as recently reported [14] by annealing of nanodiamonds (5 nm nominal particle size) at 1200°C for 6 hours under argon atmosphere to afford small spherical carbon nano-onion particles of 3–4 nm diameter and 5–6 graphitic shells. The prepared CNOs were oxidized with a mixture of sulfuric and nitric acid (3:1, v/v) for one hour to give CNO-ox [15].

4.2.4 Covalent immobilization of HRP, ALP and GOX on CNO-ox

CNO-enzyme conjugates were prepared by amidation of CNO-ox carboxylic acid groups with the amino groups of the enzymes using EDC as coupling agent (Figure 4.1). For this, 10 mg of CNO-ox were suspended in 10 mL of 0.1 M acetate buffer pH 5 and sonicated for 1 hour. The solution was cooled down in an ice bath for 30 minutes then 20 mg of EDC were added. The solution was stirred for 3 hours, then 20 mg of the corresponding enzyme were added into the solution and further stirred for 4 hours maintaining the solution at 4°C. The reaction mixture was centrifuged at 4000 rpm for 10 minutes and washed several times with Tris buffer pH 7. The CNO-enzyme conjugates were dried by lyophilization for 5 hours and stored at -20°C until use. Three batches of CNO-enzyme conjugates were prepared using this procedure.

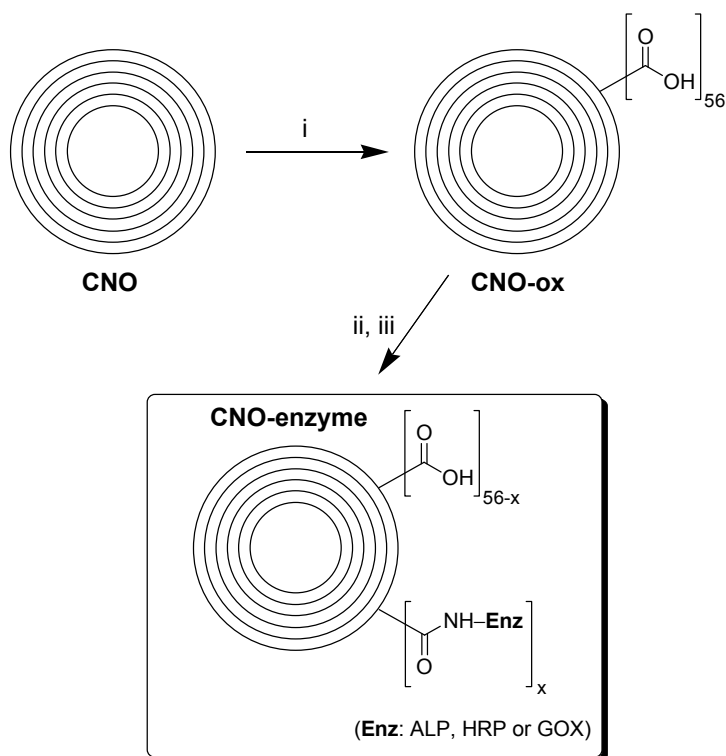


Figure 4.1: Preparation of CNO-enzyme conjugates. i) $\text{HNO}_3/\text{H}_2\text{SO}_4$ (3:1), ii) EDC, acetate buffer pH 5, iii) ALP, HRP or GOX.

4.2.5 Kinetic assays

The activity of native ALP and CNO-ALP were measured spectrophotometrically at 405 nm based on the change of solution color of *p*-nitrophenyl groups generated by the ALP-catalyzed hydrolysis of *p*-nitrophenyl phosphate (pNPP) using Alkaline Phosphatase Yellow (pNPP) Liquid Substrate System for ELISA (Sigma). The assays were carried out at pH 6-12 and at temperatures between 20°C and 70°C in 0.1 M Tris buffer containing 0.02 M MgCl₂ pH 9 using the protocol reported by Walter and Schutt [16].

The activity of native HRP and CNO-HRP were measured spectrophotometrically at 405 nm based on the change of solution color resulting from the oxidation of ABTS by HRP in the presence of hydrogen peroxide using 1-Step™ ABTS Substrate Solution (Thermo Fisher Scientific). The assays were carried out at pH 2-8 and at temperatures between 20°C and 70°C in 0.01 M Phosphate Buffered Saline pH 7 (containing 0.138 M NaCl and 0.0027M KCl) [17].

The activity of native GOX and CNO-GOX were measured spectrophotometrically at 500 nm based on the change of solution color resulting from the HRP-catalyzed oxidation of *o*-dianisidine dihydrochloride by hydrogen peroxide produced by the oxidation of glucose by oxygen-saturated GOX. The assays were carried out at pH 4-9 and at temperatures between 20°C and 70°C in 0.01 M Phosphate Buffered Saline pH 7 (containing 0.138 M NaCl and 0.0027M KCl) [18].

For the six systems, the absorbance values were measured for 10 minutes in 10 s intervals using a microplate reader. Activities were calculated from the slope of the absorbance vs. time plots taking into account the extinction coefficient of the products formed in each reaction. In all cases, the highest activity (at optimum pH or temperature) was taken as 100%. All experiments were carried out in

triplicate. In experiments comparing native with immobilized enzymes, the same amount of both enzyme forms was used in the assays.

4.2.6 Storage stability of native and CNO-enzyme conjugates

The storage stability of native and CNO-enzyme conjugates was determined in terms of the loss of enzyme activity after incubation of buffered solutions at 37°C in the same buffers used to measure the enzyme activity (see section 2.5). After incubation for determined periods of time, the residual activity of enzymes was measured as described above. The initial activity was considered as 100%.

4.3 Results and Discussion

4.3.1 Preparation and physicochemical characterization of CNO-enzyme conjugates

Figure 4.1 shows the overall procedure for the immobilization of ALP, HRP and GOX on CNOs. The first step involved an oxidation reaction to generate carboxylic groups on the graphitic shell of the CNOs to obtain CNO-ox. The carboxylic groups of CNO-ox were then linked covalently with the amino groups of the enzymes by amidation in the presence of a water soluble carbodiimide (EDC), which activates the COOH group to form a labile ester group that is further displaced by nucleophilic attack of an amino group of the enzyme to afford the corresponding CNO-enzyme conjugates (CNO-ALP, CNO-HRP and CNO-GOX). Since a large excess of both EDC and enzymes is used, enzyme self-crosslinking can occur, although most of this material is removed during the purification phase by centrifugation. The CNO conjugates formed stable suspensions when dispersed in water or buffer that did not precipitate for several days.

Figure 4.2 shows TEM images of the precursor CNOs and CNO-HRP. This conjugate forms small aggregates of 10-20 nm size that precipitate with time. Similar behavior was observed for CNO-ALP and CNO-GOX.

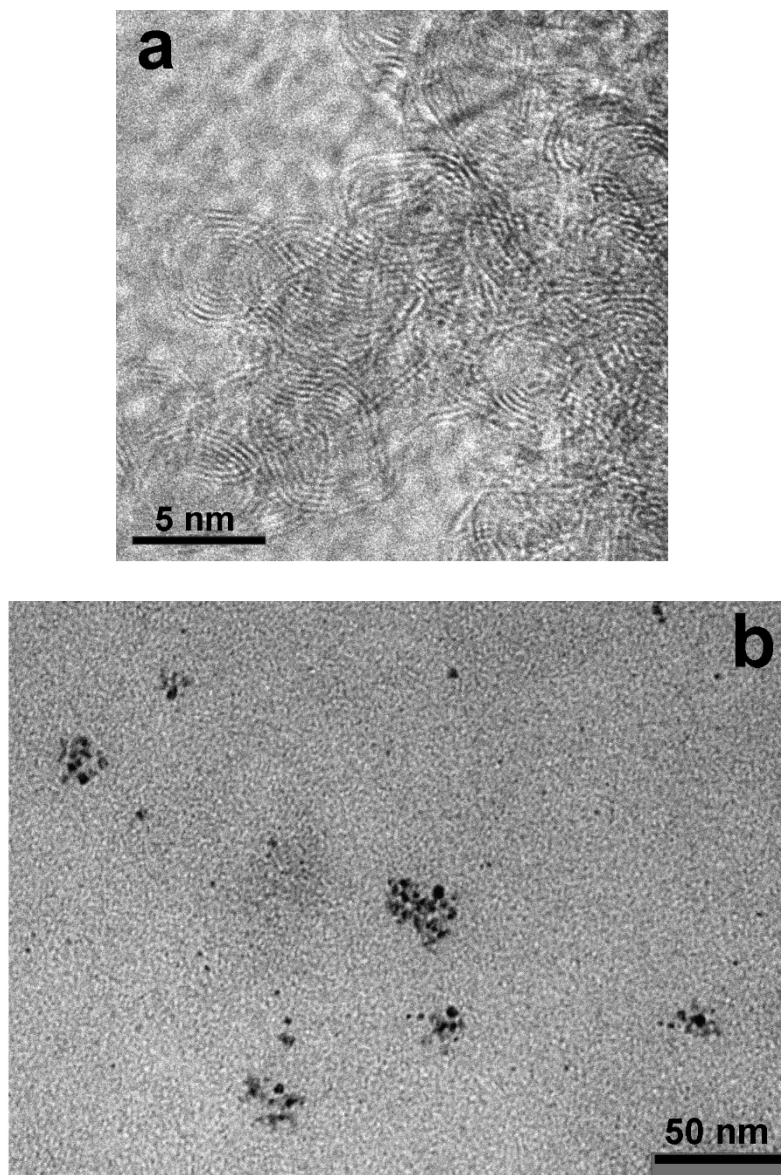


Figure 4.2: a) HRTEM image of the precursor CNOs. b) TEM image of CNO-HRP suspended in water.

The TGA profiles of the CNO conjugates is strongly dependent on the amount of immobilized enzyme. This allowed the determination of the degree of functionalization of CNO-ox and CNO-enzyme conjugates by TGA analysis under an inert atmosphere from 30°C until 1000°C using pristine CNOs as reference under the same conditions (Figure 4.3). From the TGA curves it can be seen that CNO decomposition starts at 500°C and continues decomposing until 750°C while CNO-ox exhibit two different thermal stages with a total mass loss of 3.7% between 150°C and 450°C, corresponding to the loss of the carboxylic groups from the surface of the CNOs with a further decomposition starting at 460°C.

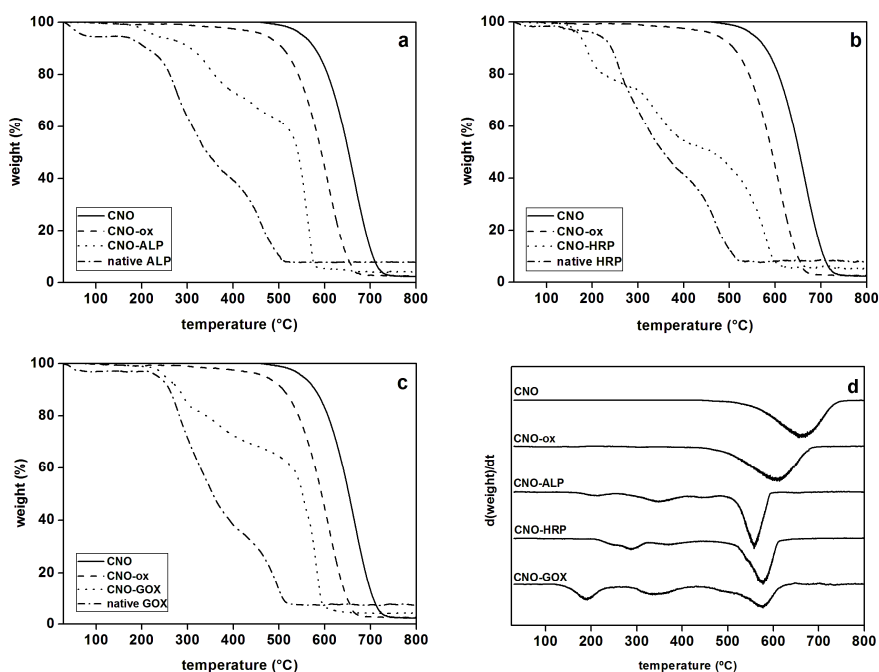


Figure 4.3: TGA curves of CNOs, CNO-ox and CNO-enzyme conjugates (a-c) and first derivative curves (d).

According to HRTEM images (Figure 4.2a), the starting CNOs have an average of six graphitic shells [14]. Considering the core is a C₆₀ fullerene, the number of carbon atoms in each shell is estimated as $60 \times n^2$ where n is the shell number,

so the first shell contains $60 \times 1^2 = 60$ carbon atoms, the second shell $60 \times 2^2 = 240$ carbon atoms, and so on. Thus, the total number of carbon atoms in one CNO containing 6 shells is 5460 with a molecular weight of $5460 \times 12 \text{ g/mol} = 65\,520 \text{ g/mol}$. The loss of weight of about 3.7% in CNO-ox indicates that there are ~ 56 COOH groups per CNO (~ 1 per

every 38 carbons of the outer shell). This value is smaller than the result reported previously by our group [15] due to a lower oxidation time used to avoid the generation of a large number of defects on the surface of the CNOs.

The CNO-ALP, CNO-HRP and CNO-GOX conjugates exhibit two main different thermal stages below 520°C with a total mass loss of 35%, 50% and 33%, respectively, corresponding to the decomposition of the proteins immobilized on the surface of the CNOs. In these cases, the decomposition of the carbon nanostructure takes place at temperatures $\sim 100^\circ\text{C}$ lower than that of pristine CNOs. This behavior is typical for modified carbon nanostructures. It is also noteworthy that the immobilized enzymes show, in general, a higher thermal stability than their native counterparts which decompose completely below 460°C , further confirming the covalent immobilization of the enzymes on the CNO surface and a positive effect of the conjugation on the stability of the enzymes.

From the results of the TGA analysis, the enzyme/CNO ratios were calculated taking into account the mass loss below 500°C and the molecular weight of the enzymes (Table 4.1). For ALP and GOX ($M = 160 \text{ kDa}$) the results indicate that there are, on average, 5 CNO particles per enzyme, while for HRP ($M = 44 \text{ kDa}$) three enzyme molecules are covalently linked with 2 CNOs (Table 4.1).

Table 4.1. Average composition and specific enzyme load for the prepared CNO-enzyme conjugates (ENZ = ALP, HRP or GOX).

Conjugate	Molar composition (CNO) _x (ENZ) _y		Specific enzyme load (mg/mg CNO)
	x	y	
CNO-ALP	5	1	0.49
CNO-HRP	2	3	0.44
CNO-GOX	5	1	0.49

The Raman spectra at 514 nm of CNO-ALP, CNO-HRP and CNO-GOX conjugates (Figure 4.4) show the typical D (~1340 cm⁻¹) and G (~1580 cm⁻¹) bands characteristic of the graphitic layers of the fullerene structure of CNOs. The 2D band is also visible at ~2700 cm⁻¹. In all cases, the I_D/I_G ratio remains essentially unaltered with respect to CNO-ox (~1.0), indicating that the conjugation of the enzymes does not induce further defects in the CNO structure. The presence of the enzymes in the conjugates is visible by the appearance of new broad bands around 1100 cm⁻¹ (C-N modes) and 2900 cm⁻¹ (C-H modes), while weak bands corresponding to the amide bonds appear at ~1440 cm⁻¹ overlapped in part between the D and G bands [19].

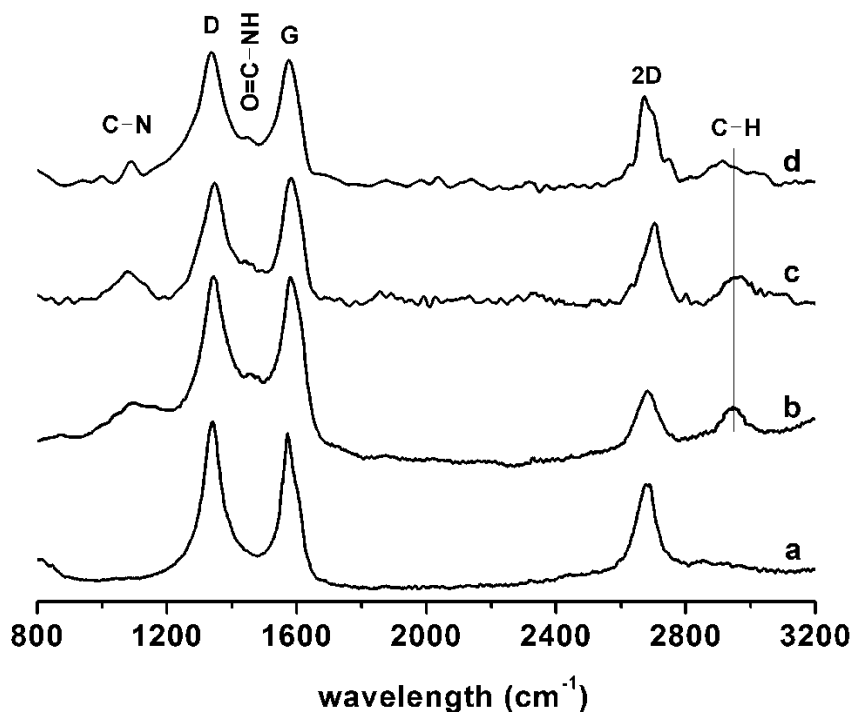


Figure 4.4: Raman spectra (514 nm) CNO-ox (a), CNO-ALP (b), CNO-HRP (c) and CNO-GOX (d).

4.2 Enzymatic activity of native enzymes and CNO-enzyme conjugates

Table 4.2 reports the catalytic properties of natives and CNO-conjugated enzymes. The CNO-ALP and CNO-GOX conjugates retained 71 and 78% of the catalytic activity of the native enzyme, while CNO-HRP kept up to 60%. This reduction could be originated from some steric hindrance produced by the attachment of the enzymes to the CNO matrix which could hinder in part the access of substrate to the active site of trypsin. Other causes could be the conditions used in the coupling reaction (pH 5, long conjugation time). However, the reduction in enzymatic activity in the CNO-enzyme conjugates was compensated by the improved stability properties, as demonstrated in the

following sections. Meanwhile, the catalytic efficiency (k_{cat}/K_m) was not markedly affected by the conjugation.

Table 4.2. Catalytic properties of native and CNO-enzyme conjugates.

Enzyme form	V_{max} (nM/s)	k_{cat} (s^{-1})	K_m (M)	k_{cat}/K_m ($M^{-1} s^{-1}$)
ALP	151 ± 2	20.1 ± 0.2	$(2.7 \pm 0.3) \times 10^{-5}$	7.3×10^5
CNO-ALP	120 ± 2	13.1 ± 0.1	$(2.5 \pm 0.2) \times 10^{-5}$	5.1×10^5
HRP	87 ± 1	15.0 ± 0.6	$(6.9 \pm 0.4) \times 10^{-5}$	2.2×10^5
CNO-HRP	50 ± 1	6.4 ± 0.2	$(3.3 \pm 0.2) \times 10^{-5}$	1.9×10^5
GOX	134 ± 2	530 ± 5	$(4.3 \pm 0.1) \times 10^{-2}$	1.2×10^4
CNO-GOX	96 ± 1	305 ± 3	$(3.6 \pm 0.2) \times 10^{-2}$	8.5×10^3

4.3 Effect of pH and temperature on the catalytic activity of native enzymes and CNO-enzyme conjugates

Solution pH is one of the most important factors in enzyme activity. The effect of pH on catalytic activities of native ALP and CNO-ALP is shown in Figure 4.5a, which shows that both CNO-ALP and native ALP reached the maximum activity at the optimum pH 9 and also the same activity at pH 8 with 95% of the maximum activity. Hence, the immobilization did not affect the optimum pH of alkaline phosphatase. For pH values lower than 8, the activities of both enzyme forms are very similar. Interestingly, CNO-ALP shows a higher activity at pH higher than the optimum pH with 12-15% of enhancement between pH 10 and 11. This behavior of immobilized ALP is similar to that reported by Hanachi et al. [20] who covalently immobilized ALP on collagen fiber using EDC as coupling agent and may be due to the presence of unmodified carboxylate groups in the surface of

the CNOs that could act as a kind of a buffer system extending the pH range of activity of the enzyme.

In the case of native HRP and CNO-HRP (Figure 4.5b), both forms reach the maximum activities at the same value of pH 3 meaning that the immobilization did not affect the optimum pH of the enzyme. Between pH 3 and 6, the activity of the CNO-HRP conjugate remained above 85% of the maximum activity, in agreement with other reports on HRP covalently immobilized on MWCTNs [21] using 1-pyrenebutanoic acid succinimidyl ester as a coupling agent. Figure 4.5c shows the effect of pH on catalytic activities of native GOX and CNO-GOX. Both native GOX and CNO-GOX reach their maximum activity at pH 6 and the activity of both enzymes is essentially the same in the studied pH range. This behavior has also been found for the conjugation of GOX with other supports such as polymer membranes [22] or silica foams [23].

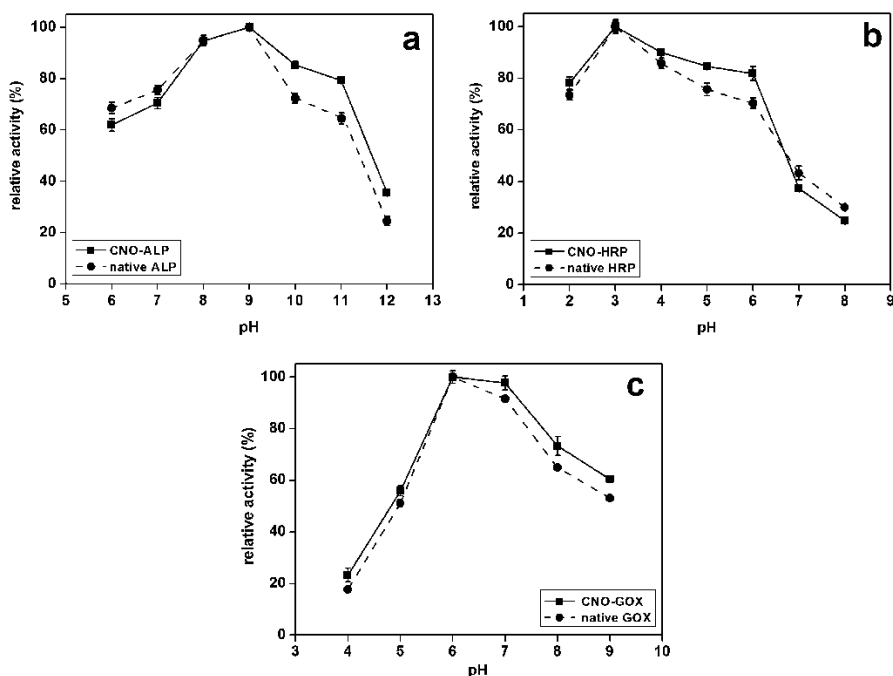


Figure 4.5. Activity vs. pH profile for native and CNO-conjugated enzymes.

4.4 Effect of temperature on the catalytic activity of native enzymes and CNO-enzyme conjugates

Temperature is another of the most important factors in enzyme activity. The effect of the temperature on the catalytic activities of native ALP and CNO-ALP is shown in the Figure 4.6a. Both native ALP and CNO-ALP reach the maximum activity at the same optimum temperature of 50°C. CNO-ALP shows between 10% and 20% higher activity than native ALP in the whole interval of temperatures, indicating that CNOs have the ability to enhance the activity of ALP when they are conjugated without altering the optimum temperature. This is in contrast to the results reported by Hanachi et al. [20] who found a lower optimum temperature for ALP immobilized on collagen fibers (40°C).

In the case of CNO-HRP and CNO-GOX, the activity vs. temperature profiles are very similar to those of the native enzymes (Figure 4.6b,c). The optimum temperature was found at 40°C in both cases, with no alteration with respect to the native enzyme. Conjugation to the CNOs affords more stable conjugates, especially in the case of HRP, which retains more than 50% of its initial activity at 60°C. For CNO-GOX, the conjugate retained more than 70% of activity even at 70°C, indicating that it can be effectively used in a wide temperature range as compared to GOX.

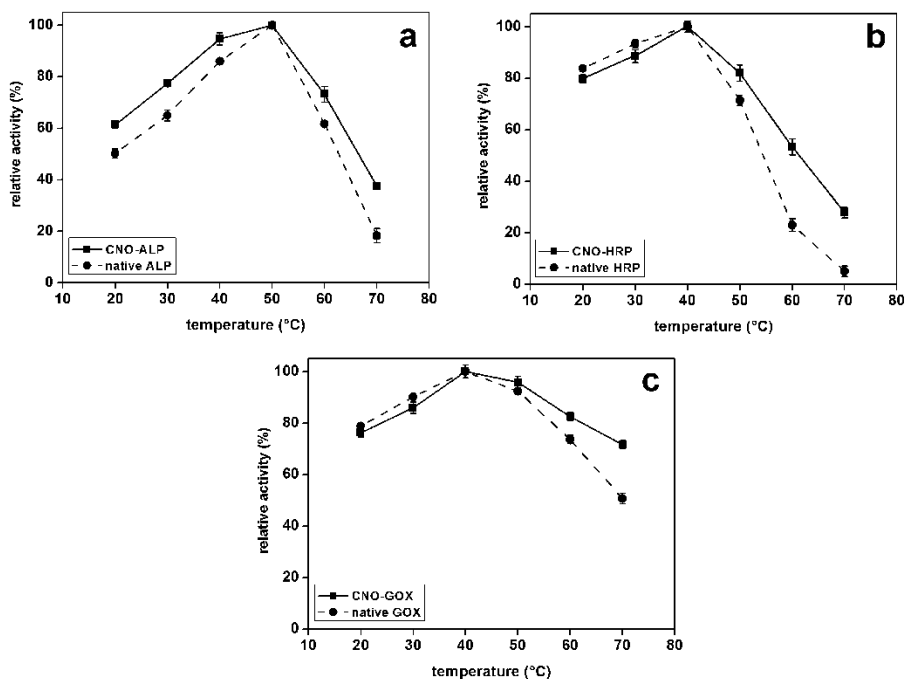


Figure 4.6. Activity vs. temperature profile for native and CNO-conjugated enzymes.

4.5 Storage stability of CNO-enzyme conjugates

The storage stability was studied for conjugates stored in buffer solution at 37°C for a given period of time and the kinetic measurements were carried out at the optimum pH and temperature for each system at room temperature. These conditions were selected as it is common to study the storage properties of biomolecules in so called “accelerated” conditions at relatively high temperatures in the absence of stabilizers.

As shown in Figure 4.7a, the results of thermal stability studies of native ALP and CNO-ALP incubated in Tris buffer pH 9 indicate a slight improvement of the stability of ALP immobilized on CNOs. The native ALP lost 67% of its initial activity whereas CNO-ALP lost 40% of its initial activity after one day. After one week, the

native ALP was completely inactivated while CNO-ALP retained 18% of its initial activity, which is equivalent to the activity of native ALP after being incubated for two days.

From the results of the thermal stability studies of native HRP and CNO-HRP stored in PBS buffer at pH 6 and 37°C (Figure 4.7b), it is clearly evident that the thermal stability of the HRP immobilized on CNO was strongly improved compared to the native HRP. The native HRP lost 95% of its initial activity after a 5-day storage while CNO-HRP retained 50% of activity. It is interesting to note that the stability profile of CNO-HRP is similar to that of HRP conjugated to an antibody [24]

In the case of GOX, this is a thermally more stable enzyme and hence its storage stability could be studied for a longer period of time. As shown in Figure 4.7c, the results of the thermal stability studies of native GOX and CNO-GOX stored in PBS buffer at pH 6 and 37°C indicate that GOX immobilized on CNO retained ~90% of activity even after six weeks of storage, while native GOX lost 50% of its initial activity.

In all cases, the conjugates stored in buffer at 4°C retained more than 95% of activity after several weeks of storage. On the other hand, the CNO-HRP conjugate was more resistant to denaturation in the presence of 2 M urea (21% activity loss) than native HRP (40% activity loss). The increased stability observed for the immobilized enzymes on CNOs might be attributed to a reduction in the enzyme structure mobility due to the anchorage to the support and subsequent translation of the rigidity to the enzyme structure thus shielding it from the denaturing effects of the environment.

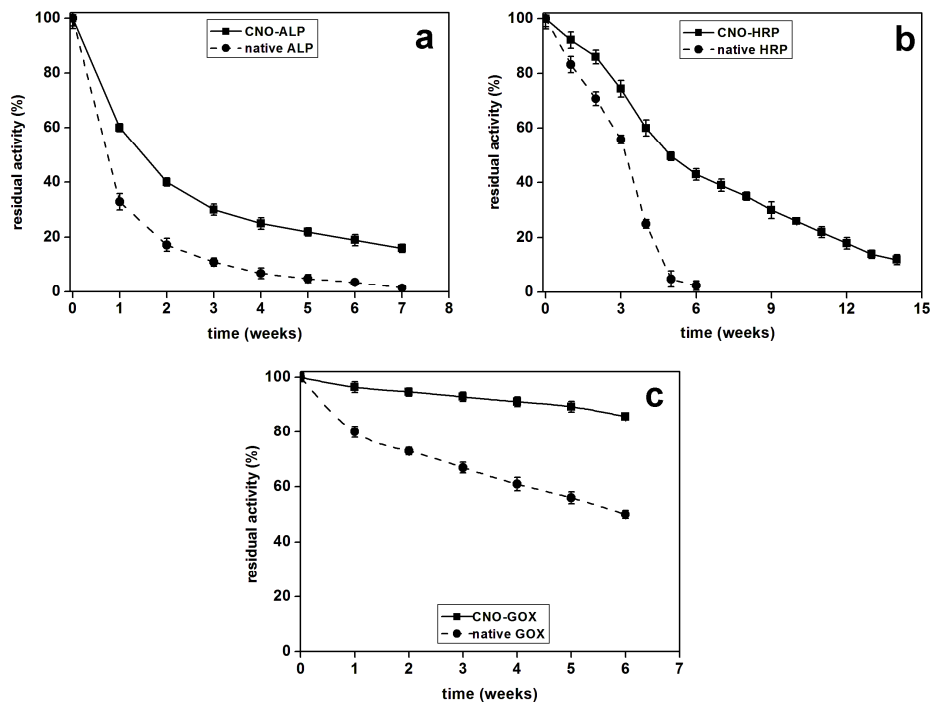


Figure 4.7. Residual enzymatic activity of native and CNO-conjugated enzymes stored in buffer solution at 37°C (see text for details).

4.4 Conclusions

ALP, HRP and GOX have been successfully immobilized on COOH-containing CNOs by amidation reactions and characterized by TEM and Raman spectroscopy. TGA analysis indicate a specific immobilization load of ~0.5 mg of protein per mg of CNOs. The conjugates retained the same optimum pH and temperature as compared with the native enzymes, with a slight improvement of their activities and are stable for longer periods of time after storage at 37°C. These properties make the prepared nanobiocatalyst of potential interest in biosensing and other biotechnological applications.

References

1. a) Sheldon, R.A.; van Pelt, S. Enzyme immobilisation in biocatalysis: why, what and how. *Chem. Soc. Rev.* 2013, 42, 6223–6235. b) Guzik, U., Hupert-Kocured, K.; Wojcieszynska, D. Immobilization as a strategy for improving enzyme properties - Application to oxidoreductases. *Molecules* 2014, 19, 8995-9018.
2. Brady, D.; Jordaan, J. Advances in enzyme immobilization. *Biotechnol. Lett.* 2009, 31, 1639-1650.
3. a) Zucca, P.; Sanjust, E. Inorganic materials as supports for covalent enzyme immobilization: methods and mechanisms. *Molecules* 19 2014, 14139-14194. b) Cui, J.; Jia, S. Optimization protocols and improved strategies of cross-linked enzyme aggregates technology: current development and future challenges. *Crit. Rev. Biotechnol.* 2015, 35, 15-28.
4. Mohamad, N. R.; Marzuki, N. H.C.; Buang, N. A.; Huyop, F.; Wahab, R. A. An overview of technologies for immobilization of enzymes and surface analysis techniques for immobilized enzymes. *Biotechnol. Equip.* 2015, 29, 205-220.
5. a) Ansari, S. A.; Husain, Q. Potential applications of enzymes immobilized on/in nano materials: A review. *Biotechnol. Adv.* 2012, 30, 512-523. b) Oliveira, S. F.; Bisker, G.; Bakh, N. A.; Gibbs, S. L.; Landry, M. P.; Strano, M. S. Protein functionalized carbon nanomaterials for biomedical applications. *Carbon* 2015, 95, 767-779.
6. Zhu, Z.; Garcia-Gancedo, L.; Flewitt, A. J.; Xie, H.; Moussy, F.; Milne, W. I. A critical review of glucose biosensors based on carbon nanomaterials: carbon nanotubes and graphene. *Sensors* 2012, 12, 5996-6022.
7. Feng, W.; Ji, P. Enzymes immobilized on carbon nanotubes. *Biotechnol. Adv.* 2011, 29, 889-895.
8. Ugarte, D. Curling and closure of graphitic networks under electron beam radiation. *Nature* 1992, 359, 707-709.
9. a) Palkar, A.; Melin, F.; Cardona, C. M.; Elliott, B.; Naskar, A. K.; Edie, D. D.; Kumbhar, A.; Echegoyen, L. Reactivity differences between carbon nano onions (CNOs) prepared by different methods. *Chem. Asian J.* 2007, 2, 625-633. b) Rettenbacher, A. S.; Perpall, M. W.; Echegoyen, L.; Hudson, J.; Smith, D. W. Radical addition of a conjugated polymer to multilayer fullerenes (carbon nano-onions). *Chem Mater.* 2007, 19, 1411-1417. c) Molina-Ontoria, A.; Chaur, M. N.; Plonska-Brzezinska, M. E.; Echegoyen, L. Preparation and characterization of soluble carbon nano-onions by covalent functionalization employing a Na-K alloy. *Chem. Commun.* 2013, 49, 2406-2408.

10. a) Sonkar, S. K.; Gosh, M.; Roy, M.; Begun, A.; Sarkar, S. Carbon nano-onions as nontoxic and high-fluorescence bioimaging agent in food chain an in vivo study from unicellular *E. coli* to multicellular *C. elegans*. *Mater. Express*. 2012, 2, 105-114. b) Luszczyn, J.; Plonska-Brzezinska, M. E.; Palkar, A.; Dubis, A. T.; Simionescu, A.; Simioescu, D. T.; Kalska-Szostko, B.; Winkler, K.; Echegoyen, L. Small nontocytotoxic carbon nano-onions: first covalent functionalization with biomolecules. *Chem. Eur. J.* 2010, 16, 4870-4880.
11. a) Bartelmeß, J.; Giordani, S. (2014) Carbon nano-onions (multi-layer fullerenes): chemistry and applications. *Beilstein J. Nanotechnol.*, 5, 1980-1998. b) Kausar, A. Carbon nano-onion as versatile contender in polymer compositing and advance application. *Fuller. Nanotub. Car. N.* 2017, 25, 109-123.
12. Bartolome, J. P.; Echegoyen, L.; Fragoso, A. Reactive carbon nano-onion modified glassy carbon surfaces as DNA sensors for human papillomavirus oncogene detection with enhanced sensitivity. *Anal Chem.* 2015, 87, 6744-6751.
13. a) Pavlidis, I. V.; Vorhaben, T.; Tsoufis, T.; Rudolf, P.; Bornscheur, U. T.; Gournis, D.; Stamatis, H. Development of effective nanobiocatalytic systems through the immobilization of hydrolases on functionalized carbon-based nanomaterials. *Bioresour. Technol.* 2012, 115, 164-171. b) Krainer, F. W.; Glieber, A. An updated view on horseradish peroxidases: recombinant production and biotechnological applications. *App, Microbiol. Biotechnol.* 2015, 99, 1611-1625. c) Bankar, S. B.; Bule, M.V.; Singhal, R. S.; Ananthanarayan, L. Glucose oxidase – An overview. *Biotechnol. Adv.* 2009, 27, 489-501.
14. Bartolome, J. P.; Fragoso, A. Preparation and characterization of carbon nano-onions by nanodiamond annealing and functionalization by radio-frequency Ar/O₂ plasma. *Fuller. Nanotub. Car. N.* 2017, 25, 327-334.
15. Wajs, E.; Molina-Ontoria, A.; Nielsen, T. T.; Echegoyen, L.; Fragoso, A. Supramolecular solubilization of cyclodextrin-modified carbon nano-onions by host-guest interactions. *Langmuir* 2015, 31, 535-541.
16. Walter, K.; Schütt, C. (1974) Alkaline phosphatase in serum. In: Bergmeyer, H. U., *Methods of Enzymatic Analysis*. 2nd edn. New York, USA, Academic Press, pp. 860–864.
17. Childs, R. E.; Bardsley, W. G. The steady-state kinetics of peroxidase with 2,2'-azino-di-(3-ethyl-benzthiazoline-6-sulphonic acid) as chromogen. *Biochem. J.* 1975, 145, 93–103.
18. Li, D.; He, Q.; Cui, Y.; Duan, L.; Li, J. Immobilization of glucose oxidase onto gold nanoparticles with enhanced thermostability. *Biochem. Biophys. Res. Commun.* 2007, 355, 488-493.

19. Rygula, A.; Majzner, K.; Marcek, K. M.; Kaczor, A.; Pilarczyk, M.; Baranska, M. Raman spectroscopy of proteins: a review. *J. Raman Spectrosc.* 2013, 44, 1061-1076.
20. Hanachi, P.; Jafary, F.; Jafary, F.; Motamedi, S. Immobilization of alkaline phosphatase on collagen surface via cross-linking method. *Iran. J. Biotech.* 2015, 13, 32-38.
21. Kim, B. J.; Kang, B. K.; Bahk, Y. Y.; Yoo, K. H.; Lim, K. J. Immobilization of horseradish peroxidase on multi-walled carbon nanotubes and its enzymatic stability. *Curr. Appl. Phys.* 2009, 9, e263-e265.
22. Rauf, S.; Ihsan, A.; Akhtar, K.; Ghauri, M. A.; Rahman, M.; Anwar, M. A.; Khalid, M. A. Glucose oxidase immobilization on a novel cellulose acetate-polymethylmethacrylate membrane. *J. Biotechnol.* 2006, 121, 351-360.
23. Balistreri, N.; Gaboriau, D.; Jolival, C.; Launay, F. Covalent immobilization of glucose oxidase on mesocellular silica foams: Characterization and stability towards temperature and organic solvents. *J. Mol. Catal. B Enzym.* 2016, 127, 26-33.
24. Laboria, N.; Fragoso, A.; O'Sullivan, C. K. Storage properties of peroxidase labeled antibodies for the development of multiplexed packaged immunosensors for cancer markers. *Anal. Lett.* 2011, 44, 2019-2030.

Chapter 5

Amperometric enzymatic biosensors based on CNO-modified surfaces for pesticide detection

Abstract

In this chapter, we have explored the possibility to use CNO-modified electrodes for the construction of amperometric enzyme biosensors based on the covalent immobilization of two enzymes on a chitosan/CNO matrix. This combination allowed the development of highly sensitive biosensors for glyphosate and 2,4,5-T based on the inhibition of tyrosinase and HRP activities, respectively. The incorporation of CNO into chitosan-enzyme composites had a positive effect in enhancing the biosensor sensitivity due to the large surface area combined with enhanced electron transfer properties of the CNO-modified electrodes. CNOs also proved beneficial to improve their stability and repeatability and the developed biosensors were tested in spiked river water samples. Our results demonstrate the feasibility of using chitosan/CNO/enzyme composites for the development of sensitive biosensors based on activity inhibition. It could be expected that this strategy can be extended to other systems.

5.1 Introduction

The immobilization of enzymes has become the subject of considerable interest due to their excellent functional properties such as reusability and cost-effectiveness. Enzyme immobilization is widely used in many fields such as industrial processes, medical diagnostics, therapy, food industry, bioenergy, etc. (1). In bioanalysis, immobilization of enzymes on the transducer surface is a necessary and critical step in the design of biosensors. Different immobilization techniques were developed to fulfill the demands for each case, including classical adsorption, covalent bonding, entrapment, cross-linking or affinity as well as combinations of them. The most common nanomaterials such as conducting polymer nanowires, carbon nanotubes or nanoparticles have been reported. The choice of the immobilization methods represents an important parameter that affects biosensor performances, mainly in terms of sensitivity, selectivity and stability, by influencing enzyme orientation, loading, mobility, stability, structure and biological activity (2).

Based on their properties, some polymers were taken in attention to entrap enzymes for biosensor development including sol-gel in HRP- (3) and acetylcholinesterase (AChE) biosensors (4), Nafion® (5), polythiophene (6), photo-crosslinkable polymers (7) and chitosan (8), among others.

In the case of pesticide biosensors, simple adsorption has been used to develop enzymatic biosensors for organophosphorous pesticides (9), thiodicarb (10), and dimethyl- and diethyldithiocarbamates (11). These biosensors were easy to fabricate but did not present a high stability.

For covalent immobilization, the most common reagent used is N-ethyl-N'-(3-dimethylaminopropyl) carbodiimide hydrochloride (EDC). Kim and his team immobilized tyrosinase on the surface of gold nanoparticle modified electrodes

via covalent bonding to develop an atrazine detection biosensor (12). Glutaraldehyde served as cross-linking agent between support and biorecognition elements for development of pesticide detection biosensors. Nafion cross-linked with butyrylcholinesterase (ChE) was used to develop organophosphorus insecticide biosensor (13). Another strategy involved bovine serum albumin (BSA) cross-linked with TYR to detect diuron, atrazine and other pesticides (14) as well as methyl parathion, carbofuran, diazinon and carbaryl (15). Finally, the capacity of enzyme entrapment and cross-linkability of chitosan makes this material especially suitable for enzymatic biosensor development. This polymer was employed as support for enzyme entrapment and being cross-linked with enzymes to develop an AChE-based biosensor for organophosphates (16), a TYR biosensor for thiodicarb detection (17) and an amperometric hydrogen peroxide biosensor (18).

Shi and co-workers made a comparison of different strategies for improving biosensor performance using different nanomaterials. Sol-gel encapsulation approaches and glutaraldehyde cross-linking strategies were applied to develop amperometric glucose biosensors based on commonly applied enzyme immobilization approaches in which carbon nanotubes were used to compare enhancement and compatibility with the enzyme and the nanomaterials (19). MWCNT was added into support composites of AChE biosensor, its presence improved electron transfer from the enzyme molecules to electrode surface and insure rapid biosensor response (20). MWNT was used as co-immobilization matrix to improve performance of an HRP biosensor (21). Graphite, graphene, and multiwalled carbon nanotubes were used to optimize the performance of a pesticide biosensor containing TYR on SPE with different immobilization techniques (22,23). Moyo and his group also utilized MWCNT in maize tassel to create a composite on glassy carbon electrode (GCE) for HRP biosensor

optimization (24) and other examples of CNT-based biosensors have been reported (25).

As mentioned in Chapter 3, since the discovery of the inhibitory effect of pesticides on tyrosinase activity, this enzyme has been widely used as biorecognition element for developing enzymatic biosensors to detect a wide variety of pesticides. Different supports and immobilization strategies were applied to develop biosensors based on tyrosinase for atrazine detection with different detection limits reported. Guan et al. immobilized the enzyme on electropolymerized poly-L-DOPA, reaching a LOD of 10 $\mu\text{g/L}$, (26) and polypyrrole with 0.1 ppm detection limit (27). Other examples include immobilizing the enzyme on vertically growth TiO_2 nanotubes (28), adsorption on a gel-like disk of the polysaccharide κ -carrageenan with 0.5 nM detection limit for atrazine (29) and gold nanoparticles electrodeposited on GCE (12). A TYR biosensor was developed based on immobilizing the enzyme in different composites to detect dichlorvos and atrazine resulting in low detection limits for each of pesticides (30). Other reported examples demonstrate the versatility of this enzyme in pesticide detection (31-35).

On the other hand, peroxidases catalyze the oxidation of various hydrogen donor compounds in the presence of peroxides. Several biosensors based on peroxidases were reported for pesticide detection, although this enzyme has been less applied than TYR. In the work of Oliveira and his team, peroxidase isolated from the atemoya fruit was immobilized in montmorillonite clay on the surface of a carbon paste electrode modified with carbon nanotubes. The enzymatic activity was measured using hydroquinone as substrate, its activity decreased in presence of glyphosate using Square Wave Voltammetry. The limit of detection of the herbicide was 30 $\mu\text{g/l}$ and the biosensor accuracy was proven by the good recovery values in spiked water samples (23). Songa developed a

biosensor by electrochemically depositing poly-(2,5-dimethoxyaniline) (PDMA) doped with poly(4-styrenesulfonic acid) (PSS) onto the surface of a gold electrode followed by electrostatic attachment of horseradish peroxidase onto the PDMA-PSS nanocomposite film. The developed biosensor was applied to detect glyphosate and its metabolite (AMPA) in the water samples using peroxide as substrate with a limit of detection of 0.16 $\mu\text{g/L}$ and 1.0 $\mu\text{g/L}$, respectively (36). Later, a similar biosensor was developed to detect glyphosate and glufosinate in spiked corn samples (37) and (38) with the same limit of detection. In the work of Zhang et al, an electrochemiluminescence (ECL) biosensor for glyphosate detection based on enzyme-assisted in situ generation of ZnS quantum dots (QDs) on ordered mesoporous carbons (OMC) substrate was developed. The HRP was introduced to expedite the generation of ZnS QDs via accelerating the reduction of $\text{Na}_2\text{S}_2\text{O}_3$ with H_2O_2 to yield H_2S that reacted Zn^{2+} ions, applied in glyphosate detection based on inhibitory effect of the herbicide on HRP activity (39).

As described previously, the possible application of carbon nano-onions (CNO) in biosensor development is still in its infancy, with many possible new developments still to come (40-42). In Chapters 2 and 3, we have seen that the inhibition constant of 2,4,5-T on HRP was the highest among the studied pesticides, while glyphosate was the best inhibitor of tyrosinase activity. We have thus selected these two systems to evaluate the performances of biosensors developed in the absence and presence of CNO on the surfaces, immobilizing the enzymes into a chitosan matrix to form a composite material that was immobilized on SPE electrodes.

5.2 Experimental

5.2.1 Materials and reagents

All chemicals and solvents were used as received. ox-CNO were prepared as reported in Chapter 3. NaOH (2M) was purchased from Scharlau. HCl (1 M) was purchased from Fluka. N-(3-dimethylaminopropyl)-N'-ethylcarbodiimide hydrochloride (EDC) and Phosphate Buffered Saline (0.138 M NaCl and 0.0027 M KCl), potassium ferricyanide (III) 99%, horseradish peroxidase salt free (lyophilized powder, 300 units/mg), chitosan from shrimp shells (50-190 kDa), glyphosate, 2,4-D, tyrosinase from mushroom (1000 units/mg), 3,3',5,5'-tetramethylbenzidine (TMB) Liquid Substrate for ELISA, and 3,4-dihydroxy-L-phenylalanine (L-DOPA) were purchased from Sigma-Aldrich. 2,4,5-T was purchased from Tokyo Chemical Industry Co. Ltd. (TCI). Acetic acid glacial (synthesis grade) was purchased from Scharlau.

Screen-printed electrodes were purchased from DropSens. All solutions were prepared with water purified using a Milli-Q water purification system (Millipore) to a resistivity of 18.2 M Ω ·cm.

5.2.2. Instrumentation

Environmental Scanning Electron Microscopy (ESEM) was recorded in a Quanta 600 microscope (FEI Company Inc.) under high vacuum at 25 kV. All electrochemical measurements were carried out using an Autolab model PGSTAT 10 potentiostat/galvanostat controlled with the general purpose electrochemical systems (GPES) software (Eco Chemie, the Netherlands), equipped with a cable connector for screen-printed electrode (DRP-CAC, from DropSens). Cyclic voltammetry studies were conducted in degassed buffers at a scan rate of 100 mV/s.

5.2.3 Preparation of HRP biosensors

Prior to modification, the bare screen-printed electrodes were cleaned/activated with 1M H₂SO₄ using cyclic voltammetry in the potential range (-1 to 1 V) for 10 cycles. Chitosan solution (1%) was prepared in 0.8% acetic acid with 3 h stirring at room temperature. The coating solutions were prepared as follows: 100 U of HRP and 0.25 mg of ox-CNO were mixed with 1 mg EDC in 200 μL phosphate buffer pH 6 and stirred at 4°C for 1h. This solution was then mixed with 200 μL of 1% chitosan and stirred overnight at 4°C. 1.5 μL of this solution were dropped on the surface of the SPEs and dried under vacuum for 2 h (SPE/Chi/CNO/HRP electrodes). The SPE/Chi/HRP electrodes were prepared in a similar way but without CNOs. The electrodes were stored in 20 mM PBS in the fridge to be utilized for measurements.

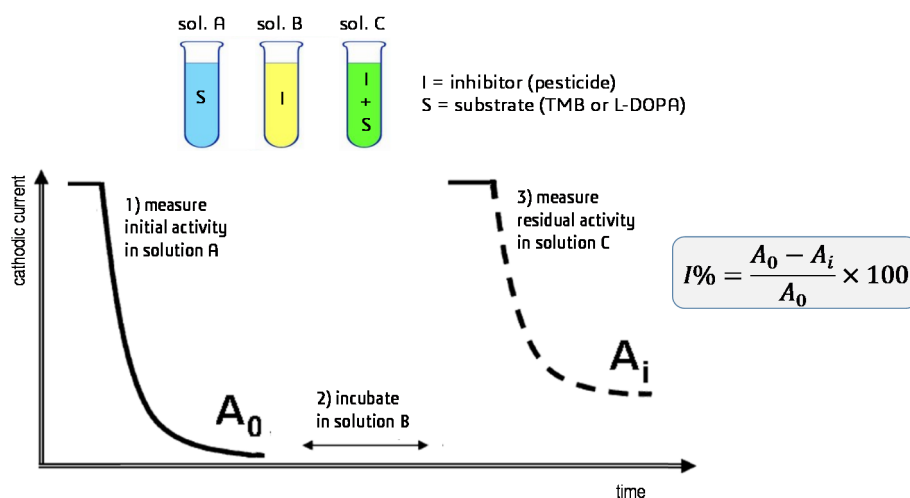
5.2.4 Preparation of TYR biosensors

In this case, the coating solutions were prepared as described above but using 100 U of tyrosinase instead of HRP. Then, the SPE/Chi/TYR and SPE/Chi/CNO/TYR electrodes were stored in 20 mM PBS in the fridge when not in use.

5.2.5 Biosensor characterization and detection procedures

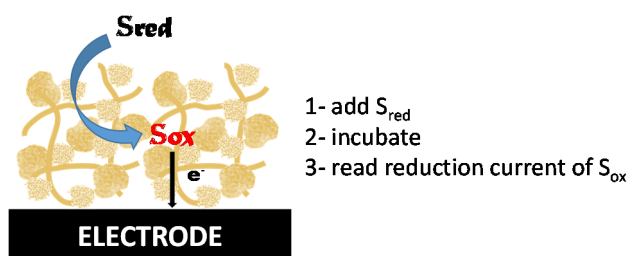
The electrochemical behavior of the developed biosensors and bare SPE was investigated by cyclic voltammetry (CV) in the potential range of -0.3 to +0.6V with scan rate 100 mV/s in 20 mM PBS pH 7 and 1 mM K₃[Fe(CN)₆] in 0.1 mM KCl. SPE/Chi/HRP and SPE/Chi/CNO/HRP were investigated by CV with the same configuration in the presence of TMB and H₂O₂ (1:1) 0.5 mM. SPE/Chi/TYR and SPE/Chi/CNO/TYR were investigated by CV in the presence of 10 mM of L-DOPA in 20 mM of PBS pH 7.

Pesticide inhibition measurements were carried out in a two-step process (Scheme 5.1). The initial response of the non-inhibited biosensor was first recorded using solution A (A_0 in Scheme 5.1), followed by incubation in the presence of the pesticide. Two solutions of the same concentration of pesticides were prepared, one without substrate for biosensor incubation (solution B) and another one with substrate for the amperometric measurements after sample incubation (solution C). On basis of amperometric response of biosensors to the substrate, the steady-state currents produced were recorded. After rinsing, the residual activity (A_i in Scheme 5.1) was then measured and the % of inhibition was calculated.



Scheme 5.1. General protocol used for biosensor measurements.

The DC amperometric measurements were carried out in stirred electrolytes (425 rpm) at an applied potential of 0.0 V for HRP biosensors and -0.20 V for TYR (vs. Ag/AgCl). According to CV, at these potentials the electrochemical reduction of the enzyme-oxidized substrates takes place. Substrate concentrations were 0.065 mM of TMB:H₂O₂ (1:1) for HRP biosensors and 1.5 mM of L-DOPA for TYR biosensors (Scheme 5.2)



Scheme 5.2. Amperometric measurement protocol used to measure A_0 and A_i . The measurements are done firstly in the absence of inhibitor (A_0), then after interaction with the pesticide (A_i).

With the responses of the biosensors, the corresponding calibration curves were built. SPE/Chi/CNO/HRP and SPE/Chi/CNO/TYR were also used to measure the presence of glyphosate and 2,4,5-T in spiked samples of water collected from the Francolí river (Tarragona city). The sample was collected on 27th June 2018 at the coordinates 41°07'12.0"N+1°14'07.8"E and filtered using a syringe filter (0.22 μ m) before use.

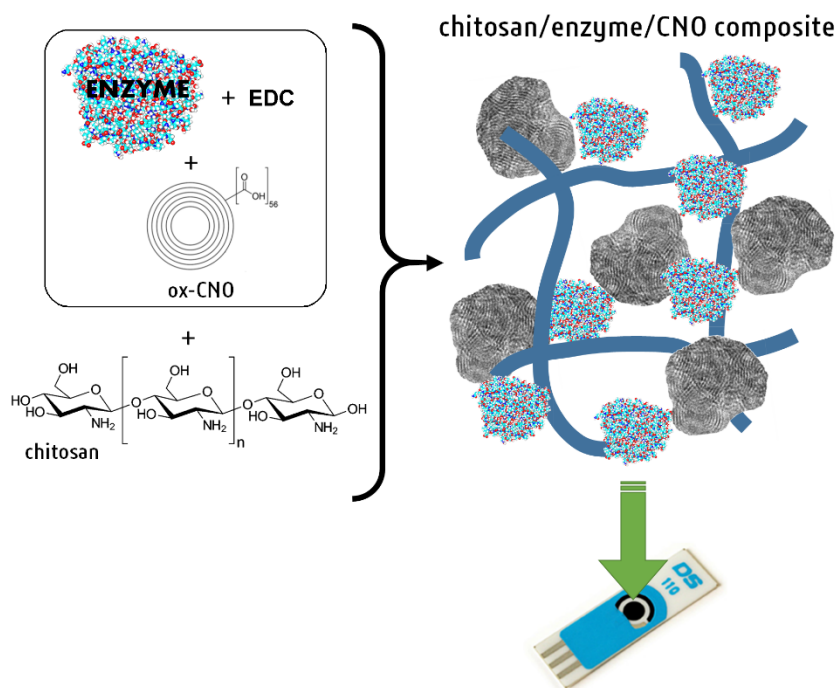
The stability of the biosensors stored in the fridge in PBS at 4°C was studied for 30 days by measuring the inhibition of enzyme activities (1 μ M glyphosate on TYR, 3 μ M 2,4,5-T on HRP). Repeatability was studied until the signal decreased by 10% with respect to the original signal for the above concentrations.

5.3 Results and Discussion

5.3.1 Electrochemical and physical properties of the modified electrodes

Chitosan is a natural polyaminosaccharide that has been widely used as a platform for enzyme immobilization in industrial and biosensing applications (43,44). It forms permeable membranes and is chemically reactive due to the many amino groups present in the structure. We thus selected this polymer as a

matrix to immobilize the enzymes (HRP or TYR) and CNO using a crosslinker that was drop-casted in a SPE to develop the pesticide biosensor (Scheme 5.2)



Scheme 5.2. Preparation of chitosan/enzyme/CNO composite.

After SPE modification, the surfaces of the electrodes were imaged by environmental scanning electron microscopy (ESEM) to distinguish the morphologies. Figure 5.1 shows the ESEM analysis of bare and modified SPEs. As shown in the images, the surface of the SPE/Chi/TYR and SPE/Chi/HRP electrodes consists of superimposed thin layers corresponding to the chitosan membrane. In the presence of CNOs, the surfaces have a markedly rough morphology due to the presence of CNO aggregates. In all cases, the composites appear to completely cover the electrode surface and evidence the successful modification of the GCE electrodes.

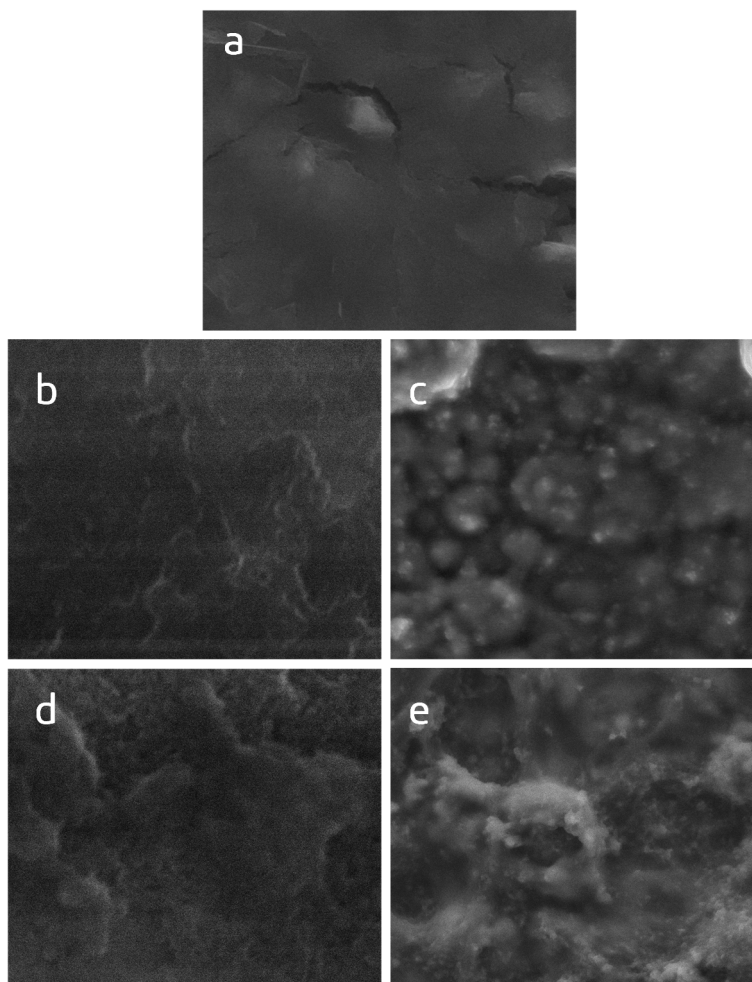


Figure 5.1. ESEM images of SPE (a), SPE/Chi/TYR (b), SPE/Chi/CNO/TYR (c), SPE/Chi/HRP (d), SPE/Chi/CNO/HRP (e). Images (a), (b) and (d) are taken at 5000X, images (c) and (e) at 2000X.

Figures 5.2 and 5.3 show the cyclic voltammograms of bare and modified electrodes using PBS as supporting electrolyte. The rectangular shape of the CVs of the modified electrodes is indicative of the deposition of the chitosan layer, that behaves as a pseudocapacitor due to its polyelectrolyte nature. This effect is increased upon incorporation of the CNOs, as recently reported for other CNO-modified surfaces (40-42).

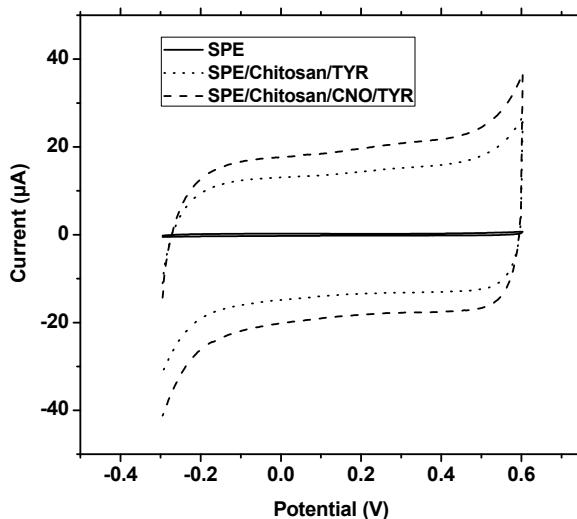


Figure 5.2. Cyclic voltammograms at SPE, SPE/Chi/CNO/TYR and SPE/Chi/TYR with scan rate 100 mV/s in the presence of 20 mM PBS, pH 7.

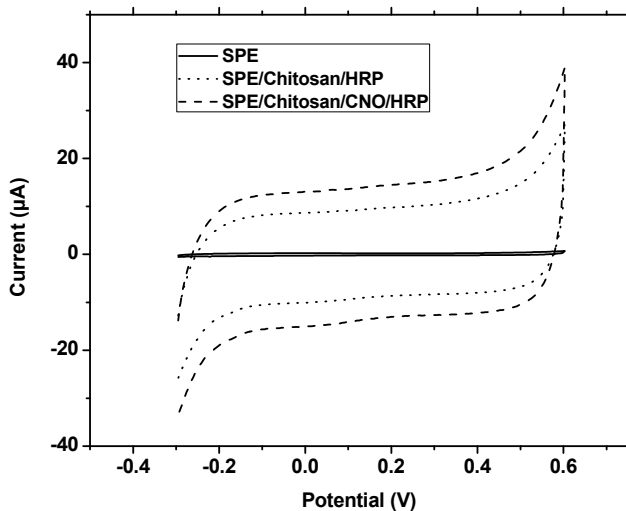


Figure 5.3. Cyclic voltammograms at SPE, SPE/Chi/CNO/HRP and SPE/Chi/HRP with scan rate 100 mV/s in the presence of 20 mM PBS, pH 7.

Figure 5.4 shows the CVs of SPE, SPE/Chi/TYR and SPE/Chi/CNO/TYR using $[\text{Fe}(\text{CN})_6]^{3-}$ in KCl as electroactive marker. SPE/Chi/CNO/TYR showed a notably higher peak current signal as compared to SPE/Chi/TYR and SPE. The electroactive

area of the mentioned electrodes accessible to the redox probe was determined using the Randles-Sevcik equation:

$$i_p = 2.69 \times 10^5 A D^{1/2} n^{3/2} v^{1/2} c$$

Where i_p is the peak current, A is the electroactive surface (cm^2), D is the diffusion coefficient of $[\text{Fe}(\text{CN})_6]^{3-}$ in dilute aqueous solution, n is the number of transferred electrons by $[\text{Fe}(\text{CN})_6]^{3-/4-}$ ($n=1$), v is the scan rate in V s^{-1} and c is the concentration of the marker. Based on this equation, by plotting the values of i_p versus $v^{1/2}$, the calculated electroactive surface of SPE/Chi/CNO/TYR is 0.775 cm^2 where SPE and SPE/Chi/TYR have surface areas 0.509 cm^2 and 0.656 cm^2 , respectively.

Similarly, figure 5.5 depicts the CVs of SPE/Chi/HRP and SPE/Chi/CNO/HRP. The calculated electroactive surfaces are 0.681 cm^2 and 0.587 cm^2 for SPE/Chi/CNO/HRP and SPE/Chi/HRP, respectively. These results indicate that the presence of both, the chitosan/enzyme composite and the CNOs in the surface coating improves the active surface of the electrodes thus enhancing the electrochemical properties of the surface. Interestingly, the prepared biosensors exhibited a good mechanical stability in aqueous solution. Treatments such as repetitive washing with water and immersion in aqueous solutions for a long time did not cause the removal of the deposited composites from the surface of SPE as revealed by inspection under an optical microscope.

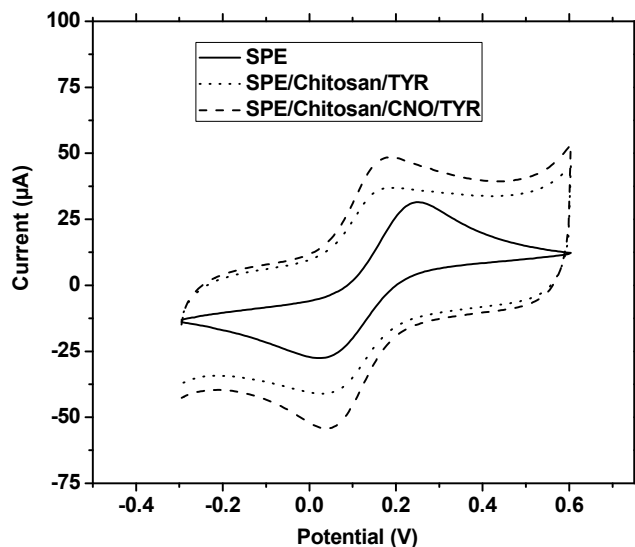


Figure 5.4. Cyclic voltammograms at SPE, SPE/Chi/CNO/TYR and SPE/Chi/TYR with scan rate 100 mV/s in the presence of 1 mM $K_3[Fe(CN)_6]$ and 0.1 mM KCl, pH 7.

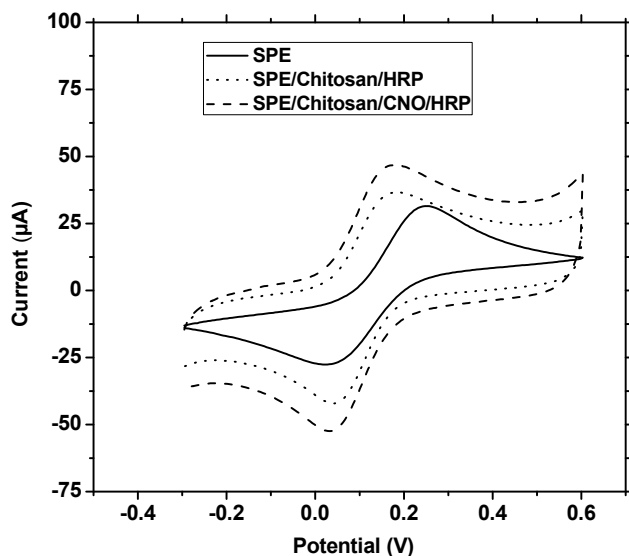


Figure 5.5. Cyclic voltammograms at SPE, SPE/Chi/CNO/HRP and SPE/Chi/HRP with scan rate 100 mV/s in the presence of 1 mM $K_3[Fe(CN)_6]$ and 0.1 mM KCl, pH 7.

Figure 5.6 shows the CVs of SPE, SPE/Chi/TYR and SPE/Chi/CNO/TYR using L-DOPA in PBS as electroactive marker. In the range of studied potentials, two peak currents appeared in both oxidation and reduction sweeps. At the bare electrode, these pairs of peaks are well resolved while in the modified electrodes the peaks are broad. The intensity of the peaks decreases in the order SPE/Chi/CNO/TYR > SPE/Chi/TYR > SPE and the peak potentials in the reduction sweep are displaced to more positive potentials, making the redox process slightly more reversible. All these features indicate that both composites are permeable to the enzyme substrate and its electroactive properties are favored with respect to the bare electrode, presumably due to an interfacial accumulation mechanism. These observations are even more evident in the case of the HRP composites using TMB as substrate. In both cases the presence of the CNOs in the surface enhanced the electroactive properties of both substrates. From these results, we selected -0.2 V and 0.0 V vs. Ag/AgCl for the amperometric measurements of TYR and HRP biosensors, respectively.

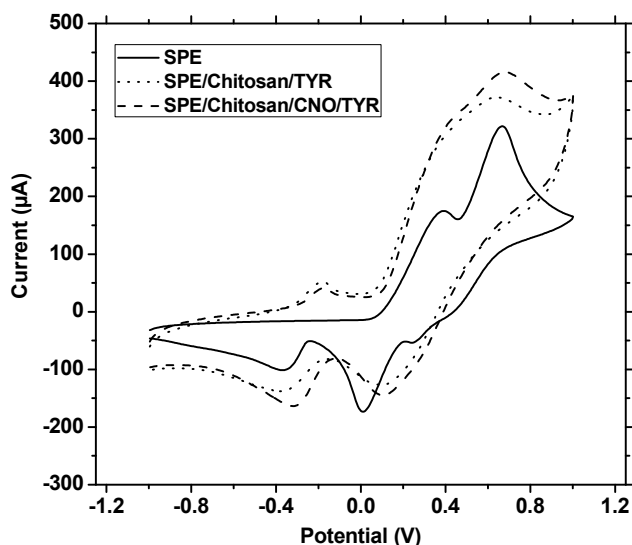


Figure 5.6. Cyclic voltammograms at SPE, SPE/Chi/CNO/TYR and SPE/Chi/TYR with scan rate 100 mV/s in the presence of 10 mM L-DOPA, pH 7.

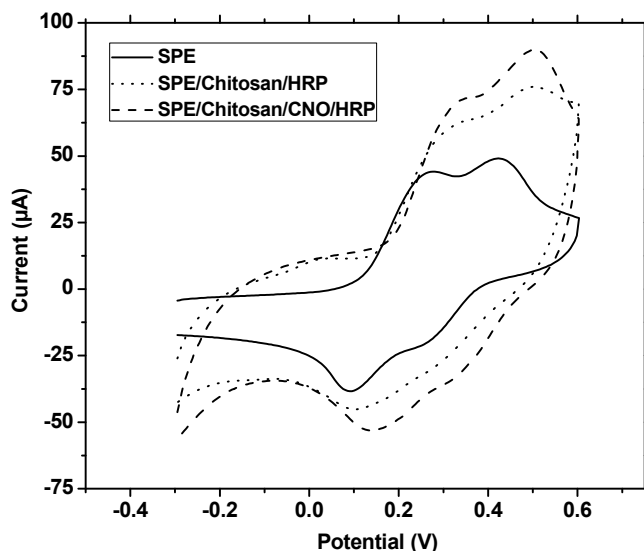


Figure 5.7. Cyclic voltammograms at SPE, SPE/Chi/CNO/HRP and SPE/Chi/HRP with scan rate 100 mV/s in the presence of 0.5 mM TMB and H_2O_2 1:1, pH 6.5.

5.3.2. Optimization of experimental conditions of the biosensors

To reach the highest sensitivity for biosensing, various conditions, including substrate concentrations and incubation times were optimized for the developed biosensors. These steps are necessary due to the heterogeneous nature of the biosensor interface given by the active membrane that has a finite permeability to ions and reagents. For this, the biosensors were incubated with the substrate for a given time and the reduction current of the product was measured at a fixed potential, depending on the enzyme and substrate used.

Figure 5.8 shows the amperometric responses of TYR biosensors with different L-DOPA concentrations. The maximum current is achieved at 1.4 mM of L-DOPA for both TYR biosensors. Above this concentration, L-DOPA started to saturate the active enzymes on the biosensors to reach maximum activity, as expected for a Michaelis-Menten kinetics. Assuming that the current response is proportional to

the enzyme activity, the K_m value of the immobilized tyrosinase was estimated to be 0.55 mM, which is lower than the value reported for the free enzyme (0.78 mM) (45). This means that the affinity of the enzyme for the substrate is improved upon immobilization. The same trend in the apparent K_m values was observed for the immobilized HRP (0.02 mM) as compared with the free enzyme (0.057 mM) (46) (Figure 5.9). In this case, saturation was achieved at 0.06 mM TMB. Interestingly, the calculated affinity values did not depend on the presence of CNOs in the composite.

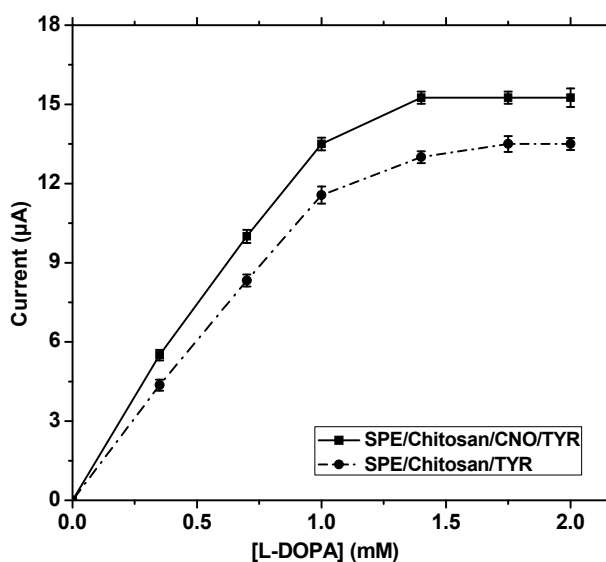


Figure 5.8. Amperometric response of SPE/Chi/CNO/TYR and SPE/Chi/TYR biosensors with different concentrations of L-DOPA in 20 mM PBS pH 7 and 2 min incubation.

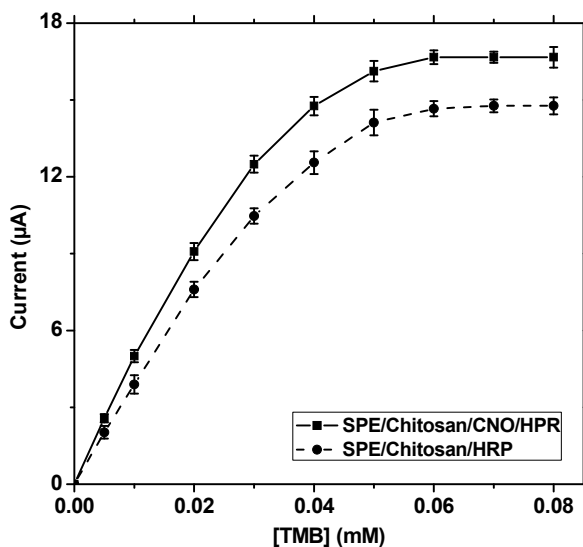


Figure 5.9. Amperometric responses of SPE/Chi/CNO/HRP and SPE/Chi/HRP biosensors with different concentrations of TMB in 10 mM PBS pH 6.5 and 2 min incubation.

Figures 5.10 and 5.11 show the current progress vs. time of SPE/Chi/CNO/TYR and SPE/Chi/CNO/HRP biosensors with and without the presence of inhibitor. As seen in the figures, the steady-state current started about 60 s after exposing the biosensors into substrate solution and the current response remained stable for several minutes. Hence, the biosensors were incubated for 1 minute after substrate addition (step 2 in Scheme 5.3) before reading the amperometric signal (step 3 in Scheme 5.3).

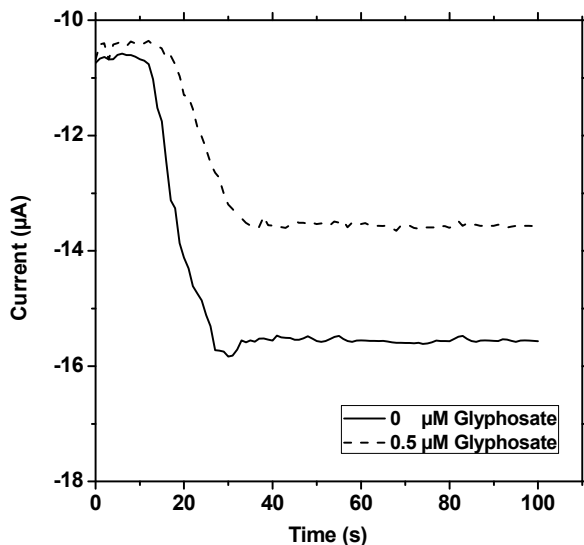


Figure 5.10. Amperometric responses of SPE/Chi/CNO/TYR to 0 and 0.5 μM of glyphosate at 425 rpm of stirring in 20 mM PBS, pH 7.

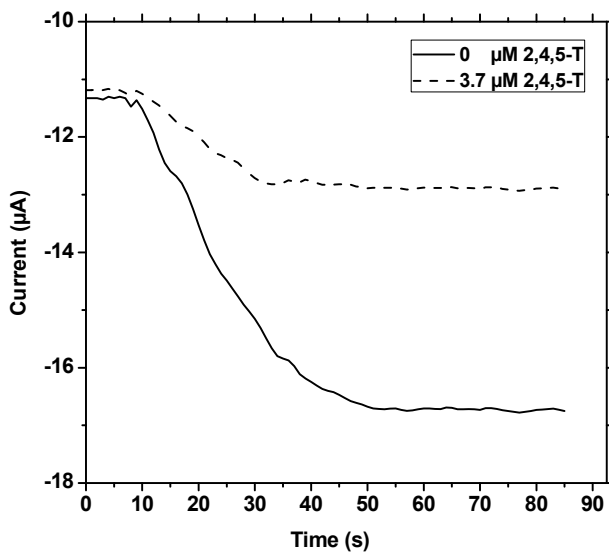


Figure 5.11. Amperometric responses of SPE/Chi/CNO/HRP to 0 and 3.7 μM of 2,4,5-T at 425 rpm of stirring in 10 mM PBS, pH 6.5.

Another important parameter to optimize in this type of systems is the time the biosensors are kept in contact with the inhibitors. In reversible competitive inhibition (as in the case of TYR and HRP with the studied pesticides), the inhibitor and substrate compete for the active site of the enzyme and for a constant substrate concentration the activity decreases with increasing inhibitor concentration. In solution this process is typically very fast but with immobilized enzymes in a rather complex matrix some time is needed to complete the diffusion of the reagents. Figures 5.12 and 5.13 show the current loss at increasing pesticide incubation times using 3.4 μM glyphosate for SPE/Chi/TYR and SPE/Chi/CNO/TYR and 2.5 μM 2,4,5-T for SPE/Chi/HRP and SPE/Chi/CNO/HRP, respectively. As seen in the figures, the biosensors need 10 and 12 minutes to achieve maximum inhibition.

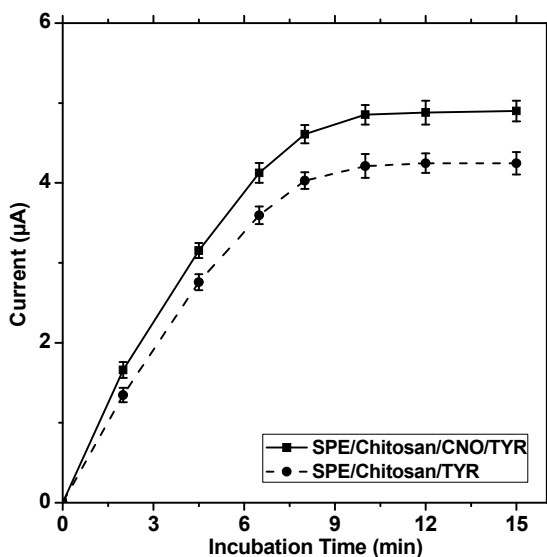


Figure 5.12. Current variations of SPE/Chi/CNO/TYR and SPE/Chi/TYR in 3.4 μM of glyphosate at different incubation times. Conditions as in Fig. 5.10.

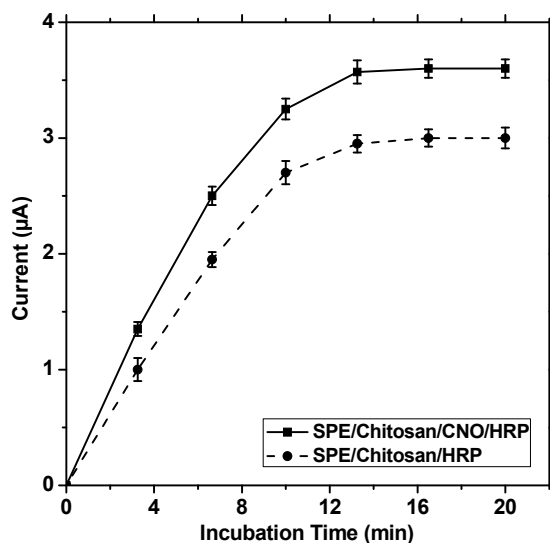


Figure 5.13. Current variations of SPE/Chi/CNO/HRP and SPE/Chi/HRP in 2.5 µM of glyphosate at different incubation times. Conditions as in Fig. 5.11.

5.3.3 Detection of pesticides using the developed biosensors

As explained in Chapter 1, the ability of many toxic substances to inhibit the catalytic activities of enzymes has contributed to the development of biosensors for the detection and quantification of pesticides. The relative inhibition of enzyme activity is correlated with the inhibitor concentration. Based on the inhibition results presented in Chapters 2 and 3, we selected in this work to apply the inhibitory effects of glyphosate on TYR response and 2,4,5-T on the HRP to develop biosensors.

The inhibition mechanism of glyphosate and 2,4,5-T on the catalytic activity of tyrosinase and horseradish peroxidase, respectively, was reversible in both cases. We thus selected the two-step approach depicted in Figure 1.8, taking into consideration that the heterogeneous nature of the enzyme-containing surface in order to optimize the incubation time, among other parameters. Hence, by

measuring the amperometric response of the biosensors in the absence and presence of the pesticides it was possible to construct the corresponding calibration plots based on percentage of signal inhibition.

5.3.3.1 Amperometric detection of glyphosate on SPE/Chi/CNO/HRP and SPE/Chi/TYR

Figure 5.14 shows the calibration curves of inhibition of glyphosate on L-DOPA response for SPE/Chi/CNO/TYR and SPE/Chi/TYR biosensors. The plots show that the inhibition percent increases almost linearly with pesticide concentration for both biosensors and then tends slowly to saturation, with the %I values not reaching 100%. A linear relationship was found up to 0.12 μM for both biosensors. The detection limits were 0.0065 μM (1.1 $\mu\text{g/L}$) for SPE/Chi/CNO/TYR and 0.009 μM (1.27 $\mu\text{g/L}$) for SPE/Chi/TYR. In the range of studied concentrations of glyphosate, the sensitivity of the SPE/Chi/CNO/TYR biosensor (taken as the slope of the linear part) is higher in comparison to SPE/Chi/TYR.

The inhibition of this pesticide on TYR in solution was found to be of a mixed type with the affinity constant of glyphosate for the enzyme $K_I = 33 \mu\text{M}$ and the affinity of glyphosate for the enzyme-L-DOPA complex $K_{IS} = 183 \mu\text{M}$. The K_I value suggest that the enzyme presents high affinity to glyphosate. The enhanced sensitivity of SPE/Chi/CNO/TYR over SPE/Chi/TYR might depend on the efficiency to maintain the bioelectrocatalytic cycle and factors such as measurement protocol, immobilization, enzyme loading, incubation time and substrate concentration. The measurement protocol and incubation times were identical for SPE/Chi/CNO/TYR and SPE/Chi/TYR, so these factors could not make the difference. In the case of reversible inhibition using free enzyme in solution, the enzyme concentration does not affect the degree of inhibition if the enzyme concentration is lower than the inhibitor concentration. In our case, the SPE/Chi/CNO/TYR contained the enzyme loaded in a CNO-containing composite

which might have enhanced electron transfer of the electroactive products, in a similar mechanism to other nanoparticles such as carbon nanotubes, carbon black, and gold nanoparticles (34,39). On other hand, the SPE/Chi/CNO/TYR has higher surface area compared to SPE/Chi/TYR, in which the enzyme might be well distributed on the sensor making enzyme with higher capability of sensing toward substrate as well as inhibitors.

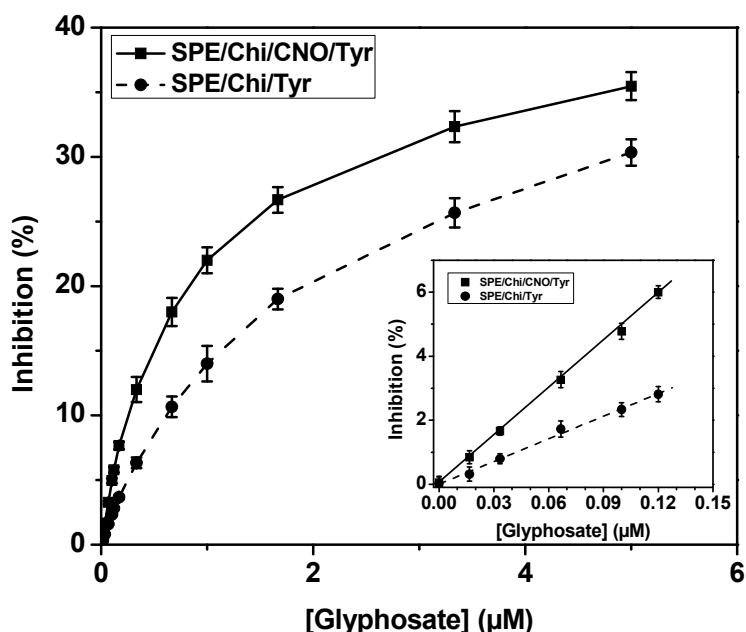


Figure 5.14. Calibration curves for biosensors SPE/Chi/CNO/TYR and SPE/Chi/TYR to different glyphosate concentrations.

To the best of our knowledge, this is the first example of tyrosinase-based biosensor for glyphosate detection, which is more sensitive in comparison to other biosensors previously reported based on HRP. Earlier reports include a biosensor based on peroxidase immobilized on a modified nanoclay with 30 μg/L of detection limit (0.1765 μM) (23) and a biosensor based on HRP adsorbed on sulfonated polymer matrix with 0.01 μM of detection limit (38).

5.3.3.2 Amperometric detection of 2,4,5-T on SPE/Chi/CNO/HRP and SPE/Chi/HRP

Figure 5.15 shows the calibration curves of inhibition of 2,4,5-T on HRP for SPE/Chi/CNO/HRP and SPE/Chi/HRP biosensors. Similarly to the TYR biosensor, the inhibition percent increases almost linearly with pesticide concentration then tends slowly to saturation, with the %I values reaching ~35% for 12 μM of 2,4,5-T. Linear relationships were found (0.0112-0.345 μM for SPE/Chi/CNO/HRP and 0.015-0.425 μM for SPE/Chi/HRP). The obtained detection limits were 0.010 μM for SPE/Chi/CNO/HRP and 0.017 μM for SPE/Chi/HRP. As seen in the graph, in the range of studied concentrations of 2,4,5-T, the sensitivity of SPE/Chi/CNO/HRP was higher than that of SPE/Chi/HRP, although in this case the difference is less pronounced than that of SPE/Chi/HRP.

In chapter 2, we found that 2,4,5-T was a competitive inhibitor of HRP with $K_I = 211 \mu\text{M}$, which corresponds to the degree of dissociation of the enzyme-2,4,5-T complex. The pesticide thus competes with H_2O_2 for the active side of the enzyme with no effect on the enzyme- H_2O_2 complex. This difference in inhibition mechanism with TYR/glyphosate may account for the differences in sensitivity between the TYR and HRP biosensors. In the first case, the pesticide is capable to inhibit both E and E-S complex, while 2,4,5-T only inhibits E. The role of CNOs in the HRP biosensor is slightly more prominent in this case with respect to the analytical parameters obtained.

The analytical data of the prepared biosensors is collected in Table 5.1.

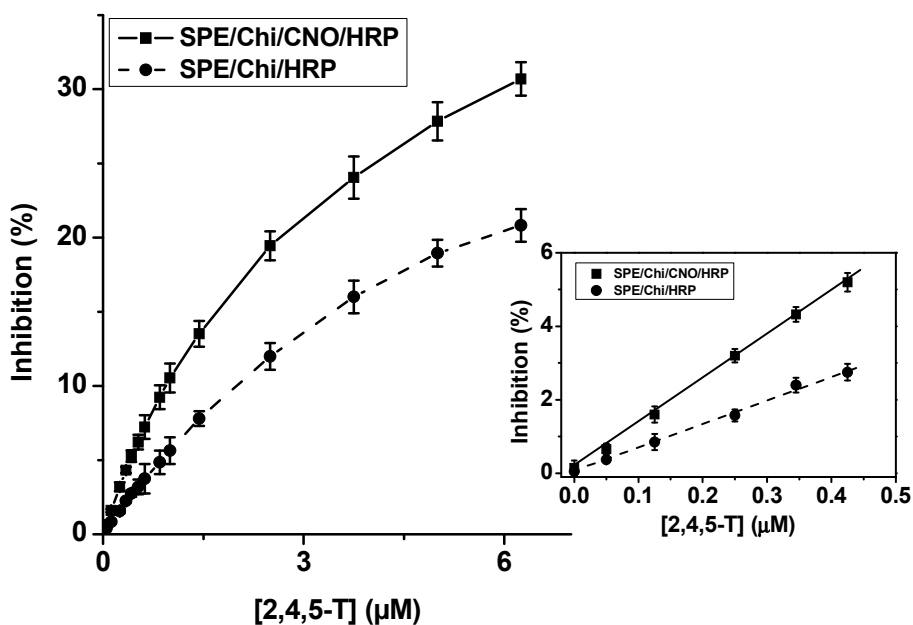


Figure 5.15. Calibration curves for biosensors SPE/Chi/CNO/HRP and SPE/Chi/HRP to different 2,4,5-T concentrations.

Table 5.1 Analytical data of the prepared biosensors (n = 3).

Pesticide	Biosensor	LOD (nM)	Sensitivity (μM^{-1})
Glyphosate	SPE/Chi/CNO/TYR	6.5 ± 0.4	51.5
	SPE/Chi /TYR	9.0 ± 0.5	23.4
2,4,5-T	SPE/Chi/CNO/HRP	10 ± 1	12.2
	SPE/Chi/HRP	17 ± 2	6.9

5.3.4 Analysis of spiked river water samples

Due to the impossibility to obtain real samples contaminated with glyphosate or 2,4,5-T, the CNO modified biosensors were tested in river water samples collected from the Francolí river in Tarragona and spiked with both pesticides

(Figure 5.16). As can be seen in Table 5.2, the recovery signals obtained for both biosensors are between 95 and 108%, demonstrating the suitability of the developed surface chemistry for pesticide detection in complex samples.



Figure 5.16 Collection site of the river water samples.

Table 5.2 Results obtained in spiked river water samples.

Pesticide	Biosensor	Concentration added (μM)	Concentration found (μM)	% Recovery
<i>Glyphosate</i>	SPE/Chi/CNO/TYR	1.0	1.08 ± 0.08	108
<i>2,4,5-T</i>	SPE/Chi/CNO/HRP	3.0	2.85 ± 0.05	95

5.3.5 Stability and repeatability of the developed biosensors

The long-term stability and repeatability of the biosensors were examined. Figure 5.17 and 5.18 show the residual activities of the immobilized enzymes on the TYR and HRP biosensors by monitoring the amperometric responses at the optimal substrate concentrations as explained above in 4-day intervals over a period of 4 weeks. As seen in figure 5.17, after one week of storage SPE/Chi/CNO/TYR and

SPE/Chi/TYR maintain 96% and 77% respectively and then decreased gradually to 62% and 38% after 4 weeks. In general, from the results of the stability studies of SPE/Chi/CNO/TYR and SPE/Chi/TYR stored in PBS buffer at pH 6.5 and 4°C it is evident that the presence of CNO in the composite of SPE/Chi/CNO/TYR biosensor significantly enhanced the stability of the biosensors compared to SPE/Chi/TYR. A similar trend was observed for HRP. Figure 5.18 illustrates that after the first week of storage, SPE/Chi/CNO/HRP and SPE/Chi/HRP maintain 96.5% and 85% respectively and then decreased to 77% and 64% after 4 weeks of storage. As seen, the presence of CNO covalently coupled with chitosan and HRP on the surface electrode has positively improved the stability of SPE/Chi/CNO/HRP compared to SPE/Chi/HRP. In general, HRP biosensors were more stable with time than tyrosinase.

The increased stability demonstrated for the enzymatic biosensors covalently coupled with CNO might be attributed to Van der Waals interactions between the carbon nanoparticles and the enzyme resulting in a reduction in the enzyme mobility due to the anchorage to the support, thus shielding it from the denaturing effects of the environment. Interestingly, these results agree with the improved stability observed for CNO-enzyme conjugates in solution as explained in Chapter 4.

Regarding repeatability, the SPE/Chi/CNO/TYR biosensor maintains stable steady-state current after 65 measurements while SPE/Chi/TYR only after 50 measurements. In case of HRP biosensors, SPE/Chi/CNO/HRP is stable for 58 measurements while SPE/Chi/HRP for 49 measurements. These results can also be explained based on the stability of the enzyme composites with CNO and the presence of the chitosan matrix.

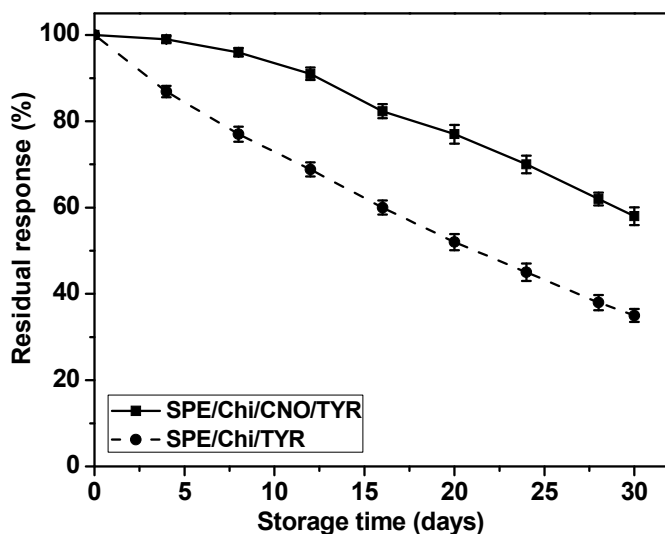


Figure 5.17. Residual activities of SPE/Chi/CNO/TYR and SPE/Chi/TYR biosensors stored in 20 mM PBS, pH 6.5 at 4°C.

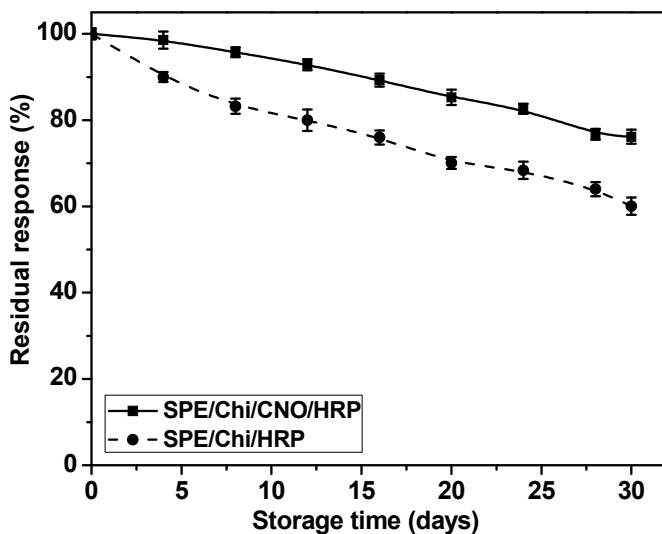


Figure 5.18. Residual activities of SPE/Chi/CNO/HRP and SPE/Chi/HRP biosensors stored in 20 mM PBS, pH 6.5 at 4°C.

5.4 Conclusions

In this chapter, we have explored the possibility to use CNO-modified electrodes for the construction of amperometric enzyme biosensors based on cross-linked and covalent immobilization of enzymes with CNO and chitosan. This combination allowed the development of highly sensitive biosensors for glyphosate and 2,4,5-T based on the inhibition of tyrosinase and HRP activities, respectively. The incorporation of CNO into chitosan-enzyme composites for biosensor development had a positive effect in enhancing the sensitivity due to the large surface area combined with enhanced electron transfer properties of the CNO-modified electrodes. CNOs also proved beneficial to improve their stability and repeatability.

Although we could not validate our results by comparison with standard methods, the simplicity of preparation, good analytical behavior and stability and ability to detect the pesticides in relatively complex samples such as river water demonstrate the feasibility of using chitosan/CNO/enzyme composites for the development of sensitive biosensors based on activity inhibition. It could thus be expected that this strategy can be further extended to develop portable pesticide detection systems for in-field agricultural or environmental applications.

References

1. H. H. Nguyen, M. Kim. An overview of techniques in enzyme immobilization. *App. Sci. Conver. Technol*, 2017. 26(6): pp. 157-163. DOI: 10.5757/ASCT.2017.26.6.157.
2. A. Sassolas, L. J. Blum, B. D. Leca-Bouvier. Immobilization strategies to develop enzymatic biosensors. *Biotechnol. Adv.*, 2012. 30(3): pp. 489-511. DOI: 10.1016/j.biotechadv.2011.09.003.
3. R. E. Sabzi, F. Rashouli, F. Kheiri. Amperometric hydrogen peroxide biosensor based on horseradish peroxidase entrapped in titania sol-gel film on screen printed electrode. *Am. J. Analyt. Chem.*, 2013. 4(11): pp. 607-615. DOI: <http://dx.doi.org/10.4236/ajac.2013.411072>.

4. A. Zejli, J. L. H. de Cisneros, I. Naranjo-Rodriguez, B. Liu, K. R. Tamsamani, J. Marty. Alimina sol-gel/sonogel-carbon electrode base don acetylcholinesteras for detection of organophosphorus pesticides. *Talanta*, 2008. 77(1): pp. 217-221. DOI: <https://doi.org/10.1016/j.talanta.2008.06.010>.
5. M. Elkaoutit, I. Naranjo-Rodriguez, M. Domínguez, M. P. Hernández-Artiga, D. Bellido-Milla, J. L. H. de Cisneros. A third-generation hydrogen peroxide biosensor based on Horseradish Peroxidase (HRP) enzyme immobilized in a Nafion–Sonogel–Carbon composite. *Electrochim. Acta.*, 2008. 53(24): pp. 7131-7137. DOI: <https://doi.org/10.1016/j.electacta.2008.04.086>.
6. C. Védrine, S. Fabiano, C. Tran-Minh. Amperometric tyrosinase based biosensor using an electrogenerated polythiophene film as an entrapment support. *Talanta*, 2003. 59(3): pp. 535-544. DOI: [https://doi.org/10.1016/S0039-9140\(02\)00540-4](https://doi.org/10.1016/S0039-9140(02)00540-4).
7. G. Valdés-Ramírez, M. Cortina, M. T. Ramírez-Silva, J. Marty. Acetylcholinesterase-based biosensors for quantification of carbofuran, carbaryl, methylparaoxon, and dichlorvos in 5% acetonitrile. *Anal. Bioanal. Chem.*, 2008. 392(4): pp. 699-707. DOI: 10.1007/s00216-008-2290-7. Epub 2008 Jul 29.
8. Q. Xu, C. Mao, N. Liu, J. Zhu, J. Sheng. Direct electrochemistry of horseradish peroxidase based on biocompatible carboxymethyl chitosan–gold nanoparticle nanocomposite. *Biosens. Bioelectron.*, 2006. 22(5): pp. 768-773. DOI: <https://doi.org/10.1016/j.bios.2006.02.010>.
9. Y. Wei, Y. Li, Y. Qu, F. Ziao, G. Shi, L. Jin. A novel biosensor based on photoelectro-synergistic catalysis for flow-injection analysis system/amperometric detection of organophosphorous pesticides. *Anal. Chim. Acta*, 2009. 643(1-2): pp. 13-18. DOI: <https://doi.org/10.1016/j.aca.2009.03.045>.
10. S. K. Mocellini, I. C. Vieira, F. D. Lima, B. G. Lucca, A. M. J. Barbosa, V. S. Ferreira. Determination of thiodicarb using a biosensor based on alfalfa sprout peroxidase immobilized in self-assembled monolayers. *Talanta*, 2010. 82(1): pp. 164-170. DOI: <https://doi.org/10.1016/j.talanta.2010.04.015>.
11. M. T. Pérez Pita, A. J. Reviejo, F. J. Manuel de Villena, J. M. Pingarrón. Amperometric selective biosensing of dimethyl-and diethyldithiocarbamates based on inhibition processes in a medium of reversed micelles. *Anal. Chim. Acta*, 1997. 340(1-3): pp. 89-97. DOI: [https://doi.org/10.1016/S0003-2670\(96\)00552-1](https://doi.org/10.1016/S0003-2670(96)00552-1).

12. G. Kim, J. Shim, M. Kang, S. Moon. Optimized coverage of gold nanoparticles at tyrosinase electrode for measurement of a pesticide in various water samples. *J. Hazard. Mater.*, 2008. 156(1-3): pp. 141-147. DOI: <https://doi.org/10.1016/j.jhazmat.2007.12.007>.
13. E. V. Gogol, G. A. Evtugyn, J. L. Marty, H. C. Budnikov, V. G. Winter. Amperometric biosensors based on nafion coated screen-printed electrodes for the determination of cholinesterase inhibitors. *Talanta*, 2000. 53(2): pp. 379-389. DOI: [https://doi.org/10.1016/S0039-9140\(00\)00507-5](https://doi.org/10.1016/S0039-9140(00)00507-5).
14. T. M. Anh, S. V. Dzyadevych, M. C. Van, N. J. Renault, C. N. Duc, J. Chovelon. Conductometric tyrosinase biosensor for the detection of diuron, atrazine and its main metabolites. *Talanta*, 2004. 63(2): pp. 365-370. DOI: <https://doi.org/10.1016/j.talanta.2003.11.008>.
15. Y. D. Tanimoto de Albuquerque, L. F. Ferreira. Amperometric biosensing of carbamate and organophosphate pesticides utilizing screen-printed tyrosinase-modified electrodes. *Anal. Chim. Acta*, 2007. 596(2): pp. 210-221. DOI: <https://doi.org/10.1016/j.aca.2007.06.013>.
16. A. C. Ion, I. Ion, A. Culetu, D. Gharase, C. A. Moldovan, R. Iosub, A. Dinescu. Acetylcholinesterase voltammetric biosensors based on carbon nanostructure chitosan composite material for organophosphate pesticides. *Mater. Sci. Eng. C*, 2010. 30(6): pp. 817-821. DOI: <https://doi.org/10.1016/j.msec.2010.03.017>.
17. F. de Lima, B. G. Lucca, A. M. J. Barbosa, V. S. Ferreira, S. K. Moccelini, A. C. Franzoi, I. C. Vieira. Biosensor based on pequi polyphenol oxidase immobilized on chitosan crosslinked with cyanuric chloride for thiodicarb determination. *Enzyme Microb. Technol.*, 2010. 47(6): pp. 153-158. DOI: <https://doi.org/10.1016/j.enzmictec.2010.05.006>.
18. Y. Miao, S. N. Tan. Amperometric hydrogen peroxide biosensor based on immobilization of peroxidase in chitosan matrix crosslinked with glutaraldehyde. *Analyst*, 2000. 125: pp. 1591-1594. DOI: 10.1039/B003483P.
19. J. Shi, J. C. Chaussen, E. S. McLamore, A. U. Haque, D. Jaroch, A. Diggs, P. C. Marzal, J. Rickus, D. M. Porterfield. A comparative study of enzyme immobilization strategies for multi-walled carbon nanotube glucose biosensors. *Nanotechnology*, 2011. 22(35): pp.355502. DOI: 10.1088/0957-4484/22/35/355502.
20. Y. Ivanov, I. Marinow, K. Gabrovska, N. Dimcheva, T. Godjevargova. Amperometric biosensor based on a site-specific immobilization of acetylcholinesterase via affinity bonds on a nanostructured polymer

- membrane with integrated multiwall carbon nanotubes. *J. Mol. Catal., B Enzym.*, 2010. 63(3-4): pp. 141-148. DOI: <https://doi.org/10.1016/j.molcatb.2010.01.005>.
21. J. Xu, J. Zhu, Q. Wu, Z. Hu, H. Chen. An amperometric biosensor based on the coimmobilization of Horseradish Peroxidase and methylene blue on a carbon nanotubes modified electrode. *Electroanalysis*, 2003. 15(3): pp. 291-224. DOI: <https://doi.org/10.1002/elan.200390027>.
 22. C. Tortolini, P. Bollela, R. Antiochia, G. Favero, F. Mazzei. Inhibition-based biosensor for atrazine detection. *Sens. Actuators B Chem.*, 2016. 224: pp. 552-558. DOI: <https://doi.org/10.1016/j.snb.2015.10.095>.
 23. G. C. Oliveira, S. K. Mocchelini, M. Castilho, A. J. Terezo, J. Possavatz, M. R. L. Magalhães, E. F. G. C. Dores. Biosensor based on atemoya peroxidase immobilised on modified nanoclay for glyphosate biomonitoring. *Talanta*, 2012. 98: pp. 130-136. DOI: <https://doi.org/10.1016/j.talanta.2012.06.059>.
 24. M. Moyo, J. O. Okonkwo, N. M. Agyei. Optimization of Horseradish Peroxidase Immobilization on glassy carbon electrode based on maize tassel-multiwalled carbon nanotubes for sensitive copper(II) ion detection. *Int. J. Electrochem. Sci.*, 2014. 9: pp. 1439-1453. DOI: [10.1016/j.enzmictec.2013.12.014](https://doi.org/10.1016/j.enzmictec.2013.12.014).
 25. J. Wang. Carbon-nanotube based electrochemical biosensors: a review. *Electroanalysis*, 2005. 17(1): pp. 7-14. DOI: <https://doi.org/10.1002/elan.200403113>.
 26. Y. Guan, L. Liu, C. Chen, X. Kang, Q. Xie. Effective Immobilization of TYRosinase via Enzyme Catalytic Polymerization of L-DOPA for Highly Sensitive Phenol and Atrazine Sensing. *Talanta*, 2016. 160(1): pp. 125-132. DOI: <https://doi.org/10.1016/j.talanta.2016.07.003>.
 27. M. E. Kaoutit, D. Bouchta, H. Zejli, N. Izaoumen, K. R. Temsamani. A simple conducting polymer-based biosensor for the detection of atrazine. *Anal. Lett.*, 2004. 37(8): pp. 1671-1681. DOI: <https://doi.org/10.1081/AL-120037595>.
 28. Z. Yu, G. Zhao, M. Liu, Y. Lei, M. Li. Fabrication of a novel atrazine biosensor and its subpart-per-trillion levels sensitive performance. *Environ. Sci. Technol.*, 2010. 44(20): pp. 7878-7883. DOI: [10.1021/es101573s](https://doi.org/10.1021/es101573s).
 29. L. Campanella, A. Bonanni, E. Martini, N. Todini, M. Tomassetti. Determination of triazine pesticides using a new enzyme inhibition tyrosinase OPEE operating in chloroform. *Sens. Actuators B*, 2005. 111-112: pp. 505-514. DOI: <https://doi.org/10.1016/j.snb.2005.03.082>.

30. J. C. Vidal, L. Bonel, J. R. Castillo. A modulated tyrosinase enzyme-based biosensor for application to the detection of dichlorvos and atrazine pesticides. *Electroanalysis*, 2008. 20(8): pp. 865-873. DOI: 10.1002/elan.200704115.
31. W. R. Everett, G. A. Rechnitz. Mediated bioelectrocatalytic determination of organophosphorus pesticides with tyrosinase-based oxygen biosensor. *Anal. Chem.*, 1998. 70(4): pp. 807-810. DOI: 10.1021/ac970958l.
32. E. Kuusk, T. Rinke. Transient phase calibration of tyrosinase-based carbaryl biosensor. *Enzyme Microb. Technol.*, 2004. 34(7): pp. 657-661. DOI: <https://doi.org/10.1016/j.enzmictec.2004.03.004>.
33. L. Campanella, D. Lelo, E. Martini, M. Tomassetti. Organophosphorus and carbamate pesticide analysis using an inhibition tyrosinase organic phase enzyme sensor, comparison by butyrylcholinesterase + choline oxidase opee and application to natural waters. *Anal. Chim. Acta*, 2007. 587(1): pp. 22-32. DOI: 10.1016/j.aca.2007.01.023.
34. G. Kim, M. Kang, J. Shim, S. Moon. Substrate-bound tyrosinase electrode using gold nanoparticles anchored to pyrroloquinoline quinone for a pesticide biosensor. *Sens. Actuators B*, 2008. 133(1): pp. 1-4. DOI: <https://doi.org/10.1016/j.snb.2008.01.055>.
35. J. Wang, V. B. Nascimento, S. A. Kane, K. Rogers, M. R. Smyth, L. Angnes. Screen-printed tyrosinase-containing electrodes for the biosensing of enzyme inhibitors. *Talanta*, 1996. 43(11): pp. 1903-1907. DOI: [https://doi.org/10.1016/0039-9140\(96\)01967-4](https://doi.org/10.1016/0039-9140(96)01967-4).
36. E. A. Songa, T. Waryo, N. Jahed, P. G. L. Baker, B. V. Kgarebe, E. I. Iwuoha. Electrochemical nanobiosensor for glyphosate herbicide and its metabolite. *Electroanalysis*, 2009. 21(3-5): pp. 671-674. DOI: <https://doi.org/10.1002/elan.200804452>.
37. E. A. Songa, V. S. Somerset, T. Waryo, P. G. L. Baker, E. I. Iwuoha. Amperometric nanobiosensor for quantitative determination of glyphosate and glufosinate residues in corn samples. *Pure Appl. Chem.*, 2009. 81(1): pp. 123-139. DOI: 10.1351/PAC-CON-08-01-15.
38. E. A. Songa, O. A. Arotiba, J. H. O. Owino, N. Jahed, P. G. L. Baker, E. I. Iwuoha. Electrochemical detection of glyphosate herbicide using horseradish peroxidase immobilized on sulfonated polymer matrix. *Bioelectrochemistry*, 2009. 75(2): pp. 117-123. DOI: <https://doi.org/10.1016/j.bioelechem.2009.02.007>.

39. Q. Zhang, G. Xu, L. Gong, H. Dai, S. Zhang, Y. Li, Y. Lin. An enzyme-assisted electrochemiluminescent biosensor developed on ordered mesoporous carbon substrate for ultrasensitive glyphosate sensing. *Electrochim. Acta*, 2015. 186: pp. 624-630. DOI: <https://doi.org/10.1016/j.electacta.2015.10.081>.
40. J. P. Bartolome, A. Fragoso. Electrochemical detection of nitrite and ascorbic acid at glassy carbon electrodes modified with carbon nano-onions bearing electroactive moieties. *Inorganica Chim. Acta*, 2017. 468: pp. 223-231. DOI: <https://doi.org/10.1016/j.ica.2017.06.024>.
41. J. P. Bartolome, L. Echegoyen, A. Fragoso. Reactive carbon nano-onion modified glassy carbon surfaces as DNA sensors for human Papillomavirus oncogene detection with enhanced sensitivity. *Anal. Chem.*, 2015. 87(13): pp. 6744-6751. DOI: 10.1021/acs.analchem.5b00924.
42. J. C. Zuaznabar, A. Fragoso. A wide-range solid state potentiometric pH sensor based on poly-dopamine coated carbon nano-onion electrodes. *Sens. Act. B, Chemical*, 2018. 273: pp. 664-671. DOI: <https://doi.org/10.1016/j.snb.2018.06.103>
43. B. Krajewska. Application of chitin-and chitosan-based materials for enzyme immobilizations: a review. *Enzyme Microb. Technol.*, 2004. 35(2-3): pp. 126-139. <https://doi.org/10.1016/j.enzmictec.2003.12.013>.
44. H. Susanto, A. M. Samsudin, N. Rokhati, I. N. Widiassa. Immobilization of glucose oxidase on chitosan-based porous composite membranes and their potential use in biosensors. *Enzyme Microb. Technol.*, 2013. 52(6-7): pp. 386-392. DOI: <https://doi.org/10.1016/j.enzmictec.2013.02.005>.
45. Q. Wu, Z. Xu, Y. Duan, Y. Zhu, M. Ou, X. Xu. Immobilization of tyrosinase on polyacrylonitrile beads: biodegradation of phenol from aqueous solution and the relevant cytotoxicity assessment. *RSC Adv.*, 2017. 7(45): pp. 28114-28123. DOI: 10.1039/C7RA03174B.
46. E. I. Karasyova, I. V. Nauchik, D. I. Metelitz. Activation of peroxidase-catalyzed oxidation of aromatic amines with 2-aminothiazole and melamine. *Biochemistry (Moscow)*, 2003. 68(1): pp. 54-62.

Conclusions and Future Work

As we have demonstrated in the preceding Chapters, there is currently a strong concern on the use of pesticides in agriculture and their possible side effects, which justifies the need for sensitive and robust detection systems as an important step in this direction. The overall objective of this thesis was to study the interaction of different pesticides with peroxidase and tyrosinase with the aim to develop biosensors for pesticide detection based on CNO-modified electrodes.

In the first part of this thesis, we determined that the inhibition of peroxidase and tyrosinase activities by three of the most used pesticides (2,4-D, 2,4,5-T and glyphosate) follows a reversible mechanism. This conditioned to a certain extent the immobilization and measurement strategies of the developed biosensors in order to obtain the maximum possible sensitivity. We later showed that oxidized CNOs can be used as supports for the immobilization of enzymes, retaining most of their catalytic and functional properties and enhancing the stability of the immobilized enzymes. Finally, we combined the previous studies in a novel composite material based on a chitosan matrix containing the immobilized enzymes and CNO to develop electrochemical biosensors to detect glyphosate, based in tyrosinase inhibition, and 2,4,5-T, based on peroxidase activity. The incorporation of CNOs into chitosan-enzyme composites had a positive effect in enhancing the sensitivity of the biosensors and proving to be beneficial to improve their stability and repeatability.

This thesis has thus been a contribution to a rapidly growing field related with the development of new classes of nanomaterial-based detection systems applied, in our case, to solve a challenging environmental problem of present times.

Although some of the biosensor platforms developed in this work were not fully optimized and could not be compared with standard methods, it is clear that the use in biosensing of carbon nano-onions combined with enzymes has many promising advantages over other nanomaterials. It also seems evident that there is a possibility to apply these materials to detect other contaminants. We thus recommend to continue the research work in this direction.

UNIVERSITAT ROVIRA I VIRGILI

AMPEROMETRIC ENZYME-BASED DETECTION OF AGRICULTURAL PESTICIDES ON NOVEL CARBON NANO-ONION COMPOSITES

Vibol Sok



UNIVERSITAT
ROVIRA i VIRGILI